Development and Application of Semi-Active Prosthetic Foot-Ankle Systems

By

Kieran Nichols

A dissertation submitted in partial fulfillment of the
requirements for the degree of

Doctor of Philosophy
(Mechanical Engineering)

at the
UNIVERSITY OF WISCONSIN-MADISON
2023

Date of final oral examination: 6/28/2023
The dissertation is approved by the following members of the Final Oral Committee:

Peter Adamczyk, Associate Professor, Mechanical Engineering (Advisor)
Darryl Thelen, Professor, Mechanical Engineering
Katherine Fu, Associate Professor, Mechanical Engineering
Aaron Dingle, Senior Scientist, School of Medicine
Xiaobin Xiong, Assistant Professor, Mechanical Engineering
Kristen Pickett, Associate Professor, Kinesiology

ABSTRACT

There is a need for improved design and function of prosthetic devices to aid walking in persons with transtibial amputations. This dissertation focused on two semi-active ankle-foot prosthetic devices, the Variable Stiffness Foot (VSF) and Two Axis aDaptable Ankle (TADA), which allow users to change biomechanical ankle-foot functions using simpler designs, lower costs, and less power than active prostheses. The background for this dissertation explored the main lower-limb biomechanical principles of prosthetic design, prosthetic-walking mechanics, and sensor feedback. The VSF manuscript investigated the mechanical impact of adjusting stiffness on lower limb mechanics using a prosthetic foot, which can modulate forefoot stiffness. A less stiff VSF resulted in increased ankle dorsiflexion angle, decreased ankle plantarflexor moment, decreased knee extension, decreased knee flexor moment, and increased magnitudes of prosthetic energy storage, energy return, and push-off power. These findings suggest that a less stiff VSF may offer advantages in lower joint moments and greater ankle angle range of motion for individuals with lower-limb prostheses. The Two Axis aDaptable Ankle (TADA) is a semi-active prosthetic ankle that offers independent modulation of sagittal and frontal ankle angles. The first TADA study modified a Raspberry Pi 4 for real-time control of brushless direct-current motors, allowing for precise and reliable ankle angle adjustments. The control system employed CANopen over EtherCAT (CoE) for synchronized communication between the Raspberry Pi and motor controllers. The results demonstrated improved movement times, lower movement errors, and higher data transmission rates. As a continuation, the final TADA study aimed to create an ankle prosthesis that can synchronously record lower-body kinematics and kinetics and assess the sensitivity of those mechanics to different walking speeds and ankle angles for an unimpaired participant. Using a pylon load cell, the results showed that peak magnitudes and impulses increased for plantarflexor moments with increased plantarflexion angle and for evertor moments with increased inversion angles. Moreover, the peak sagittal pylon moments increased with higher walking speeds. The integrated control system of the TADA effectively controls ankle angles, can affect lower-body mechanical outcomes, and can allow for efficient adaptation to various speeds and terrains in users with transtibial amputations.

OVERVIEW

Persons with unilateral transtibial amputations have lost their biological ankle and foot. To regain functional walking, they can utilize ankle-foot prostheses. These prostheses can vary in cost and complexity depending on their adaptability, weight, and comfort. The simplest and cheapest designs exist as passive mechanical prostheses, and the most complex and expensive designs are from active robotic prostheses. In between these two extremes of passive and active prostheses, semi-active prostheses allow users to modulate mechanical functions with simpler design, lower cost, and less power than active prostheses. In addition, they could replicate more of the biological ankle-foot functions than passive prostheses.

The background for this dissertation (Chapter 1) explored the main principles of prosthetic design, prosthetic-walking mechanics, and sensor feedback. Many users adapt their walking with passive transtibial prostheses with biomechanical gait deviations like hip circumduction, toe scuffing, weak prosthetic side push-off, hyperextension on the prosthetic side, and higher intact-side collision energy. Knee osteoarthritis on the intact side may become an eventual consequence of those gait deviations. Current semi-active prosthetics attempt to minimize those gait deviations with improved design and sensor feedback. This document presents the biomechanical evaluation of a Variable Stiffness Foot (VSF) and presents the design and biomechanical evaluation of a Two-Axis aDaptable Ankle (TADA). These two prostheses were chosen to give users modulation of the essential ankle-foot functions of stiffness and ankle angle.

Chapter 2 focused on the sensitivity analysis of the Variable Stiffness Foot. The manuscript examined the effects of the Variable Stiffness Foot (VSF) on joint mechanics during level-ground walking for individuals with transtibial amputations. The study investigated the mechanical impact of adjusting stiffness on knee and ankle mechanics using the VSF. The results demonstrated that a stiffer VSF leads to reduced ankle dorsiflexion angle, increased ankle plantarflexor moment, increased knee extension, increased knee flexor moment, and decreased magnitudes of prosthetic energy storage, energy

return, and power. These findings suggest that a less stiff VSF may offer advantages in lower joint moments and greater ankle angle range of motion for individuals with lower-limb prostheses.

Chapter 3 focused on the implementation and results of controlling the Two-Axis aDaptable Ankle (TADA) prosthesis. The study modified a Raspberry Pi 4 for real-time control of brushless direct-current motors, allowing for precise and reliable ankle angle adjustments. The control system employed CANopen over EtherCAT (CoE) for synchronized communication between the Raspberry Pi and motor controllers. The experimental results demonstrated improved movement times, lower movement errors, and higher data transmission rates compared to the previous TADA version. These software and hardware enhancements enable the TADA system to efficiently adapt to various speeds and terrains, enhancing its functionality and performance.

Chapter 4 presented the Two Axis aDaptable Ankle (TADA) as a semi-active prosthetic ankle that offers independent modulation of sagittal and frontal ankle angles, and can synchronously record lower-body kinematics and kinetics. The study using one unimpaired participant investigated the influence of changes in TADA angles and walking speed on prosthetic pylon moments during flat-ground walking. The results showed that peak sagittal (plantarflexor) moments and impulses increased with increased plantarflexion angles, frontal (evertor) peaks and impulses increased with increased inversion angles, and peak frontal moments increased with increased plantarflexion angles. Moreover, the peak sagittal pylon moments increased with higher walking speeds. The integrated TADA system effectively controls ankle angles and can affect lower-body mechanical outcomes. Additionally, Chapter 5 – 8 were dedicated to the Nomenclature, List of Figures and Tables, and References of the Introduction and Discussion sections. Chapters 2 – 4 have their respective references.

Acknowledgments

Thank you to my partner, Marie, for your love and support. You have been adaptable, caring, and understanding through my Ph.D., and I'm glad that I've shared the experience with you. I'm grateful to my mother, Cheryl, and brother, Keanu, who have loved, supported, and believed in me. I thank my

family and friends who have been with me through it all. I appreciate my identity as a person from Trinidad and Tobago and how that identity has contributed to my strength and perseverance. I sacrificed a lot to pursue this Ph.D. and am grateful for my past and who I have become.

I am thankful for my time in BADGER Lab. Dr. Peter Adamczyk, you accepted me into your lab and helped me grow as a scientist and engineer. I appreciate the Mechanical Engineering department for giving me a chance to try, when I transferred into the Ph.D. program from Kinesiology. I was fortunate to explore biomechanics and engineering in the UWNCL under the guidance of Kreg Gruben. Thank you to the members of BADGER Lab, especially Becca, Heidi, Stephanie, and Jenny. You helped me grow, process the grad student experience, and your friendship means a lot to me. And a final thanks to my committee members who were willing to discuss my research and were helpful in the process of finishing my graduate career.

Table of Contents

Chapter 1. BACKGROUND

(a) Introduction

People with lower-limb amputations account for about one million people in the United States of America, with about 28% being individuals with transtibial amputation (TTA)[1,2]. Besides the high average cost of about $81,000 for TTA amputation and associated rehabilitation services[3], prosthetic users spend about $1600 per year for a prosthetic device that lasts on average 1.3 years[4]. The primary function of these lower limb prostheses is to regain walking on level ground but are also necessary for standing, walking on stairs and ramps, and uneven terrain. These prosthetic devices attempt to return walking functionality by mimicking some aspects of the human ankle-foot mechanics that were lost. This attempt to return to walking for these persons with unilateral transtibial amputations is difficult as the necessary walking mechanics are not fully understood. The problems of high cost and difficulty in recreating the human ankle-foot system instigate a need for improved mechanical adaptabilities and characteristics of the prostheses.

(b) Main Principles of Prosthetic Design

(i) Common characteristics of prosthetic walking

To mechanically connect to a person with TTA, the prosthetic foot-ankle device has an attachment area on its residual limb via a socket-suspension interface. This interface allows the prosthetic lower limb to be attached to the residual limb, which distributes the loading forces through a liner and its many contact points on the remaining part of the residual limb. The socket-suspension interface connects to a pylon adaptor that allows height adjustability. The pylon adaptor then connects to the prosthetic device.

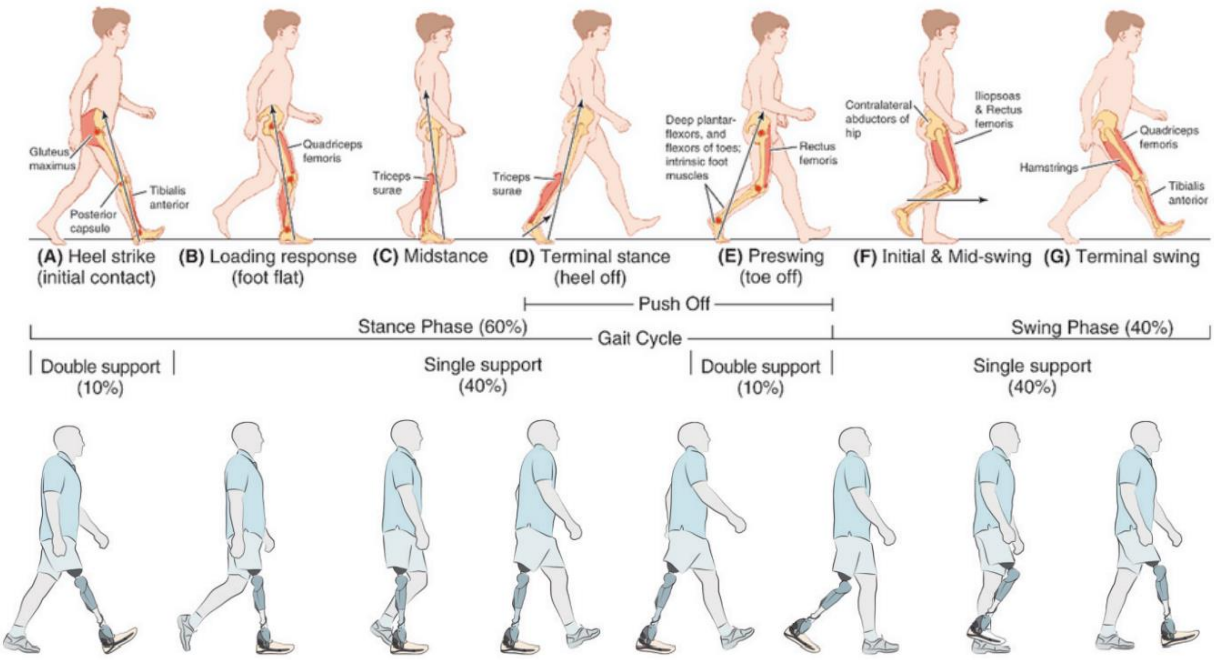

Figure 1: graphical representation of gait events of a non-disabled person and person with a prosthetic leg from Rajukova et al.[7]

Human walking (see figure 1) involves a periodic cycle where the two legs move the body forward in two phases: stance (about 60% of the cycle) and swing (about 40% of the cycle)[5]. During the swing, only one leg is in contact with the ground, and one or two legs are in contact with the ground during stance. Typically, the foot first contacts the ground with a heel strike, transitions to foot flat, heel off, and ends with toe-off. Non-disabled humans (no amputations) depend on their multiple leg muscles that cross the hip, knee, or ankle joints to modulate the joint position and moment to apply the appropriate ground reaction forces.

The hip, knee, and ankle mechanics' nomenclature will be introduced in the following sentences. Mechanically, hip motion is described by hip flexion and extension with moments of hip flexor and extensor. Knee motion is described by knee flexion and extension with moments of knee flexor and extensor. Ankle motion is described by ankle dorsiflexion and plantarflexion with moments of ankle dorsiflexor and plantarflexor[6] (see figure 2). A person with a transtibial amputation typically relies on an ankle-foot prosthesis (transtibial prosthesis) to walk. They have lost the original functionality of the ankle-foot system and must rely on the replacement passive or powered ankle-foot prosthesis.

Persons with transtibial amputations have many biomechanical issues, which they must compensate for by adjusting their gait. Issues[7] include vaulting where the person steps up with their intact side to complete the prosthetic side swing, circumduction consisting of the prosthetic foot swinging outward during the swing phase, hyperextension (locking) of the knee on the prosthetic side, and lateral trunk bending consisting of the person having a forward-leaning torso during prosthetic side stance. These issues could be caused by improper fitting and alignment and be reduced by a more suitable prosthesis. Prosthesis research aims to improve prosthesis design and fitting to minimize the need for these compensations.

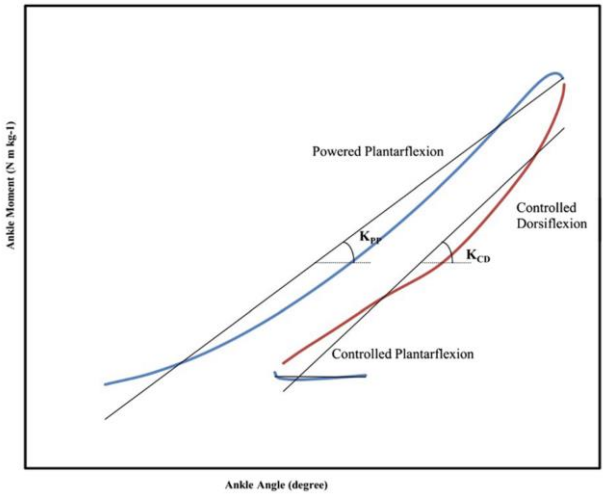

Figure 2: Non-disabled ankle moment vs. angle of the stance phase of typical walking from Safaeepour et al.6 Stance phase starts with controlled plantarflexion, transitions to controlled dorsiflexion, and ends with powered plantarflexion. Stiffness relates to the slope of ankle moment and angle.

(ii) Design of Lower Limb Prostheses

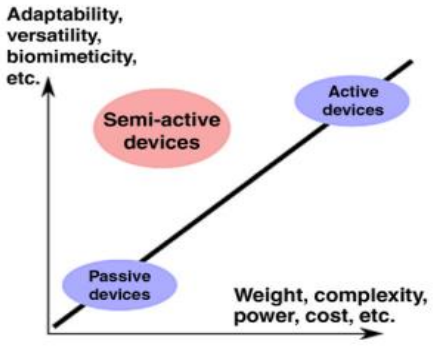

Figure 3: Various considerations in developing passive, active, and semi-active prostheses from Adamczyk[8]

The main aim of the prosthetic design is to allow the users to have a functional gait when interacting with the prosthetic device. Prosthetic devices restore standing, walking, and running locomotion, giving users mobile self-sufficiency instead of using crutches or a wheelchair. Prostheses can be categorized in terms of adaptability into three main groups: passive, semi-active, and active (see figure 3). Passive prostheses which have static mechanical properties are more widely accessible and affordable. On the other side of the adaptability spectrum (see figure 3), active (robotized) prostheses offer users an extensive range of biomimetic functions, including modulation of posture, impedance, and

power. Still, their disadvantages stem from their weight, increased size, expensive, high energy demand, and control complexity[8].

Energy Storage and Return (ESR) prostheses are useful passive prostheses that offer some passive adaptability and returned functionality to persons with transtibial amputations. ESR prostheses absorb mechanical energy using viscoelastic deformation in early-to-mid-stance and return it during mid-to-late stance. In addition, ESR prostheses offer biological ankle-foot functions like impact absorption, gradual center of pressure advancement, and some push-off energy due to viscoelastic recoil[9,10,11]. To assess the usefulness of the ESR prostheses, one proposal[12] created standardized tests to establish essential features to evaluate prosthetic feet for prescription, including pylon, heel, and axis tests. Another report[13] put forward that ankle-foot prostheses can be differentiated by two main factors: normal stiffness (superior-inferior direction to foot) and foot geometry/alignment, which includes ankle angle. Ankle-foot stiffness and foot geometry/alignment are essential for passive prosthesis design as they affect all parts of prosthetic gait. For example, higher foot stiffness is associated with lower push-off work and gait asymmetry during late stance[9,] and an overly long foot is associated with more toe scuffing during the swing phase[14].

In between the adaptability extremes of passive and active prostheses exist the semi-active prostheses. Semi-active prostheses allow some modulation of mechanical properties but cannot supply positive energy during the stance phase. Their mechanical properties[8] range from exploiting the gait cycle by changing swing phase ankle angle where ankle loads are low, combining non-backdrivability and high static forces by benefiting from friction on an inclined plane, and using springs to replace motors by using a spring-loaded ankle mechanism to match ankle angle according to the slope of the ground. Though positive energy is not supplied during stance, these prostheses can allow users more adaptability at a fraction of the cost, weight, and sometimes complexity. Adamczyk[8] proposed essential questions to ask when designing an appropriate prosthetic foot-ankle device to be, “How could a semi-active device accomplish the goal, and how and when should the prosthesis adapt?” To evaluate the prosthesis

performance, they proposed that we ask: “Does it work, does it have the intended effect, and do people like it.”

Three prominent types of semi-active mechanisms are hydraulic devices, adaptable stiffness, and ankle angle control. Hydraulic prostheses use pressurized fluid to dampen joint motion. Several ankle-foot systems[8] use variable hydraulic dampers like Endolite *Elan*[15], Freedom Innovations *Kinnex*[16], and the Ottobock *Meridium*[17]. Adaptable stiffness prostheses like the *Variable Stiffness Foot* and *Variable Stiffness Prosthetic Ankle* change ankle-foot stiffness to affect ankle and knee mechanics. The Ossur *Proprio* foot[18] changes the ankle angle in swing phase under active control[8,18].

To further understand how to create main principles for ankle-foot prosthetic design, we must describe the observable walking mechanics common in walking for persons using transtibial prostheses.

(c) Prosthetic Sagittal Mechanics in walking

Firstly, much of walking mechanics focuses on sagittal kinematics and kinetics as walking moves along the anterior-posterior (sagittal) axis (forward direction of walking). The sagittal plane breaks the body into right and left with its perpendicular axis predominantly describing flexion/extension. Its dimensions are vertical and anterior-posteriorly horizontal. The lower-leg prostheses primarily affect the hip, knee, and ankle joints and their relevant upper-leg, lower-leg, and foot segments. Also, summative mechanics like the center of mass work and acceleration give valuable information for describing the effect of lower leg prosthetics on walking. This section will describe the prosthetic sagittal walking mechanics by starting with the ankle-foot system, then knee mechanics and hip, and ending with the center of mass (COM) summative metrics.

(i) Ankle-foot mechanics

Adamczyk[8] proposed three different concepts of ankle-foot functions: Foot roll-over where the center of pressure (COP) as a function of the lower leg angle can be related with the instantaneous effective radius of the ankle-foot; angular stiffness where ankle moment is related to ankle angle like a lever mounted to a torsional spring; ankle angle control where the neutral ankle angle or set point by

which the spring/shape like behavior is relative to that neutral angle. These ankle-foot concepts are different ways to model ankle-foot behavior.

Raschke et al.[19] found that persons with TTA preferred less stiff feet while walking, associated with 15% lower peak sagittal prosthetic socket moments. Furthermore, Fey[20] offered that decreased foot stiffness leads to increased prosthetic ankle range of motion, mid-stance energy storage, and late stance energy return. Also, Klodd et al.[10] reported that dorsiflexion angle and ankle plantarflexor moments increased with a stiffer forefoot. To further explore the effect of foot stiffness on walking mechanics, Adamczyk et al.[9] examined the hind/forefoot stiffness effects on prosthetic walking for different stiffnesses and walking speeds. In general, they found that a stiffer hindfoot yields decreased prosthesis energy return, larger vertical ground reaction force (GRF) loading rate, larger knee flexion angle (stance phase), and knee extensor moment. They also found that a stiffer forefoot yielded decreased prosthetic ankle and COM push-off work and larger knee extension angle and knee flexor moment in late stance.

Glanzer and Adamczyk[21] created a Variable Stiffness Foot (VSF) as an adaptable stiffness prosthetic foot. It offers a semi-active modulation of its forefoot stiffness during the swing phase. The VSF has a rigid ankle, and its forefoot acts as an overhung beam that can modulate the forefoot stiffness by adjusting a support fulcrum to change the overhang length. They reported that VSF users displayed greater energy storage and return with lower stiffnesses.

As another stiffness-based prosthesis, the Variable Stiffness Prosthetic Ankle (VSPA)[22] utilizes a cam-based transmission to allow selectable nonlinear ankle torque-angle curves and modulate forefoot stiffness through motorized leaf spring configurations. VSPA allows the users to set their ankle and foot stiffnesses according to their preferences and mobility tasks. Gait testing with VSPA resulted in increased peak plantarflexor moment and increased peak dorsiflexion angle with increased stiffness. Quraishi et al.[23] further adapted the VSPA to have decoupled energy storage and return where energy was stored at heel strike and during loading and returned later in the gait cycle. These mechanics can also allow suitable ankle changes for toe clearance and increased push-off power during the swing phase.

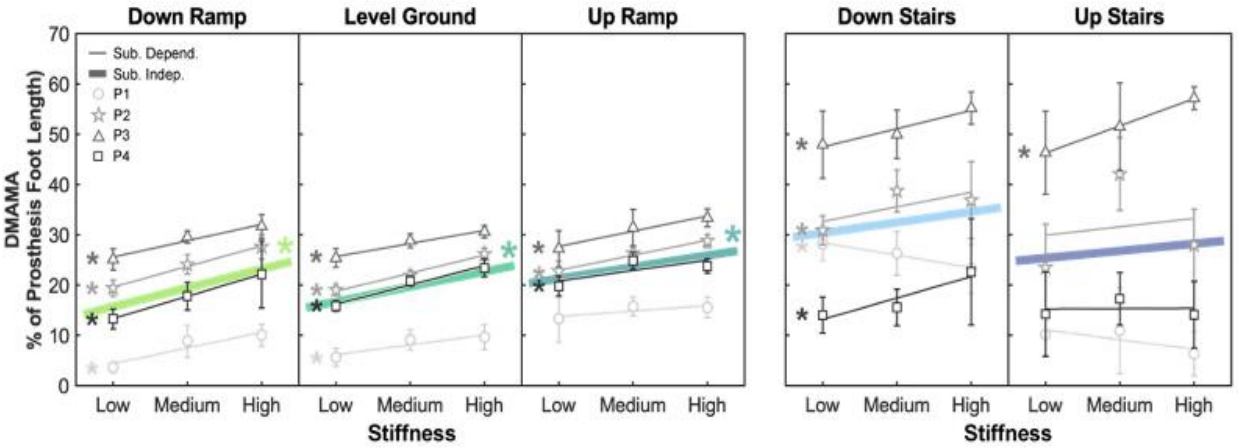

Figure 4: linear mixed model trends showing the relationships of prosthetic forefoot stiffness on DMAMA for various locomotion modes from Leestma et al.[18] The persons with transtibial amputations walked on level ground, up and down ramps, and up and downstairs. Color lines represent the subject-independent linear mixed effect regressions. Gray markers, vertical bars, and lines show each person's average, standard deviation, and subject-specific linear fit. The asterisk (*) represents a significant linear trend (p-value < 0.05).

Effective control of the stiffness modulation in walking and running can be connected to the Dynamic Mean Ankle Moment Arm (DMAMA)[24]. DMAMA represents the ratio of sagittal ankle moment impulse to vertical ground reaction force impulse during the stance phase of gait. Adamczyk[24] results showed that GRFs move closer to the ankle (less forward) with increased walking speed in natural gait. As a follow-up, Leestma et al. [18] analyzed persons with transtibial amputations walking on level ground, ramps, and stairs. They found a positive linear sensitivity of DMAMA (more forefoot dominated) to stiffness and ground incline while walking with the VSF (see figure 4). This metric, DMAMA, could be used as a control loop variable to adapt semi-active prostheses to various locomotion modes like

standing and walking on level, ramps, and stairs. In addition, DMAMA could also evaluate the biomimetic performance of various passive and active prostheses.

Persons with ankle-foot prostheses have poor proprioception in their lower leg due to the transtibial amputation. As they interact with these prostheses, they use their residual limbs to perceive the prosthetic ankle-foot mechanics. Shepherd et al.[26] added that persons with TTA can repeatably select their preferred stiffness within a mean coefficient of variation of 14.2% and could identify a 7.7% change in ankle stiffness with a 75% accuracy. Along with stiffness, individuals also can perceive ankle damping. For example, Azocar et al.[27] reported that persons with amputations could perceive damping changes of at least 12.0% at the ankle and highlighted those persons with amputations could perceive changes of at least 11.6% and 13% for ankle and knee stiffness, respectively.

(ii) Knee and hip mechanics

The prosthetic ankle-foot directly affects a prosthetic user's ability to modulate their ankle torque and angle. These ankle mechanics also influence more proximal joints like the knee and hip. Ankle mechanics have dominant contributions to the center of pressure excursion, push-off power, and energy storage and release. In contrast, knee and hip mechanics heavily contribute to body support during the stance phase and swinging the leg without floor contact during the swing phase. Common knee and hip issues with persons with TTA are hyperextended (locked) knees during stance phase, toe scuffing, and more hip effort during swing phase.

Ingraham et al.[28] proposed that even though excess prosthetic ankle work (more than biological values) has been thought to help reduce hip effort compensations, it may be a diminishing negative return. In the intact leg, the bi-articular (knee and ankle) gastrocnemius muscle help reduce excessive knee extension during stance. However, in a prosthetic foot-ankle that does not have that bi-articular restraint, excessive ankle plantarflexor moment is associated with knee hyperextension[13,21].

Wu et al.[30] explored the determinants of ground foot clearance during leg swing and found that foot movement is not only determined by the separate costs of lifting the foot high (positive foot clearance) or scuffing your foot on the ground (negative foot clearance). They found that the cost for scuffing increased twice as steeply as that for lifting (see figure 5) and indicated that it might also be due to movement variability, which influences the average cost of walking.

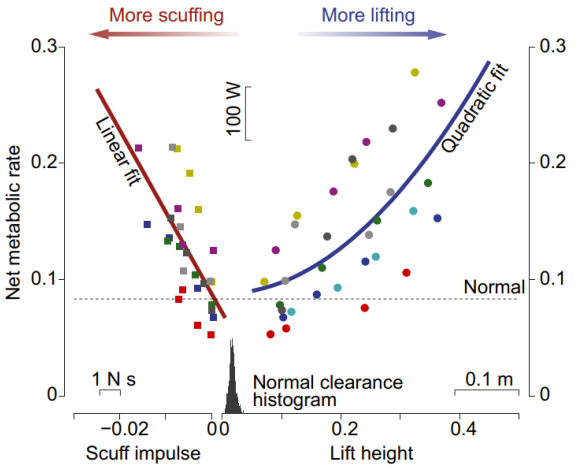

Figure 5: Net metabolic rate as a function of measured scuff impulse and toe lift height from Wu et al.[24] The toe clearance height and scuff impulse were normally distributed, meaning that more of the scuffs had low magnitude scuffs and low lift height.

To investigate energy storage and return in walking, Adamczyk et al.[31] found that push-off impairment and its related compensations are related to some asymmetries in walking for people with unilateral transtibial amputations. Lower prosthetic energy return leads to lower push-off work by the impaired limb, leading to greater energy loss in the intact leg/ground collision. Prosthesis users may compensate by adding positive hip work during the intact leg or prosthetic leg stance phase. That compensation was observed with a semi-active energy-recycling prosthesis, the controlled energy storage, and return (CESR) prosthesis[32]. Segal et al.[33] showed that using CESR with low stiffness increased prosthetic push-off (energy return) and decreased intact limb COM collision work compared to using a conventional foot.

(iii) Whole-body metrics: center of mass

Beyond the prosthetic energy flow, whole body metrics like energy expenditure and center of mass mechanics (COM) also need to be discussed. Zelik and Adamczyk[34] showed a unified effect of ankle energy return that contributes to both leg swing and COM acceleration in able-bodied walking. Zelik et al.[35] found that lower prosthetic foot stiffnesses led to higher energy storage, energy return, and prosthetic limb center of mass (COM) push-off work. Walking energy expenditure in their participants with TTA was lowest for intermediate stiffness. This statement agreed with Klodd et al.'s suggestion[10] that there might be biomechanical disadvantages to the lowest stiffness despite higher energy return. One biomechanical disadvantage involved the "drop-off" effect in late stance, which is reduced ankle plantarflexor moment that allows the COM to "drop off" the end of the foot during load transfer from the prosthetic side to the intact side[10]. The persons with TTA from Zelik et al.[28] showed higher hip work with lower energy transfer from the prosthesis to the COM, which could be attributed to higher energy dissipation at the knee. Spring compliance (inverse of stiffness) influences push-off but has co-occurring biomechanical trade-offs limiting how push-off can benefit the walking economy (lower metabolic cost). Additionally, Clites et al.[36] agreed that subject-preferred stiffness had no correlation with energy expenditure, but it also found that stiffness tended to be lower for self-selected speed.

(iv) Summary

The distinctive features of sagittal prosthetic mechanics include sagittal ankle, knee, and hip angles, work, and moments, push-off energy and energy storage, vertical ground reaction force, DMAMA, and foot clearance.

(d) Prosthetic frontal mechanics in walking

Along with sagittal plane compensations, people with transtibial amputations also have distinctive frontal (coronal) plane issues. The frontal plane divides the body into front and back. Common descriptors of frontal plane motion are inversion/eversion and adduction/abduction. Moments are described as invertor/evertor and adductor/abductor.

(i) Ankle-foot mechanics

Kim et al.[37] performed a test with an ankle-foot prosthesis emulator that modulated inversion/eversion moments using stiffness trajectories and found that positive ankle inversion stiffness could lower the active control requirements compared to zero stiffness conditions in flat ground walking. They alluded to active control being managed by foot placement variability[38], margin of stability[39], and intact limb center of pressure control[40]. Additionally, Velzen et al.[41] found that the systematic effects of prosthetic misalignment were evident in horizontal magnitude and moment arm from the ankle of the frontal ground reaction force (GRF) during late prosthetic stance. They showed that the magnitude of the mediolateral horizontal GRF was significantly less with an internally rotated prosthesis (inward rotation of knee along the tibial long axis), compared to knee adduction (knocked knees) and externally rotation (outward rotation of knee along the tibial's long axis). Also, the moment arm was more lateral when the prosthesis was externally rotated.

van Hal et al.[32] demonstrated that mediolateral balance is dominated by hip frontal moments and that passive mechanical stability is dependent on the curvature of the loaded prosthetic foot. In addition, they investigated the prosthetic roll-over curvatures and found that a limiting factor for applying frontal moments is the lagging (hysteresis) of the center of pressure displacement due to material compliance and slip of the shoe, which suggests that shoe design to prevent these issues is essential to consider.
Segal and Klute[43,44] found that recovery strategies differ minimally between stiff and compliant prosthetic feet. They suggested that prosthetic mediolateral compliance is less necessary, and hip frontal moments during the stance phase may be necessary.

Ramstrand and Nilsson[45] showed no significant difference in stair walking between persons with amputations and non-disabled individuals in foot placement (foot entirely on the stair) and foot clearance. However, for stair ascent and descent, the persons with amputations walked with a slower velocity and cadence, increased stance phase and double support time, and increased their step width compared to the non-disabled individuals.

(ii) Knee/Hip mechanics

Boone et al.[36] investigated the perturbation effects of TTA prosthetic misalignment on the sagittal and frontal (coronal) socket reaction moments. These prostheses had misalignment perturbations of 3 and 6 deg rotation (adduction/abduction) and 5 and 10 mm translations (medial and lateral). Compared to normal alignment, frontal socket moments had the most statistically significant differences at 30% and 75% of the stance phase for all angles and translation perturbations (see figure 6). Royer and Wasilewski[47] demonstrated that persons with unilateral transtibial amputations had 46% and 39% higher peak knee and hip internal abduction moments on the intact side compared to the prosthetic side. The participants also had 17% and 6% higher peak knee and hip external abduction moments on the intact side compared to the prosthetic side. These results suggest higher joint loading on the intact side, which may predispose the participants to premature joint degeneration like knee osteoarthritis.

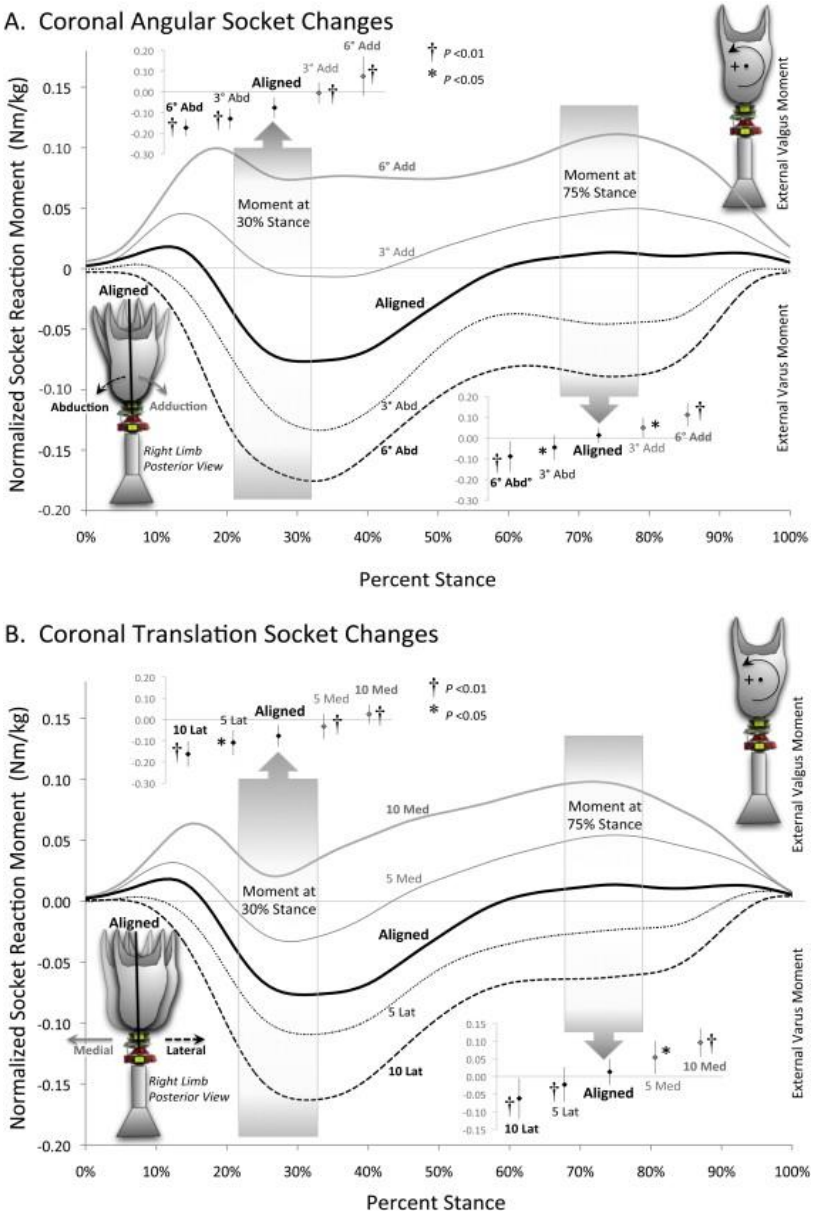

Figure 6: Normalized socket reaction moment in response to frontal (coronal) angular and translational socket changes from Boone et al.[36] The frontal socket reaction moments were shown for angular perturbations (Graph A) and translational perturbations (Graph B).

Morgenroth [48] investigated the potential contributors to knee osteoarthritis in persons with lower-limb amputations (see figure 7). They found a negative correlation of higher prosthetic push-off with lower first peaks of intact knee external adduction moments (KEAM). Jin et el[49] added that higher first peaks of KEAM and higher loading rates were also associated with using higher damped prosthetic feet vs. lower damped ones. When looking at sloped walking, Doyle et al.[50] showed that the first peak of KEAM and the rate at which KEAM increased (KEAM loading) were the only significant results where downhill had the largest KEAM loading compared to flat, uphill, and right and left cross slopes.

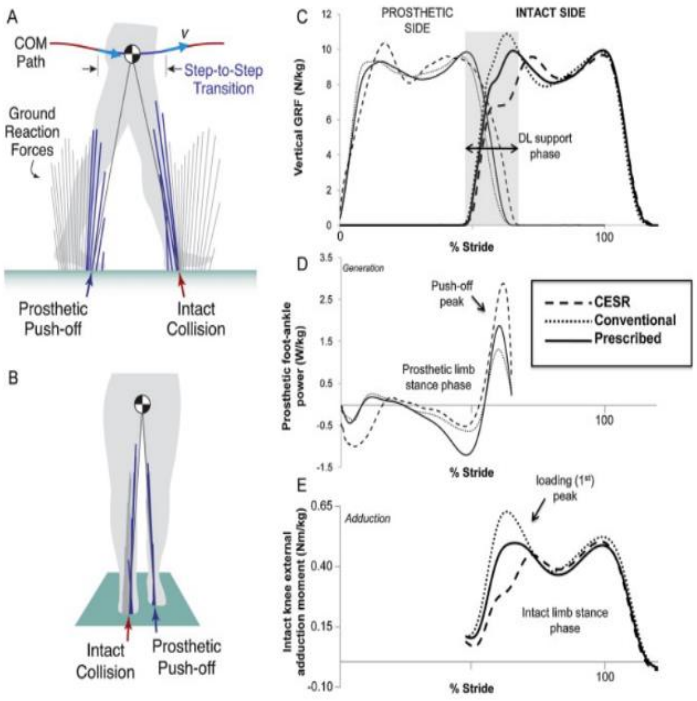

Figure 7: sagittal and frontal representations (A and B) of prosthetic and intact side collision and push-off. Graphs of vertical GRF (C), prosthetic foot-ankle power (D), and intact knee external adduction moment (E) vs. percentage of stride were shown from Morgenroth et al.[41]

Rueda et al.[51–53] showed that participants with TTA walked with less hip abductor and valgus (knee) moments on the prosthetic side compared to the intact side and the non-disabled subjects. They also found that the thorax frontal range of motion increased, indicating mediolateral compensation to accommodate the prosthetic vs. intact frontal moments. Ventura et al.[54] showed that subjects who walked along a circular path primarily relied on larger sagittal hip joint work to turn compared to persons with no amputations who relied on more sagittal ankle work with the residual leg in and outside of the turn. Additionally, Segal et al.[33] found that persons with TTA have decreased prosthetic mediolateral ground reaction impulse and stride length suggesting a more centered COM over the base of support, which may lower the risk of falling.

(iii) Whole-body metrics: center of mass and angular momentum

A useful measure of dynamic walking stability is the margin of stability (MOS), which incorporates the relationship of COM movement and foot placement in the person staying upright while walking[55]. The margin of stability is the mediolateral distance between the edge of a person's base of support and the velocity-adjusted (extrapolated) position of the center of mass at an instant of time. Gates et al.[39] found that persons with TTA who walked on a loose rock surface had larger average minimum margins of stability (min MOS) than their non-disabled participants. In addition, persons with TTA had decreased min MOS on their prosthetic limb compared to the intact limb. Overall, these non-disabled people and persons with TTA had increased step width mean and variability, COM range of motion, and peak COM velocity when walking on a rocky surface. Interestingly, the persons with TTA had higher variability of step width and min MOS, which may indicate that they are making larger step-to-step corrections to achieve the same average result.

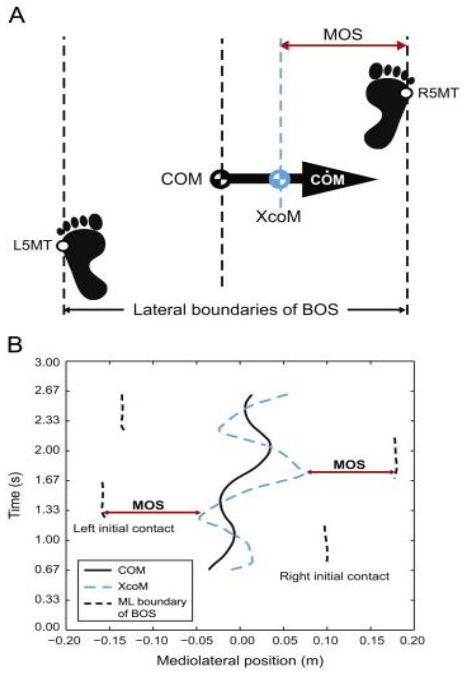

Figure 8: conceptual diagram (A) and numerical graph (B) showing the relationship of the center of mass (COM) mediolateral position, extrapolated COM (xCOM), base of support (BOS), and margin of stability (MOS) from Beltran et al.[46]

Beltran et al.[56] tested persons with TTA and non-disabled individuals on walking trials on the Computer Assisted Rehabilitation eNvironment (CAREN). The conditions involve no perturbations and pseudo-random mediolateral translations of the visual field and platform (see figure 8 for MOS representation). Persons with TTA had a larger mean and variance of the MOS in the platform oscillations compared to the non-disabled walkers, but not the visual oscillations, which the authors attributed was due to people with TTA having a lack of active ankle control and ankle proprioception. [57]

In Miller's Master's thesis[58], they looked at the balance recovery mechanisms of persons with TTA following

mediolateral translational perturbations using a pneumatic device attached to the ankle. They found that participants had decreased range of frontal angular momentum and increased hip joint work for lateral perturbations and decreased hip joint work and increased range of frontal angular momentum for medial perturbations. Shell et al.[59] investigated the mechanical effects of decreased frontal stiffness of the prosthetic ankle with persons with TTA walking on a circular path. When their residual limb was on the inside of a 1m circular turn, the frontal hip work increased, decreased residual and increased intact limb vertical ground reaction impulses, and the frontal range of whole-body angular momentum decreased.

(iv) Summary

The distinctive features of prosthetic frontal mechanics include frontal ankle, knee, and hip moments and work, step width, mediolateral and vertical ground reaction force, margin of stability, and frontal angular momentum.

(e) Lower limb sensor feedback in prosthetic walking

(i) Identifying prosthetic state

There are many ways of identifying the spatiotemporal properties of a person wearing a prosthetic lower limb. Several measurements systems that are utilized contain force or pressure plates, optoelectronic, wearable motion capture devices (inertial measurement units), and smart clothes. In the laboratory, one of the most common methods utilizes the motion capture system with infrared cameras (optoelectronic) and reflective markers, and force plates. This method yields high precision and intra-trial repeatability but lacks portability, and its results are sensitive to setup. A methodology that has become more popular[5,60] and helps determine the human body's kinematics (translational and rotational position, velocity, and acceleration) is the use of Inertial Measurement Units (IMUs). To add further information about the interaction of the prosthetic device with the environment, load cells[5] can be used to identify the kinetic interaction (translational and rotational forces and moments).

(ii) Kinematic and kinetic sensing of gait events

Many currently produced IMUs contain gyroscopes, accelerometers, and magnetometers that measure rotational velocity, translational acceleration, and earth's magnetic North (to help with integration drift). Several IMU-based methods[5] have been used to identify gait events like heel contact and toe-off with IMUs attached to the foot, pelvis, or shank. When combined with portable force sensors like load cell or foot pressure soles, the gait detection algorithms[5] improved the robustness of identifying transitions between gait events (stance to swing) and sub-phase events of stance and swing.

Washabaugh et al.[61] showed that IMUs had moderate to high validity of spatiotemporal gait parameters in healthy young adults among multiple days of walking speeds and were repeatable on treadmill and overground walking. In addition, they found that motion reconstruction, which depended on foot IMUs, gave better gait parameters than placing the IMU at the ankle.

Li et al.[62] developed and tested a walking speed estimator that used a shank-mounted IMU (gyroscope and accelerometer) with relatively high accuracy (under 5% error) for various treadmill speeds and slopes. The estimator was statically calibrated to determine the gravity axis and modeled the shank's movement like an inverted pendulum. This model sets the horizontal velocity of the IMU to zero when the shank is vertical (around mid-stance).

Rebula et al.[63] demonstrated that a foot-mounted IMU could be used to estimate mean stride lengths and duration within 1% of motion capture. They displayed the success of motion reconstruction using the zero-velocity property when the foot is flat on the ground (referred to as a zero-velocity update). Also, they offered the algorithm steps for motion reconstruction of step segmentation, rotational orientation estimation, translational velocity estimation, and trajectory formation (see figure 9 on the following page). Kitagawa et al.[64] added foot clearance calculations as an output to the previous motion

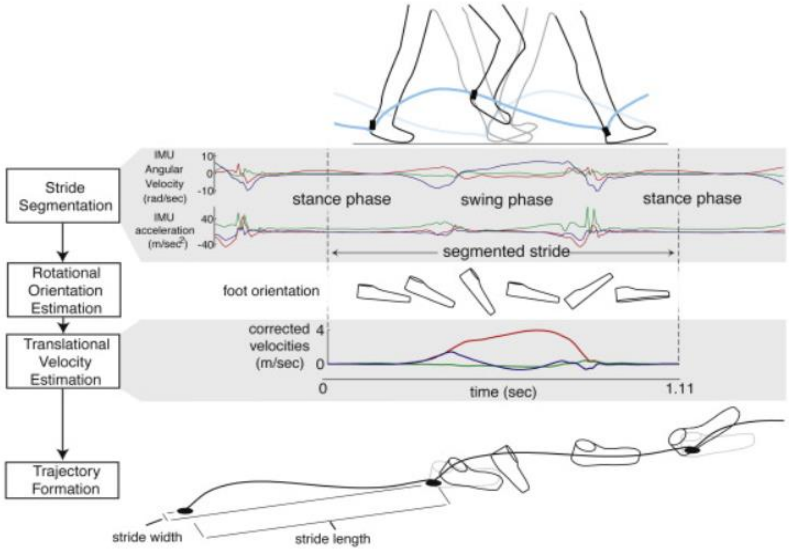

Figure 9: Motion reconstruction steps with representative data trajectories from Rebula et al.[57]

reconstruction method. They used a foot IMU with an adjusted zero vertical displacement assumption across multiple strides. They found that mean accuracy and precision for foot clearance were 2±7 mm. Previous researchers[64,65] have defined foot clearance during the swing phase as the vertical displacement of the foot IMU from the floor. The minimum foot clearance (MTC) is associated with tripping and falling if the value is too low[30].

(iii) Locomotion modes

Previous work[66] has shown the validity of locomotion mode classification in transtibial prostheses discerning between level-ground walking, stair ascending, stair descending, ramp ascending, and ramp descending. They used two IMUs (shank and foot), where the studies had more than a 95% recognition accuracy for each locomotion mode. Sup et al.[67] showed that two slope angles (5 and 10 degrees) were detected and estimated in knee/ankle prosthetic walking. They used a three-axis accelerometer attached axially along the prosthetic shank and two load cells (one under heel and another under ball of foot) to detect when the prosthetic foot is parallel with the ground.

(iv) Feedback in lower limb prosthetic walking

Feedback in prosthetic gait is essential to help the users achieve functional gait. Ankle-foot stiffness and ankle angle have commonly been used as the feedback variable to adjust gait mechanics. Clites et al.[36] found that participants with transtibial amputations preferred lower ankle stiffness at self-selected treadmill walking speeds and the same/higher stiffness for faster self-selected overground

walking. These preferred stiffnesses were associated with kinematic symmetry between prosthetic and intact joints but not with body mass or metabolic rate.

Best et al.[68] presented a phase variable controller for a powered knee-ankle prosthesis that adjusted knee and ankle mechanics depending on various speeds and inclines. They developed a task estimator with a joint position controller, and it identifies steady gait, speed estimation, incline estimation. Their closed-loop controller contained a knee and ankle actuator, one IMU on the thigh, and a load cell at the ankle. It was robust to discontinuous task changes and converged in less than five steps to the specified target.

(v) Summary

The key uses of lower limb sensor feedback in prosthetic walking include: using inertial measurement units and load cells to detect prosthetic state; estimating gait events like heel strike, toe-off, and leg swing; reconstructing prosthetic movement, ground reaction forces, and joint moments; classifying if the gait is over flat or sloped ground; and finally using the prosthetic sensor feedback to adjust ankle-foot stiffness and angle.

(f) Gaps and research opportunities

Persons with unilateral transtibial amputations need appropriate ankle-foot prostheses for walking. They have typical gait deviations and compensations of hip circumduction, toe scuffing, weak prosthetic side push-off, hyperextension on the prosthetic side, higher intact side collision work, and knee osteoarthritis on the intact side. A passive prosthetic ankle-foot device replaces some of the functionalities of the biological structures of the ankle-foot system. Semi-active prostheses attempt to recover more of the biological ankle mechanics. This dissertation will focus on designing and testing two semi-active prosthetic properties of stiffness and ankle angle control: Variable Stiffness Foot (VSF) and Two-Axis aDaptable Ankle (TADA). These semi-active prostheses will be built to sense ankle angle, foot motion, and ankle moments using intrinsic position sensors, an IMU, and a load cell. Though these prosthetic sensors are limited to detecting ankle kinematics and kinetics, data will also be collected for the knee, hip,

and summative mechanics to observe the effects of the ankle-foot prosthetics on the prosthetic user. The main objective of this dissertation is to create semi-active ankle-foot prostheses based on stiffness and ankle angle control properties. It will also characterize their effectiveness using ankle, knee, hip angles and moments, pylon moments and impulses, ground reaction force, and center of mass movements.

(g) Research Questions for this Dissertation

The main research questions for this dissertation are as follows:

1. What are the biomechanical effects of modulating forefoot stiffness on knee and ankle mechanics on persons with transtibial amputations walking with the Variable Stiffness Foot?
2. How to implement a real-time motor control for the new Two Axis aDaptable Ankle using a Raspberry Pi, ROS, and CANopen over EtherCAT?
3. What is the Influence of Prosthetic ankle-angle and walking speed on Pylon moments of the Two Axis aDaptable Ankle?

Chapter 2. Sensitivity Analysis of Variable Stiffness Foot

(a) Introduction

The objective of the past work was to identify the significant sagittal joint mechanics that are affected by changes in forefoot stiffness using the Variable Stiffness Foot (VSF) in flat overground walking with human participants with transtibial amputation. The VSF[21] is a prosthetic foot that allows real-time modulation of forefoot stiffness during the swing phase of walking. This objective focused on exploring moments, and powers, vertical ground reaction forces, and energy and power flow through the prosthesis)[69]. Forefoot stiffness is one of the main variables that allows prosthetic users the ability to adapt their gait. Adaptable stiffness of a prosthetic ankle-foot is important as many commercially available passive prostheses are constant-stiffness devices, so a user with an adaptable stiffness prosthesis replaces the functionality of multiple commercial prostheses that each have one stiffness option.

(b) Variable Stiffness Foot (VSF) Description

The Variable Stiffness Foot (VSF)[21] offers a semi-active foot prosthesis that modulates forefoot stiffness during the swing phase. The VSF has a rigid ankle, and its forefoot acts as an overhung beam that can modulate the forefoot stiffness by adjusting a support fulcrum to change the overhang length. The VSF is a semi-active device where power is not supplied to move the body while the foot is on the ground. Instead, it supplies minimal power when the foot is in the air moving the fulcrum while the motor load is low. The fulcrum position is changed with a motor, belt, and pulley system and is positionally tracked using a potentiometer. This semi-active nature allows the VSF to be lightweight and low power compared to active prostheses, where power is supplied during foot/ground interaction. The VSF's motor commands and data collection are managed using a microcontroller with embedded software programming in the C language. The microcontroller also has an embedded inertial measurement unit (IMU) to track the foot's trajectory in real-time.

(c) Sensitivity of Joint Mechanics to Various Forefoot Stiffnesses of the Variable Stiffness Foot (VSF) in level-ground walking

Published in Journal of Biomechanics (manuscript below is the published material)[70]

Abstract

This paper presents the effects of the Variable Stiffness Foot (VSF) on lower-limb joint mechanics in level-ground walking. Persons with transtibial amputations use lower-limb prostheses to restore level-ground walking, and foot stiffness and geometry have been shown to be the main factors for evaluating foot prostheses. Previous studies have validated the semi-active and stiffness modulation capabilities of the VSF. The core aim of this study is to investigate the mechanical effects of adjusting stiffness on knee and ankle mechanics for prosthetic users wearing the VSF. For this study, seven human participants walked with three different stiffnesses (compliant, medium, stiff) of the VSF across two force plates in a motion capture lab. Linear mixed models were utilized to estimate the significance and coefficients of determinations for the regression of stiffness on several biomechanical metrics. A stiffer VSF led to decreased ankle dorsiflexion angle ($p < 0.0001$, $r^2 = 0.90$), increased ankle plantarflexor moment ($p = 0.016$, $r^2 = 0.40$), increased knee extension ($p = 0.021$, $r^2 = 0.37$), increased knee flexor moment ($p = 0.0007$, $r^2 = 0.63$), and decreased magnitudes of prosthetic energy storage ($p < 0.0001$, $r^2 = 0.90$), energy return ($p = 0.0003$, $r^2 = 0.67$), and power ($p < 0.0001$, $r^2 = 0.74$). These results imply lower ankle, knee, and hip moments, and more ankle angle range of motion using a less stiff VSF, which may be advantageous to persons walking with lower-limb prostheses. Responsive modulation of the VSF stiffness, according to these findings, could help overcome gait deviations associated with different slopes, terrain characteristics, or footwear.

Introduction

The primary function of lower-limb prostheses for persons with amputations is to restore overground walking. Still, these prosthetic devices are also necessary for standing and walking on stairs, ramps, and uneven terrain. In particular, transtibial prostheses attempt to return walking functionality by mimicking some aspects of the lost human ankle-foot mechanics. These lost mechanics include altered

ankle push-off energy and power, and ankle angle motion (Adamczyk et al., 2017; Adamczyk and Kuo, 2015; Fey, 2011). This attempt to restore walking for prosthetic users is difficult as the influence of prosthetic parameters like stiffness and geometry on ankle and knee mechanics is not fully understood, and is variable across terrains and locomotor behaviors. The difficulty in universally recreating the human ankle function in terms of ankle-foot geometry and ankle angle and torque relations instigates a need for improved mechanical adaptability of the prostheses (Adamczyk et al., 2017).

Energy Storage and Return (ESR) prostheses are the standard solutions to offer some passive adaptability and returned functionality to prosthetic users. ESR prostheses absorb mechanical energy using viscoelastic deformation as they are loaded and return that energy when unloaded during push-off. To assess the usefulness of the ESR prostheses, one proposal[12] created standardized tests to establish essential features to evaluate prosthetic feet for prescription. Another report (Major et al., 2011) put forward that transtibial prostheses can be differentiated by three main factors: normal stiffness (superior-inferior direction to foot) and foot geometry, and to a lesser extent, shear stiffness. (Raschke et al., 2015) found that persons with amputations preferred less stiff (normal stiffness) feet while walking, which was associated with 15% lower peak sagittal prosthetic socket moments. Furthermore, (Fey et al., 2011) found that decreased foot stiffness leads to an increased prosthetic range of motion (ankle), mid-stance energy storage, and late stance energy return. These factors of prosthetic socket moments, ankle angle range, and energy storage and return are affected by changes in foot stiffness, and are important when considering the adaptability of ESR prostheses.

To further explore the effect of foot stiffness on walking mechanics, (Adamczyk et al., 2017) examined the hind/forefoot stiffness effects on prosthetic walking for various stiffnesses and walking speeds. They found that increasing hindfoot stiffness yields decreased prosthesis energy return and increased ground reaction force (GRF) loading rate, knee flexion angle (stance phase), and knee extensor moment. Moreover, they found that increasing forefoot stiffness yields decreased prosthetic ankle and center of mass push-off work, and larger knee extension angle and knee flexor moment in late stance.

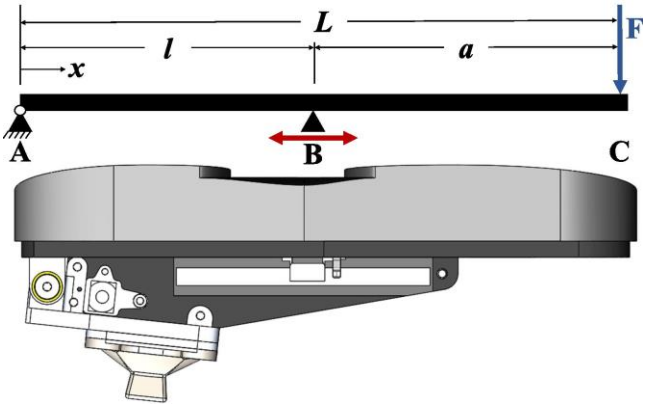

Fig. 10. Side drawing of the Variable Stiffness Foot (VSF) highlighting the cantilever mechanics from Glanzer and Adamczyk, 2018. The ground reaction force on the foot acts at "F," the beam is supported at "B," and pinned at "A" © 2018

Also, (Klodd et al., 2010) reported that dorsiflexion angle and ankle plantarflexor moments increased with a stiffer forefoot.

To alter ankle and knee mechanics, the Variable Stiffness Foot (VSF) offers a semi-active foot prosthesis that can modulate its forefoot stiffness during the swing phase. The VSF (Glanzer and Adamczyk, 2018) has a rigid ankle, and its forefoot acts as an overhung beam that can modulate the forefoot stiffness by adjusting a support fulcrum to change the overhang length (parameter a in Fig. 10). The VSF is a semi-active device where power is not supplied to move the body while the foot is on the ground, but minimal power is supplied when the foot is in the air to move the fulcrum, while the motor load is low. This semi-active nature allows the VSF to be lightweight and low power compared to active prostheses, where power is supplied during foot/ground interaction. (Glanzer and Adamczyk, 2018) reported that VSF users displayed greater energy storage and return with lower stiffnesses.

The VSF offers the ability to change forefoot stiffness during movement, so the mechanical effects of the stiffness change and its benefits to different tasks need to be experimentally determined. This study focuses on characterizing the kinetic and kinematic response of participants with transtibial amputation in level-ground walking using the VSF at three different stiffnesses. Based on the findings from fixed component stiffness changes (Adamczyk et al., 2017), we hypothesize that increasing forefoot stiffness will lead to kinematic changes, including decreasing ankle dorsiflexion and increasing stance-phase knee extension angles; joint moment changes, including increasing plantarflexor moment and knee flexor moment; changes in energy and power, including decreasing prosthetic energy storage, energy return, and peak power output; and GRF changes, including increasing second peak of vertical ground reaction force and increasing off-loading rate.

Subject	Age (years)	Sex	Amputated side	Number of years post-amputation (years)	Body mass (kg)	Body height (m)	Leg length(m)	Walking speed (m/s)
1	70	M	L	14	83.8	1.8	0.978	1.24
2	61	F	R	8	63.8	1.63	0.874	1.22
3	34	M	R	15	77.3	1.81	0.942	1.25
4	46	M	R	5	104	1.9	1.06	1.42
5	51	M	R	8	111	1.75	0.95	1.18
6	44	M	L	19	75	1.72	0.93	0.679
7	56	M	R	3	105	1.83	0.96	0.653
Average	51.7	-	-	10.3	88.6	1.78	0.956	1.09
Standard deviation	11.9	-	-	5.82	18.1	0.087	0.056	0.301

Table 1. Subject characteristics with mean and standard deviations of age, sex, amputated side, number of years post-amputation, body mass, body height, leg length, and walking speeds for seven subjects.

Methods

Seven participants (characteristics shown in Table 1) with unilateral transtibial amputation were included in this study after giving written informed consent according to procedures approved by the University of Wisconsin-Madison Health Sciences Institutional Review Board (protocol #2017-0678). Participants were included under the criteria: having a unilateral transtibial amputation with stable socket fit, being at least six months post-surgery, being able to comfortably walk a minimum of 30 minutes without aid, and being able to walk comfortably on level ground, stairs, and ramps. Exclusion criteria included the presence of neuromuscular disorders, sores or current injuries, or surgery within the past six months. The VSF was fitted onto the participants and aligned in its Medium stiffness setting (see settings below) by a certified prosthetist. Subjects were given a short (ten-minute) acclimation period in which they walked freely about the laboratory space.

The participants performed three over-ground walking trials for each of the three different VSF stiffness settings. Compliant, Medium, Stiff settings ranged from 13 to 32 N/mm. Body mass was used for scaling the Compliant stiffness to ensure that the minimum stiffness prevented the prosthetic keel from contacting the internal safety limit. The Compliant condition had an estimated mean and standard

deviation of 15.4±1.53 N/mm. The Stiff condition was set to be 32 N/mm, and the Medium condition (23.8±0.74 N/mm) was set as the halfway point of the Compliant and Stiff conditions. Body kinematics were recorded using optical motion capture (twelve Optitrack Prime 13 cameras, Natural-Point, Inc., Corvallis, OR, USA). Marker clusters were placed on each segment of both lower limbs (thighs, shanks, and feet), with additional markers placed on anatomical landmarks (medial and lateral malleoli on the intact ankle, medial and lateral epicondyles bilaterally, bony prominences of the pelvis), and several locations on the VSF prosthesis. Three markers were placed on the pylon/VSF rigid frame, and three more each on the heel and toe areas (center, lateral, and medial). Minor adjustments were made to accommodate differences in individuals' prosthesis componentry. Ground reaction forces were collected using two force plates (Bertec, Inc., Columbus, OH, USA). Motion capture and force plate data were recorded at 200 and 1000 Hz, respectively. All signals were resampled and scaled to 0 to 100% stance phase, approximately 0 to 60% stride cycle.

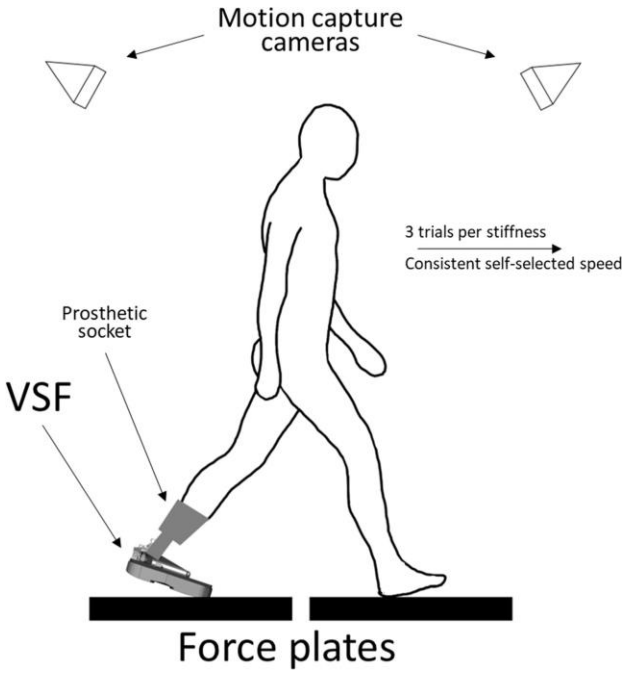

Fig. 11. Side facing diagram showing a person with a transtibial amputation walking with the Variable Stiffness Foot (VSF) across two force plates in a motion capture lab. They walked at a consistent speed for 3 trials per stiffness (total of 9 trials).

Walking speed was tracked as subjects walked across the force plates using the pelvis segment from motion capture (Fig. 11). At the beginning of the trials, a comfortable target walking speed was selected for each subject (see Table 1), and subjects were asked to maintain that speed consistently. Trials were rejected if the speed exceeded the bounds ± 0.12 m/s or the feet were not cleanly on force plates. Attempts continued until three successful trials were recorded in each condition. Testing was repeated similarly for the other conditions in randomized order, with five minutes between to rest and then to acclimate to each

stiffness setting by walking in the laboratory area. Stiffness settings were concealed from the participant and prosthetist by referring to them only by randomized condition numbers, although subjects could likely perceive the stiffness changes during use.

Standard lower-body joint kinematics and inverse dynamics were computed using a lower-body model in Visual 3D (C-Motion, Inc., Germantown, MD, USA). Functional joint centers for the hips and knees were calculated using the Gillette algorithm (Schwartz and Rozumalski, 2005) to establish the rotation axes. The point along that axis representing the knee joint center was determined as a projection from the midpoint of the medial and lateral epicondyles. An estimated anatomical joint center was used for the intact ankle (midpoint between malleoli). A chosen geometric location was used to specify the VSF ankle joint on the prosthetic side (0.1 m above the floor and 0.05 m anterior to the heel marker). This geometric definition of the VSF ankle was arbitrary because it lacks a true joint rotation axis; it was chosen as a systematic way to define the prosthetic ankle joint for all subjects. Leg length was measured from the floor to the greater trochanter. The segments' masses were estimated from body mass according to standard anthropometric tables within Visual3D; prosthetic leg mass was not changed from this anthropomorphic assumption. All body segments were modeled as 6-degree-of-freedom rigid bodies (Cappello et al., 1997).

Motion and force data were low-pass filtered using 4th order, bidirectional Butterworth filters with 10 and 25 Hz cutoffs, respectively. Lower-limb joint angles, moments and powers were estimated from standard inverse dynamics calculations. The prosthesis's power and energy absorption and return were calculated using the unified deformable segment model (UD power) (Takahashi et al., 2012) to avoid reliance on the precise ankle joint definition. Energy storage and return in the keel were calculated as the negative and positive parts of the time integral of UD power, excluding initial heel contact (the first 20% of the stride) to capture only the forefoot contribution. Energy was separated into storage (negative) and return (positive; also known as push-off) regions to investigate these separate consequences of forefoot stiffness modulation.

The results were sorted, processed, and graphed using MATLAB (The Mathworks, Natick, MA USA) in the form of hip, knee, and ankle angles, moments, and powers (Adamczyk et al., 2017). Peak values on the prosthetic side were recorded for the following variables: ankle dorsiflexion angle, ankle plantarflexion moment, midstance knee extension angle, midstance knee flexor moment, UD Power, the second peak of vertical Ground Reaction Force (vGRF), prosthetic energy storage, prosthetic energy return, and vGRF off-loading rate (slope of vGRF vs. time between the time-point of 250 N to the 0 N time-point (Adamczyk et al., 2017)). The "midstance" peaks were chosen between 30% and 55% of the stride cycle. Each metric was averaged across all trials for each stiffness setting to give one mean value per stiffness for each subject.

Linear mixed-effects (LME) models (Leestma et al., 2021) were used to estimate the sensitivity of these prosthetic-side metrics to stiffness settings, their significance (p-value), and the coefficients of determination (r^2) of their regressions. To investigate the participant-independent effects of the stiffness changes on joint mechanics, the LME model treated the stiffnesses as the fixed effects. The differing offset across participants was modeled as a random effect. Coefficients of determination were adjusted to account only for the explanatory value of the linear term and not the individualized offsets (random participant effects). All outcome measures were redimensionalized (Adamczyk et al., 2017) using an average subject's body mass ($M = 88.6\ kg$), standing leg length ($L = 0.956\ m$, greater trochanter to floor), and gravitational acceleration (g, 9.807 m/s/s). We used Mg for forces, MgL for work and moment, $Mg\sqrt{gL}$ for power, and $Mg\sqrt{\frac{g}{L}}$ for force rate of change.

Results

Representative joint mechanics data are shown in Fig. 12, and comprehensive statistical results of the LME regression are shown in Table 2 and Fig. 13.

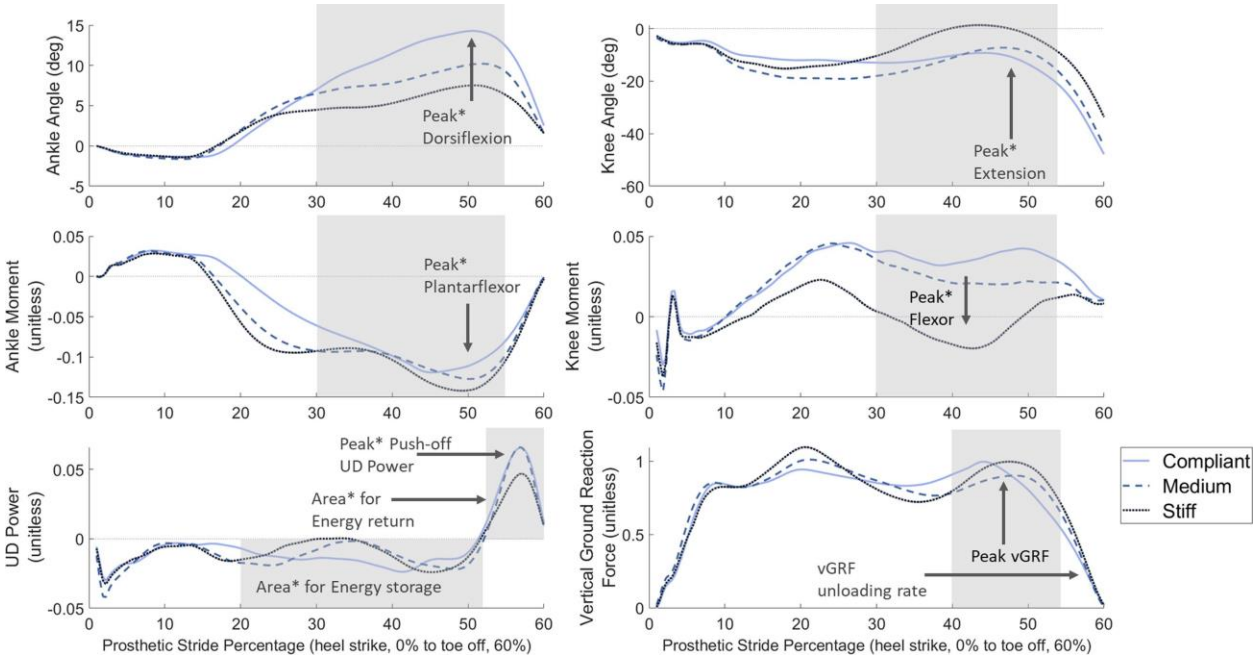

Fig. 12. Prosthetic-side joint mechanics for a representative subject walking with the Variable Stiffness Foot (VSF). First row is prosthetic angles for ankle and knee; second row is the prosthetic moments for the ankle and knee; the third row is the Unified Deformable-body (UD) push-off power and vertical ground reaction force for the prosthetic side. Mean curves across trials for each stiffness condition are plotted, and data is shown for the prosthetic stance phase from heel strike to toe-off. Grey rectangles represent the region of concern for each variable where the peaks or areas are considered. Asterisks (*) were included after the words, "area" and "peak" to highlight the variables which had statistical significance with changes in stiffness.

A software fix was implemented to synchronize the data for three subjects due to an unexpected sampling rate change in the instrumentation, where the motion capture and force plate lost synchronization. Based on observed toe-off events from the other subjects, the first vertical ground reaction force frame before toe-off with a magnitude below 10N was synced with the maximum inferior displacement of the toe marker relative to the foot reference frame, which occurred due to recoil of the elastic keel just as the foot left the ground.

Some trials were rejected during post-processing due to participants' incomplete contact with force plates, missing markers, and faults in the VSF (Subject 6). Subjects 2 – 4 and 6 were missing a trial at the highest stiffness, Subject 6 was missing a trial at the lowest stiffness, and Subject 4 did not

complete testing for the lowest stiffness. In total, 55 of the original 63 trials were kept for statistical analyses.

Prosthetic Side		Non-dimensionlized										Redimensionlized							
	Peak	Comp. Mean	Comp. SD	Med. Mean	Med. SD	Stiff Mean	Stiff SD	Slope	Intercept	Adjusted r^2	p-val of slope	Units	Comp. Mean	Comp. SD	Med. Mean	Med. SD	Stiff Mean	Stiff SD	Slope	Intercept
Ankle	Angle (dorsiflexion +)	9.41	2.35	7.8	2.04	5.46	1.9	-2.2	12.1	0.899	**<0.0001**	Deg	9.41	2.35	7.8	2.04	5.46	1.9	-2.2	12.1
	Moment (dorsiflexor +)	-0.148	0.0218	-0.148	0.0229	-0.154	0.0224	-0.00582	-0.136	0.396	**0.016**	Nm	-123	18.1	-123	19	-128	18.6	-4.84	-113
Knee	Angle (extension +)	-5.19	4.76	-3.7	6.28	-1.82	6.72	1.95	-7.63	0.372	**0.0205**	Deg	-5.19	4.76	-3.7	6.28	-1.82	6.72	1.95	-7.63
	Moment (extensor +)	0.00079	0.0176	-0.00806	0.0199	-0.0199	0.0235	-0.0114	0.0144	0.632	**0.0007**	Nm	0.653	14.6	-6.69	16.6	-16.5	19.5	-9.45	12
GRF	Vertical 2nd peak	0.959	0.0263	0.935	0.0667	0.959	0.0832	0.0124	0.918	0.12	0.225	N	833	22.8	812	57.9	833	72.3	10.8	797
	Vertical Off-loading Rate	-7.46	2.82	-8.02	2.73	-8.4	3.21	-0.33	-7.39	0.227	0.0848	N/s	-20800	7850	-22300	7590	-23400	8930	-918	-20600
UD	Energy Storage	-0.0133	0.00387	-0.00937	0.0043	-0.00671	0.0031	0.0029	-0.0153	0.903	**<0.0001**	J	-36.9	3.21	-7.78	3.53	-5.57	2.56	2.4	-12.7
	Energy Return	0.0174	0.0055	0.0177	0.0059	0.0142	0.0055	-0.00232	0.0216	0.672	**0.0003**	J	48.3	4.57	14.7	4.93	11.8	4.54	-1.93	17.9
	Push-off Power	0.0559	0.0203	0.0568	0.0259	0.0453	0.0245	-0.00921	0.0736	0.739	**<0.0001**	W	156	56.5	158	72.1	126	68.2	-25.6	205

Table 2. Assessed biomechanical metrics with their associated means for each stiffness (Compliant, Medium, Stiff), slope of the Linear Mixed Effects regression against stiffness (the slope indicates the change in the relevant quantity per level of stiffness), mean intercept across subjects, adjusted r^2, and p-value. GRF represents Ground Reaction Force, SD represents Standard deviation, and UD represents Unified Deformable-body. Results are presented in dimensionless form and redimensionalized according to average subject characteristics.

Joint Angle: Results showed that during late stance, the peak dorsiflexion angle significantly decreased with increasing stiffness (p<0.0001, r^2=0.90). During mid-stance, the peak knee extension angle significantly increased (less negative) with increasing stiffness (p=0.021, r^2=0.37).

Joint Moment: Results showed that during late stance, the peak plantarflexor ankle moment increased in magnitude (more negative) with increased stiffness (p=0.016, r^2=0.40). Likewise, peak knee flexor moment during midstance increased in magnitude (more negative) with increasing stiffness (p=0.0007, r^2=0.63).

Prosthesis energy storage, energy return, and power flow: Results showed significantly decreased magnitudes of energy storage (p<0.0001, r^2=0.90), energy return (p=0.0003, r^2=0.67), and peak UD power (p<0.0001, r^2=0.74) with increasing stiffness.

Ground reaction forces: Results showed no significant dependence on stiffness for the 2nd peak of vGRF (p=0.23, r^2=0.12) and the off-loading rate of the prosthetic foot (p=0.085, r^2=0.23).

Hip mechanics: Additional to the hypotheses, prosthetic-side hip mechanics were also calculated to observe the effect of VSF forefoot stiffness. With increasing VSF stiffness, there was a trend toward

increasing peak magnitude of hip flexor moment (p=0.045, r^2=0.30). There were no significant trends for early-stance hip flexion angle, late-stance hip extension angle, late-stance hip power, and net stance-phase hip work.

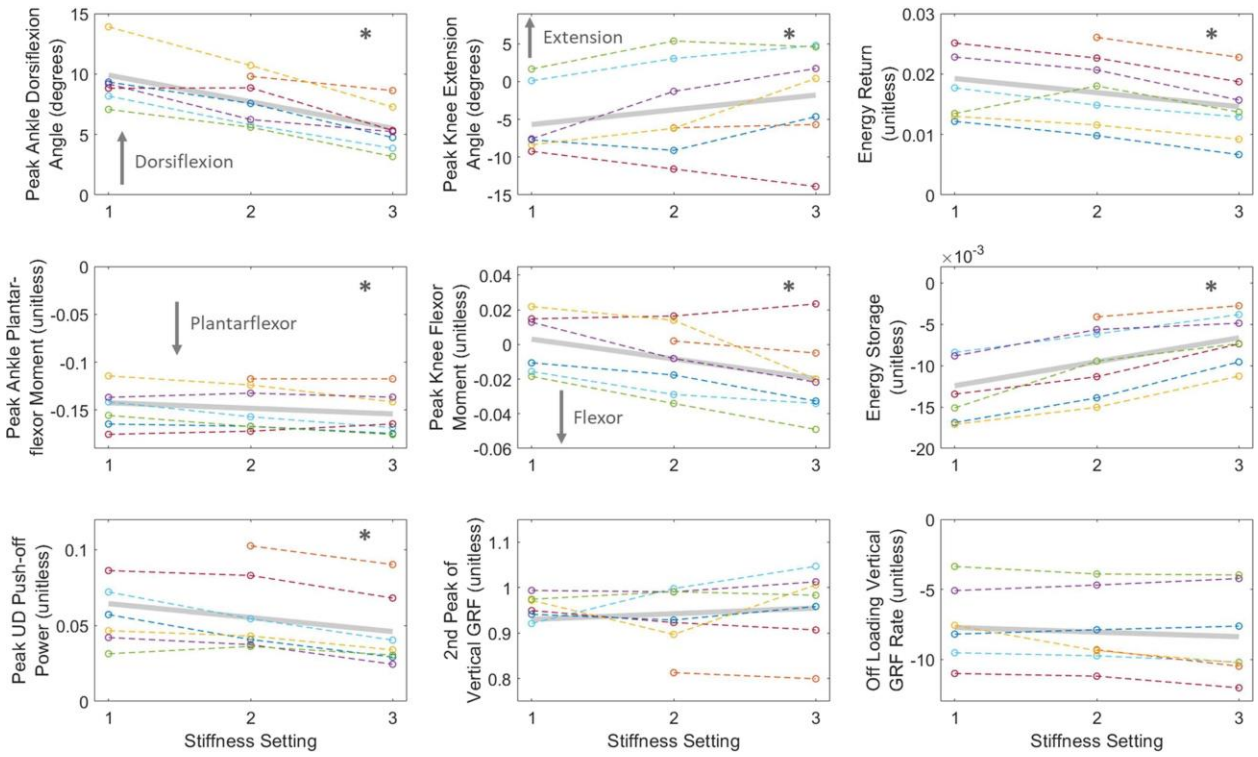

Fig. 13. Linear mixed-effect regressions for ankle and knee angles and moments, Unified Deformable-body (UD) power, prosthesis energy storage and energy return, vertical Ground Reaction Force (vGRF), and vGRF offloading rate for the non-dimensionalized data, with respect to stiffness settings. Stiffness settings 1, 2, 3 relate to Compliant, Medium, and Stiff stiffnesses, respectively. The grey bar represents the linear mixed effects fit of all subjects. One subject did not have data for the lowest stiffness setting. Asterisks (*) were included in the top right area for the variables which had statistical significance with changes in stiffness.

Discussion

The main purpose of this study is to examine the influence of modulating forefoot stiffness on knee and ankle mechanics for prosthetic users wearing the Variable Stiffness Foot (VSF). Results (Fig. 13) showed that increased VSF stiffness led to decreased peak ankle dorsiflexion angle, increased peak plantarflexor moment, increased peak flexor knee moment, increased peak knee extension angle, decreased magnitudes of energy storage, energy return, and peak UD power. These results supported most of our hypotheses. These results imply lower ankle, knee, and hip moments and more ankle angle range of motion using a less stiff VSF. According to these findings, responsive modulation of VSF stiffness could

help overcome gait deviations associated with different slopes (e.g. knee hyperextension on uphills or instability on downhills), terrain characteristics (e.g. soft ground), or footwear. In addition, persons with transtibial amputations tend to have problems with knee hyperextension (Adamczyk and Kuo, 2015), so a less stiff VSF can help reduce knee extension.

Previous stud[9] (Adamczyk et al., 2017; Raschke et al., 2015) proposed that active people with transtibial amputations tend to prefer soft (less stiff) prostheses due to the dominance of kinetics over kinematics in ESR interactions, compared to stiffer settings of an adjustable stiffness prosthetic foot (Adamczyk et al., 2017) and other commercial prostheses (Raschke et al., 2015). Also, softer forefoot associated with higher energy return could help with ground clearance due to increased leg swing acceleration (Darter and Wilken, 2014; Wu and Kuo, 2016; Zelik and Adamczyk, 2016).

In the ESR prosthetic literature, three (Glanzer and Adamczyk, 2018; Lecomte et al., 2021; Shepherd and Rouse, 2017) semi-active devices specialize in giving prosthetic users the customizability to change the ankle and forefoot stiffness: Variable Stiffness Prosthetic Ankle (VSPA), Variable Stiffness Ankle (VSA), and Variable Stiffness Foot (VSF). VSPA (Clites et al., 2020; Shepherd and Rouse, 2017) utilizes a cam-based transmission to allow selectable nonlinear ankle torque-angle curves to mimic intact gait and modulate forefoot stiffness through motorized leaf spring configurations. Similarly, the VSA (Lecomte et al., 2021) used a variable leaf-spring design within an ankle module atop a standard flexible prosthesis. Gait testing with both VSPA (Shepherd and Rouse, 2017) and VSA (Ármannsdóttir et al., 2021) demonstrated decreased peak dorsiflexion angles, and the VSPA showed increased peak plantarflexor moment with increased stiffness. Together with the present study and prior studies of fixed-component stiffness changes (Adamczyk et al., 2017), this evidence builds up the mechanistic understanding of how parametric changes in prosthesis properties affect typical walking.

Another important consideration is the VSF's potential contribution to the musculoskeletal health of its users. The higher push-off work of the lower VSF stiffnesses could contribute to lower first peaks of intact-side knee external adductor moment, potentially leading to a reduced risk of knee osteoarthritis

(Baliunas et al., 2002; Morgenroth et al., 2011), which is a major issue for persons with unilateral amputation (Struyf et al., 2009). Prosthesis users also face difficulties with gait symmetry (Dingwell et al., 1996). Asymmetric gait for persons with unilateral amputation may be unavoidable because passive prostheses cannot completely replace the lost prosthetic-side push-off work (Adamczyk and Kuo, 2015); but, fortunately, these compensations can be reduced. Preferred stiffness using the VSF could increase the kinematic symmetry between the intact and prosthetic sides, as shown with the VSPA (Clites et al., 2021). Finally, the VSF could have beneficial effects in mitigating knee hyperextension or instability on up- or down-slopes, respectively. Knee hyperextension can be caused by high socket moments when the uphill ground moves the center of pressure (COP) toward the toes (Leestma et al., 2021) and can be uncomfortable and potentially injurious to the prosthetic-side knee. Softening the VSF may help to limit this effect. On the other hand, down-slope gait can keep the COP too near the heel (Leestma et al., 2021), forcing the knee into flexion, which many persons with amputation find difficult to control and which may lead to falls (Williams et al., 2006). Stiffening the VSF forefoot can help stabilize against such instability. These potential benefits require not just prostheses of different stiffnesses, but rather the ability to actively modulate stiffness as different environments are encountered, as enabled by the VSF and related technologies.

Effective control of the stiffness modulation can be connected to the Dynamic Mean Ankle Moment Arm (DMAMA) (Adamczyk, 2020). DMAMA represents the ratio of sagittal ankle moment impulse to sagittal ground reaction force impulse in stance phase, capturing how forefoot-dominated the ground interaction is. Tests (Adamczyk, 2020) of DMAMA showed that in natural gait, GRF impulse moves closer to the ankle (less forward) with increased walking speed. As a follow-up, (Leestma et al., 2021) analyzed companion data from level-walking, ramps, and stairs in a subset of the present study's subjects, and found a positive linear sensitivity of DMAMA (more forefoot dominated) to both forefoot stiffness and ground incline while using the VSF. Thus, stiffness control of the VSF could target

DMAMA as a control loop variable to adapt to walking on level-ground, ramps, stairs, and potentially standing.

It is important to investigate whether the more capable weight support of a stiffer foot or larger energy return of a compliant foot are of contrasting benefit when deciding optimal stiffness in walking. While the energy return is usually considered good and users prefer more compliant prostheses[19], there can also be a "drop-off" effect if the foot is too compliant (Klodd et al., 2010). This effect can appear as a low "effective foot length ratio" (EFLR) that fails to mimic an intact limb appropriately. For example, prostheses with short or very soft internal keels have a low EFLR, while those with longer or stiffer keels achieve EFLR closer to the physiological value (Hansen et al., 2004). This trade-off is fundamental to the mechanics of a passive compliant prosthesis, so the right choice or balance may come down to individuals' preferences or the use of semi-active, adaptable prostheses like the VSF to adjust the behavior for different circumstances. Simultaneously achieving both the low impedance and high energy return of a compliant prosthesis and the firm weight support of a stiffer foot may fundamentally require a powered foot-ankle system or a more complex mechanism such as energy recycling (Collins and Kuo, 2010; Segal et al., 2011; Shepherd and Rouse, 2017).

Beyond the prosthetic energy flow, whole body metrics like energy expenditure and center of mass mechanics (COM) must also be considered. [34] showed a unified effect of ankle energy return that contributes to both leg swing and COM acceleration. Ankle energy return is a defining characteristic of the VSF since stiffness directly affects push-off power and work. (Zelik et al., 2011) and (Segal et al., 2012) found that lower stiffnesses led to higher energy storage, energy return, and prosthetic limb center of mass (COM) push-off work in a semi-active energy-recycling prosthesis, the controlled energy storage and return (CESR) prosthesis. They showed that using CESR with low stiffness increased prosthetic push-off (energy return) and decreased intact limb COM collision work compared to using a conventional foot. Walking energy expenditure in their participants with TTA was lowest for intermediate stiffness, suggesting biomechanical disadvantages to low stiffness despite higher energy return. Agreeing with

previous results from (Adamczyk and Kuo, 2015), people with TTA showed higher hip work with lower energy transfer from the prosthesis to the COM, which could be attributed to higher energy dissipation at the knee. These results showed that spring stiffness influences push-off but has a co-occurring biomechanical trade-off that limits how push-off can benefit walking economy. Additionally,(Clites et al., 2020) found that subject-preferred stiffness did not correlate with energy expenditure but tended to be lower for self-selected speed than fast or slow speeds.

The ability to control properties without varying components may allow the VSF and similar systems to support the development of predictive computational models of gait mechanics. Through a combination of mechanical modeling and user testing in catch-trial and adaptation protocols, models could be developed to anticipate how users will respond to changes and perhaps how they will select optimal settings. Already, we have incorporated the VSF into a computational contact model (McGeehan et al., 2021a), a study predicting the resultant and center of pressure of the ground reaction force (McGeehan et al., 2021b) under stiffness changes, and a study that predicts the normal pressure and shear stress of the residual limb-socket interface with changing stiffness (McGeehan et al., 2022).

Improvements to the experimental design of this research study could include increasing the number of participants, having more trials per stiffness category, and giving participants more acclimation time with the VSF for each stiffness. Another practical limitation is the fixed foot length of the VSF; the same foot length was used for all subjects despite varying body masses and heights. Technologically, the VSF achieved a very high range of stiffness modulation, but only at the forefoot; a future step may be to build a second keel and carriage to allow for heel stiffness modulation, improving heel strike and energy storage in the early stance. Also, combining the VSF function with a repositionable ankle (e.g., Ossur Proprio) could help with swing-phase ankle dorsiflexion to improve toe clearance and minimize tripping. A further limitation involves the wide range of our participants' self-selected walking speeds and the potential influence of walking speed on lower body mechanics. An alternative experiment with controlled speeds (Adamczyk et al., 2017) would have emphasized mechanistic effects, but we used self-selected

speeds to observe the effects on participants' most realistic use conditions. The analysis using a Linear Mixed-Effect Model partially accounts for this variation by accommodating speed-related shifts in the outcome measures. Where possible, future research on the effects of prosthesis properties should include both controlled and self-selected speeds to include both perspectives.

These improvements will depend on control, so further work must focus on real-time algorithms for gait measurement and stiffness modulation across various locomotive conditions. Using biomimetic, experimentally-optimized target values of DMAMA, or the joint mechanics measured in this study, embedded sensors (e.g. inertial sensors (Glanzer and Adamczyk, 2018) or load cells (Leestma et al., 2021)) could feed a control loop that iteratively modulates stiffness for optimal gait mechanics. Upgrades to the VSF feedback controller could include detecting previously validated kinematic variations (Kitagawa and Ogihara, 2016; Li et al., 2021; Washabaugh et al., 2017) while walking on and transitioning among various speeds, ramps, stairs, and standing still.

Conclusion

The variable stiffness foot (VSF) enables biomechanical knee and ankle adjustments through controlled modulations of forefoot stiffness. Mainly, ankle dorsiflexion angle and plantarflexor moment; knee extension angle and extensor moment; and unified deformable energy storage, energy return, and power were affected by changes in forefoot stiffness of the VSF. Future closed-loop control of VSF stiffness could be used to achieve continuous real-time modulation for optimized gait mechanics.

Acknowledgments: This work was supported by NIH HD074424, DOD W81XWH-20-1-0884, and institutional funds from the University of Wisconsin–Madison.

Conflicts of interest: No reported conflicts of interest

References

Adamczyk, P.G., 2020. Ankle Control in Walking and Running: Speed- and Gait-Related Changes in Dynamic Mean Ankle Moment Arm. J Biomech Eng 142. https://doi.org/10.1115/1.4045817

Adamczyk, P.G., Kuo, A.D., 2015. Mechanisms of gait asymmetry due to push-off deficiency in unilateral amputees. IEEE Transactions on Neural Systems and Rehabilitation Engineering 23, 776–785.

Adamczyk, P.G., Roland, M., Hahn, M.E., 2017. Sensitivity of biomechanical outcomes to independent variations of hindfoot and forefoot stiffness in foot prostheses. Human Movement Science 54, 154–171. https://doi.org/10.1016/j.humov.2017.04.005

AOPA, 2010. Prosthetic Foot Project Report. American Orthotic and Prosthetic Association.

Ármannsdóttir, A.L., Lecomte, C., Brynjólfsson, S., Briem, K., 2021. Task dependent changes in mechanical and biomechanical measures result from manipulating stiffness settings in a prosthetic foot. Clinical Biomechanics 89, 105476. https://doi.org/10.1016/j.clinbiomech.2021.105476

Baliunas, A.J., Hurwitz, D.E., Ryals, A.B., Karrar, A., Case, J.P., Block, J.A., Andriacchi, T.P., 2002. Increased knee joint loads during walking are present in subjects with knee osteoarthritis. Osteoarthritis and Cartilage 10, 573–579. https://doi.org/10.1053/joca.2002.0797

Cappello, A., Cappozzo, A., La Palombara, P.F., Lucchetti, L., Leardini, A., 1997. Multiple anatomical landmark calibration for optimal bone pose estimation. Human Movement Science, 3-D Analysis of Human Movement - II 16, 259–274. https://doi.org/10.1016/S0167-9457(96)00055-3

Clites, T.R., Shepherd, M.K., Ingraham, K.A., Rouse, E.J., 2020. Patient Preference in the Selection of Prosthetic Joint Stiffness, in: 2020 8th IEEE RAS/EMBS International Conference for Biomedical Robotics and Biomechatronics (BioRob). Presented at the 2020 8th IEEE RAS/EMBS International Conference for Biomedical Robotics and Biomechatronics (BioRob), pp. 1073–1079. https://doi.org/10.1109/BioRob49111.2020.9224405

Clites, T.R., Shepherd, M.K., Ingraham, K.A., Wontorcik, L., Rouse, E.J., 2021. Understanding patient preference in prosthetic ankle stiffness. Journal of NeuroEngineering and Rehabilitation 18, 128. https://doi.org/10.1186/s12984-021-00916-1

Collins, S.H., Kuo, A.D., 2010. Recycling Energy to Restore Impaired Ankle Function during Human Walking. PLoS ONE 5, e9307. https://doi.org/10.1371/journal.pone.0009307

Darter, B.J., Wilken, J.M., 2014. Energetic consequences of using a prosthesis with adaptive ankle motion during slope walking in persons with a transtibial amputation. Prosthet Orthot Int 38, 5–11. https://doi.org/10.1177/0309364613481489

Dingwell, J.B., Davis, B.L., Frazder, D.M., 1996. Use of an instrumented treadmill for real-time gait symmetry evaluation and feedback in normal and trans-tibial amputee subjects. Prosthetics and Orthotics International 20, 101–110. https://doi.org/10.3109/03093649609164426

Fey, N.P., 2011. The influence of prosthetic foot design and walking speed on below-knee amputee gait mechanics (thesis).

Fey, N.P., Klute, G.K., Neptune, R.R., 2011. The influence of energy storage and return foot stiffness on walking mechanics and muscle activity in below-knee amputees. Clinical Biomechanics 26, 1025–1032. https://doi.org/10.1016/j.clinbiomech.2011.06.007

Glanzer, E.M., Adamczyk, P.G., 2018. Design and Validation of a Semi-Active Variable Stiffness Foot Prosthesis. IEEE Transactions on Neural Systems and Rehabilitation Engineering 26, 2351–2359. https://doi.org/10.1109/TNSRE.2018.2877962

Hansen, A.H., Sam, M., Childress, D.S., 2004. The Effective Foot Length Ratio: A Potential Tool for Characterization and Evaluation of Prosthetic Feet. Journal of Prosthetics and Orthotics 16, 41–45. https://doi.org/10.1097/00008526-200404000-00002

Kitagawa, N., Ogihara, N., 2016. Estimation of foot trajectory during human walking by a wearable inertial measurement unit mounted to the foot. Gait & Posture 45, 110–114. https://doi.org/10.1016/j.gaitpost.2016.01.014

Klodd, E., Hansen, A.H., Fatone, S., Edwards, M., 2010. Effects of prosthetic foot forefoot flexibility on gait of unilateral transtibial prosthesis users. J Rehabil Res Dev 47, 899–910.

Lecomte, C., Ármannsdóttir, A.L., Starker, F., Tryggvason, H., Briem, K., Brynjolfsson, S., 2021. Variable stiffness foot design and validation. Journal of Biomechanics 122, 110440. https://doi.org/10.1016/j.jbiomech.2021.110440

Leestma, J.K., Fehr, K.H., Adamczyk, P.G., 2021. Adapting Semi-Active Prostheses to Real-World Movements: Sensing and Controlling the Dynamic Mean Ankle Moment Arm with a Variable-Stiffness Foot on Ramps and Stairs. Sensors 21, 6009. https://doi.org/10.3390/s21186009

Li, T., Wang, L., Yi, J., Li, Q., Liu, T., 2021. Reconstructing Walking Dynamics from Two Shank-Mounted Inertial Measurement Units (IMUs). IEEE/ASME Transactions on Mechatronics 1–1. https://doi.org/10.1109/TMECH.2021.3051724

Major, M.J., Twiste, M., Kenney, L.P.J., Howard, D., 2011. Amputee Independent Prosthesis Properties—A new model for description and measurement. Journal of Biomechanics 44, 2572–2575. https://doi.org/10.1016/j.jbiomech.2011.07.016

McGeehan, M.A., Adamczyk, P.G., Nichols, K.M., Hahn, M.E., 2022. A simulation-based analysis of the effects of variable prosthesis stiffness on interface dynamics between the prosthetic socket and residual limb. Journal of Rehabilitation and Assistive Technologies Engineering 9, 20556683221111984. https://doi.org/10.1177/20556683221111986

McGeehan, M.A., Adamczyk, P.G., Nichols, K.M., Hahn, M.E., 2021a. A Reduced-Order Computational Model of a Semi-Active Variable-Stiffness Foot Prosthesis. Journal of Biomechanical Engineering 143. https://doi.org/10.1115/1.4050456

McGeehan, M.A., Adamczyk, P.G., Nichols, K.M., Hahn, M.E., 2021b. A Computational Gait Model With a Below-Knee Amputation and a Semi-Active Variable-Stiffness Foot Prosthesis. Journal of Biomechanical Engineering 143. https://doi.org/10.1115/1.4052108

Morgenroth, D.C., Segal, A.D., Zelik, K.E., Czerniecki, J.M., Klute, G.K., Adamczyk, P.G., Orendurff, M.S., Hahn, M.E., Collins, S.H., Kuo, A.D., 2011. The effect of prosthetic foot push-off on mechanical loading associated with knee osteoarthritis in lower extremity amputees. Gait & Posture 34, 502–507. https://doi.org/10.1016/j.gaitpost.2011.07.001

Raschke, S.U., Orendurff, M.S., Mattie, J.L., Kenyon, D.E.A., Jones, O.Y., Moe, D., Winder, L., Wong, A.S., Moreno-Hernández, A., Highsmith, M.J., Sanderson, D.J., Kobayashi, T., 2015. Biomechanical characteristics, patient preference and activity level with different prosthetic feet: A randomized double blind trial with laboratory and community testing. Journal of Biomechanics 48, 146–152. https://doi.org/10.1016/j.jbiomech.2014.10.002

Schwartz, M.H., Rozumalski, A., 2005. A new method for estimating joint parameters from motion data. Journal of Biomechanics 38, 107–116. https://doi.org/10.1016/j.jbiomech.2004.03.009

Segal, A.D., Orendurff, M.S., Czerniecki, J.M., Schoen, J., Klute, G.K., 2011. Comparison of transtibial amputee and non-amputee biomechanics during a common turning task. Gait & Posture 33, 41–47. https://doi.org/10.1016/j.gaitpost.2010.09.021

Segal, A.D., Zelik, K.E., Klute, G.K., Morgenroth, D.C., Hahn, M.E., Orendurff, M.S., Adamczyk, P.G., Collins, S.H., Kuo, A.D., Czerniecki, J.M., 2012. The effects of a controlled energy storage and return prototype prosthetic foot on transtibial amputee ambulation. Human Movement Science 31, 918–931. https://doi.org/10.1016/j.humov.2011.08.005

Shepherd, M.K., Rouse, E.J., 2017. The VSPA Foot: A Quasi-Passive Ankle-Foot Prosthesis With Continuously Variable Stiffness. IEEE Transactions on Neural Systems and Rehabilitation Engineering 25, 2375–2386. https://doi.org/10.1109/TNSRE.2017.2750113

Struyf, P.A., van Heugten, C.M., Hitters, M.W., Smeets, R.J., 2009. The prevalence of osteoarthritis of the intact hip and knee among traumatic leg amputees. Arch Phys Med Rehabil 90, 440–446. https://doi.org/10.1016/j.apmr.2008.08.220

Takahashi, K.Z., Kepple, T.M., Stanhope, S.J., 2012. A unified deformable (UD) segment model for quantifying total power of anatomical and prosthetic below-knee structures during stance in gait. Journal of Biomechanics 45, 2662–2667. https://doi.org/10.1016/j.jbiomech.2012.08.017

Washabaugh, E.P., Kalyanaraman, T., Adamczyk, P.G., Claflin, E.S., Krishnan, C., 2017. Validity and repeatability of inertial measurement units for measuring gait parameters. Gait & Posture 55, 87–93.

Williams, R.M., Turner, A.P., Orendurff, M., Segal, A.D., Klute, G.K., Pecoraro, J., Czerniecki, J., 2006. Does Having a Computerized Prosthetic Knee Influence Cognitive Performance During Amputee Walking? Archives of Physical Medicine and Rehabilitation 87, 989–994. https://doi.org/10.1016/j.apmr.2006.03.006

Wu, A.R., Kuo, A.D., 2016. Determinants of preferred ground clearance during swing phase of human walking. Journal of Experimental Biology jeb.137356. https://doi.org/10.1242/jeb.137356

Zelik, K.E., Adamczyk, P.G., 2016. A unified perspective on ankle push-off in human walking. Journal of Experimental Biology 219, 3676–3683. https://doi.org/10.1242/jeb.140376

Zelik, K.E., Collins, S.H., Adamczyk, P.G., Segal, A.D., Klute, G.K., Morgenroth, D.C., Hahn, M.E., Orendurff, M.S., Czerniecki, J.M., Kuo, A.D., 2011. Systematic Variation of Prosthetic Foot Spring Affects Center-of-Mass Mechanics and Metabolic Cost During Walking. IEEE Transactions on Neural Systems and Rehabilitation Engineering 19, 411–419. https://doi.org/10.1109/TNSRE.2011.2159018

(d) Published Collaboration Manuscripts

(i) A Reduced-Order Computational Model of a Semi-Active Variable-Stiffness Foot Prosthesis[71]

Authors: Michael A. McGeehan, Peter G. Adamczyk, Kieran M. Nichols, Michael E. Hahn

Abstract: Passive energy storage and return (ESR) feet are current performance standard in lower limb prostheses. A recently developed semi-active variable-stiffness foot (VSF) prosthesis balances the simplicity of a passive ESR device with the adaptability of a powered design. The purpose of this study was to model and simulate the ESR properties of the VSF prosthesis. The ESR properties of the VSF were modeled as a lumped parameter overhung beam. The overhung length is variable, allowing the model to exhibit variable ESR stiffness. Foot-ground contact was modeled using sphere-to-plane contact models. Contact parameters were optimized to represent the geometry and dynamics of the VSF and its foam base. Static compression tests and gait were simulated. Simulation outcomes were compared to corresponding experimental data. Stiffness of the model matched that of the physical VSF (R2: 0.98, root-mean-squared error (RMSE): 1.37 N/mm). Model-predicted resultant ground reaction force (GRFR) matched well under optimized parameter conditions (R2: 0.98, RMSE: 5.3% body weight,) and unoptimized parameter conditions (R2: 0.90, mean RMSE: 13% body weight). Anterior–posterior center of pressure matched well with $R2 > 0.94$ and $RMSE < 9.5\%$ foot length in all conditions. The ESR properties of the VSF were accurately simulated under benchtop testing and dynamic gait conditions. These methods may be useful for predicting GRFR arising from gait with novel prostheses. Such data are useful to optimize prosthesis design parameters on a user-specific basis.

(ii) A Computational Gait Model With a Below-Knee Amputation and a Semi-Active Variable-Stiffness Foot Prosthesis[72]

Authors: Michael A. McGeehan, Peter G. Adamczyk, Kieran M. Nichols, Michael E. Hahn

Abstract: Introduction: Simulations based on computational musculoskeletal models are powerful tools for evaluating the effects of potential biomechanical interventions, such as implementing a novel prosthesis. However, the utility of simulations to evaluate the effects of varied prosthesis design

parameters on gait mechanics has not been fully realized due to the lack of a readily-available limb loss-specific gait model and methods for efficiently modeling the energy storage and return dynamics of passive foot prostheses. The purpose of this study was to develop and validate a forward simulation-capable gait model with lower-limb loss and a semi-active variable-stiffness foot (VSF) prosthesis. Methods: A seven-segment 28-DoF gait model was developed and forward kinematics simulations, in which experimentally observed joint kinematics were applied and the resulting contact forces under the prosthesis evolved accordingly, were computed for four subjects with unilateral below-knee amputation walking with a VSF. Results: Model-predicted resultant ground reaction force (GRFR) matched well under trial-specific optimized parameter conditions (mean R2: 0.97, RMSE: 7.7% body weight (BW)) and unoptimized (subject-specific, but not trial-specific) parameter conditions (mean R2: 0.93, RMSE: 12% BW). Simulated anterior-posterior center of pressure demonstrated a mean R2 = 0.64 and RMSE = 14% foot length. Simulated kinematics remained consistent with input data (0.23 deg RMSE, R2 > 0.99) for all conditions. Conclusions: These methods may be useful for simulating gait among individuals with lower-limb loss and predicting GRFR arising from gait with novel VSF prostheses. Such data are useful to optimize prosthesis design parameters on a user-specific basis.

(iii) A simulation-based analysis of the effects of variable prosthesis stiffness on interface dynamics between the prosthetic socket and residual limb[73]

Authors: Michael A. McGeehan, Peter G. Adamczyk, Kieran M. Nichols, Michael E. Hahn

Abstract: Loading of a residual limb within a prosthetic socket can cause tissue damage such as ulceration. Computational simulations may be useful tools for estimating tissue loading within the socket, and thus provide insights into how prosthesis designs affect residual limb-socket interface dynamics. The purpose of this study was to model and simulate residual limb-socket interface dynamics and evaluate the effects of varied prosthesis stiffness on interface dynamics during gait. A spatial contact model of a residual limb-socket interface was developed and integrated into a gait model with a below-knee amputation. Gait trials were simulated for four subjects walking with low, medium, and high prosthesis

stiffness settings. The effects of prosthesis stiffness on interface kinematics, normal pressure, and shear stresses were evaluated. Model-predicted values were similar to those reported previously in sensor-based experiments; increased stiffness resulted in greater average normal pressure and shear stress ($p < 0.05$). These methods may be useful to aid experimental studies by providing insights into the effects of varied prosthesis design parameters or gait conditions on residual limb-socket interface dynamics. The current results suggest that these effects may be subject-specific.

(e) Development of VSF with hind and forefoot properties

The VSF allows for adaptable fore-foot stiffness modulation and has been shown to affect the knee and ankle mechanics. The VSF's ankle is rigid, and the forefoot mainly affects mid to late prosthetic stance. Adamczyk et al.[14] examined both hind and forefoot stiffness effects on persons with transtibial amputations walking for various controlled stiffnesses and walking speeds. They found similar ankle and knee mechanical effects as was seen in the VSF results, but they also showed that a stiffer hindfoot yields decreased prosthesis energy return, larger ground reaction force (GRF) loading rate, larger knee flexion angle (stance phase), and knee extensor moment.

To improve prosthetic walking adaptability, some of my work involved working with a team of students to upgrade the VSF design to include two keels (VSF2K): one forefoot and one hindfoot. The overhung beam (keel) and carriage system for the original VSF were replicated and shrunk for the hindfoot. The two keels are mounted at a common axis near the ankle (see figure 14) and are diagonally extended downwards to mimic the midfoot arch. Two motors will move the hind and forefoot carriages to change the hind and forefoot stiffness of the VSF2K. The foot stiffness was designed to range from 7 to 30 N/mm.

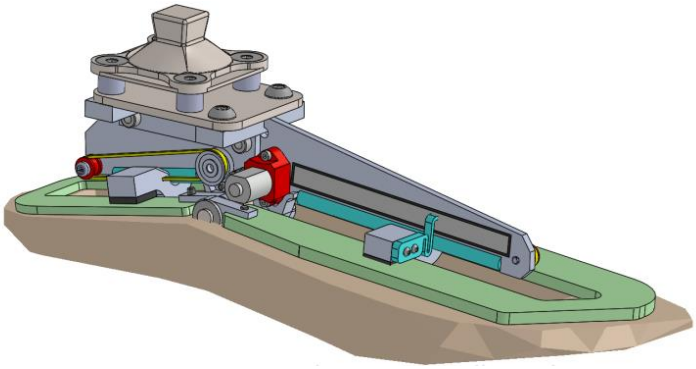

Figure 14: proposed design of the Variable Stiffness Foot with two keels (VSF2K)

The collection and construction of the individual parts are nearly complete, and other students are currently assembling them for the first physical build of the VSF2K. Future steps for those students will include developing the VSF2K software controller to modulate the hind and fore-foot stiffness and testing its effects on humans. Feedback for control will involve foot IMU motion reconstruction, motor control to move the carriage, and potentiometer readings of carriage position to change the stiffness. Tests will include many of the same outcomes observed in the study described here, as well as effects due to hindfoot stiffness and tests on non-level terrain.

(f) Conclusion

This past work explored the effect of three stiffnesses (compliant, medium, and stiff) of the Variable Stiffness Foot on the sagittal ankle and knee angles, moments, and powers, vertical ground reaction forces, and unified deformable energy and power. Forefoot stiffness is one of the main variables that allows prosthetic users to adapt their functional gait, and another main variable is ankle angle control. A computational contact model was developed for the VSF to replicate its energy return and storage properties, and it predicted the resultant and center of pressure of the ground reaction force under the prosthesis. Additionally, a Variable Stiffness Foot with two keels (VSF2K) was designed to allow for hind and fore-foot stiffness modulation.

Chapter 3. Design of the Motor Control of the Two Axis aDaptable Ankle

Real-time Motor Control of the New Two Axis aDaptable Ankle using a Raspberry Pi, ROS, and CANopen over EtherCAT

Intended Journal: MDPI Actuators

a) Abstract

This paper will focus on the implementation method and results of control of a second-generation Two-Axis aDaptable Ankle (TADA) prosthesis, with emphasis on modifying a Raspberry Pi 4 for real-time control of brushless direct-current motors. Kinematic algorithms for setting ankle angles of zero to ten degrees in any combination of sagittal (dorsiflexion/Plantarflexion) and frontal (inversion/eversion) angles were implemented and commanded to the motors. Real-time control was implemented using CANopen over EtherCAT (CoE) to synchronize the communication between the Raspberry Pi and the motor controllers. To achieve reliable motor communication, where the motors continuously move, the distributed clock synchronization of Linux and Motor driver systems needs to have Proportional Integral (PI) compensation and sampling period specifically tuned for the Raspberry Pi and motor driver system. We hypothesized that the variability of the sampling period of the clock synchronization would be lower for higher I and P gains, and that the CPU loads would be lower for larger sampling periods of the clock synchronization thread. We further hypothesized that the motors would have lower movement times and errors than the previous TADA version. Data collection involved moving the TADA through 33 unique pre-selected ankle configurations nine times. Results show that distributed clock synchronization with consistent sampling periods with lower CPU loads had an actual sampling period of 249.98±4.51 microseconds and 12.48±21.3% for CPU loads. Also, the ankle angle movements had mean values of 0.1278 sec for 95% Rise Time, 0.1928 sec for Settling Time, and less than 0.1 degrees for Movement errors. These software and hardware improvements to the TADA system allow for quicker (low movement times), more reliable (continuous movements with low sampling period variability), and more

precise (low movement error) ankle angle changes, and also higher data transmission rates with modest CPU loads compared to the original TADA. These improvements aim to allow the TADA to efficiently adapt to various speeds and terrains, like walking on slopes, stairs, or around corners.

b) Introduction

Real-time control of lower-limb prosthetics has been an emerging area of academic interest. There is a need for prosthetic devices to sense the person and their environment and actuate appropriately to aid in functional walking. Semi-active prosthetic devices (Adamczyk, 2020) can return some functionalities of the lower-limbs to their users by combining the benefits of passive mechanical properties and robotic control. They do not supply power to the body and use minimal power to reconfigure or adjust when off the ground. The increasing popularity of research in semi-active devices pushed the field to improve the mechanical benefits of passive prosthetic elements while reducing the cost, weight, and computational demand of the electronic components. These semi-active prostheses can help make lower-limb prostheses more accessible and have the potential to be more widely applicable due to the potential adaptability of the prosthetic software as it interacts with the sensors and actuators.

Several recent prostheses have chosen to use a Raspberry Pi (a small and versatile computer with quad-core CPUs and WIFI, Bluetooth, and Ethernet capability) as the embedded controller (Azocar et al., 2018; Lenzi et al., 2019). However, these examples use separate circuit boards to communicate with the embedded motor controllers or use reduced motor control functionality by communicating through simplified channels such as analog voltages, whereas the full capabilities of the motor controllers are realized only with comprehensive digital communication. One goal of this paper is to describe the implementation of such comprehensive digital communication directly on the Raspberry Pi to achieve real-time control and communication.

One communication protocol that allows real-time communication is CANopen over EtherCAT (CoE). CoE is a protocol that allows CANopen-capable devices (Voss, 2008) to be connected to EtherCAT-capable devices. EtherCAT (Sung et al., 2011) is used to specify how the data is transmitted,

and CANopen specifies how the data is defined. Simpler communication protocols like USB, serial (RS-232, 485), and ethernet are limited in their real-time control abilities. CoE (Chen et al., 2010) offers data transmission with a high data rate and throughput, reliability (has error detection and correction), and deterministic data transfer (events will occur in a specific and predictable amount of time). CoE is also flexible in its control loop as it can handle multiple managers to multiple client control. Timing constraints are managed on CoE with a distributed clock synchronization (Giridhar and Kumar, 2006), where all devices on the network adjust their clock based on a single reference clock on the manager. Data transmission in CoE provides real-time communication (Wei et al., 2016) with low latency and jitter. CoE is an ideal choice to use with a Raspberry Pi and motor drivers to set up real-time control of motors.

It is possible to have real-time control with a Raspberry Pi, but the software needs to be adjusted and optimized to have stable CoE communication. Our semi-active device, the Two Axis aDaptable Ankle, an ankle angle adaptor (Adamczyk, 2020) was improved to include brushless DC motors, a Raspberry Pi 4 as the computer board, and CoE for communication with separate embedded motor controllers. This improvement allows quicker and more accurate changes in ankle angle that are necessary to efficiently adapt to various terrain like walking on slopes, stairs, or around corners. The TADA can modulate ankle angle up to ten degrees in the sagittal and frontal planes. Low-power motors rotated two angled cams, and as these turned, their angled faces changed the orientation of the foot.

This paper will focus on the implementation method and results of programming a Raspberry Pi 4 for real-time motor control in a new version of the TADA. The real-time control was implemented using CANopen over EtherCAT to allow precise and reliable communication between the Raspberry Pi and two motor drivers, which control the movement of the motors. We hypothesized that the mean and standard deviation of the sampling period of the clock synchronization would scale with Proportional and Integral gains used to synchronize the clocks, respectively, and that the CPU loads would be lower for larger sampling periods of the clock synchronization thread. We further hypothesized that the motors would

have lower movement times and errors than the previous TADA version, indicating improved performance.

c) Hardware Design

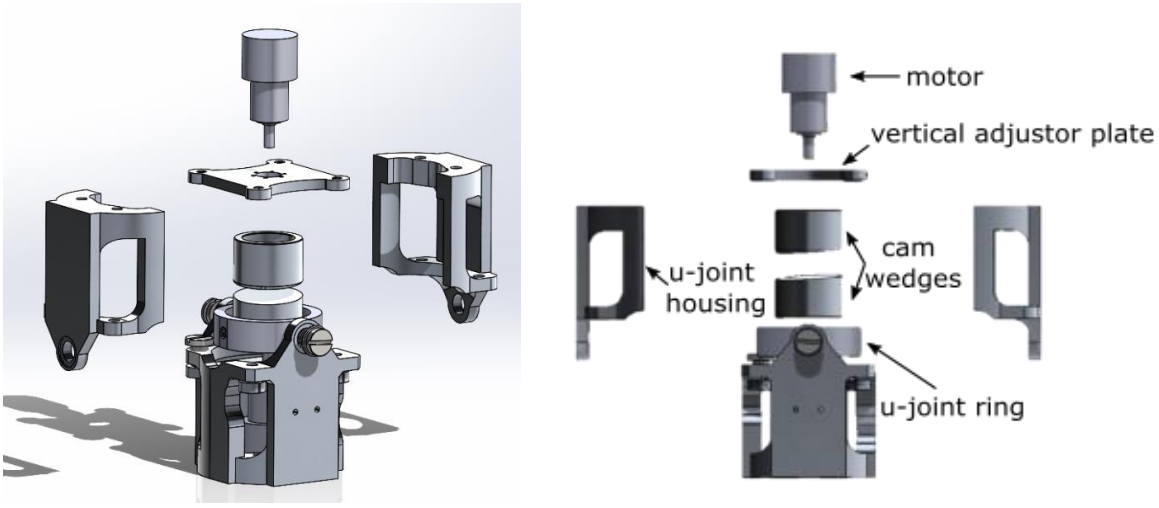

Figure 15: exploded views of the new TADA design

The new version (Figure 15) of the semi-active prosthesis – TADA – consists of an external universal-joint whose movement is driven by brushless DC motors rotating two cylindrical wedge cams. Four housing pieces make up the frame and pivot points of the U-joint and hold the motors in place. The TADA concept requires precisely coincident joint centers between (i) the two wedge cams and (ii) the intersecting axes of the U-joint, to avoid binding due to overconstraint. The updated TADA has modular alignment plates supporting the wedge cams for fine vertical adjustments and locations on the outside of the U-joint to place shims for fine horizontal adjustments to prevent this issue.

The new TADA uses brushless Direct Current (DC) motors (Faulhaber 3216W012BXTHIEF3-1024L) with 14:1 gearboxes (Faulhaber 22GPT 14:1) having a rated torque output of 0.532 Nm and rated speed of 4.59 revolutions per second. These motor parameters allow for quick motor rotations that can reorient the distal side of the TADA, which is attached to a prosthetic foot, during a single leg swing in walking. The motor shaft is connected to the wedges by a spider coupling to help account for any additional misalignments. As with the previous version, the mating faces of the two wedge cams have an

angle of five degrees relative to the axis of the motor; as these cams rotate, they can plantarflex, dorsiflex, invert, and evert the ankle anywhere between zero to ten degrees. The centered U-joint holds the two cylindrical wedges in contact with each other, allowing them to move freely in swing phase but lock in place during stance phase as the applied ankle moment causes friction between the cams.

The TADA electronics are powered by three 12 V lithium polymer batteries (120C, 1.5Ah each). The 12V source powers the two Faulhaber brushless DC motors through two standalone motor controllers (Elmo Gold Twitter) and is also connected to a step-up voltage regulator to provide a 24V power line to the motor controller. The motor controller powers the hall sensors of the motors with 5V wires. A step-down voltage regulator (12 to 5V) from the second battery powers the Raspberry Pi computer. The electronics are mounted to a waist pack that houses the motor drivers, Raspberry Pi, batteries, voltage regulators, and power distribution circuits. The wires are bundled and can be strapped to the leg to power the TADA ankle. A low-profile foot prosthesis (Steplite Low Profile - 3/4" (18mm) KC01) is mounted to the distal end of the TADA for ground contact.

The Raspberry Pi 4 has a Broadcom (BCM2711) quad-core Cortex-A72 with 4 GB of LPDDR4 SDRAM memory. It is overclocked to 2.0 GHz to ensure high performance. Its Ethernet port was used to connect the Raspberry Pi to the motor controllers for the CoE physical layer. To collect the experimental data to a file, a Windows computer communicated with the Raspberry Pi over WIFI. The Windows laptop was a Lenovo Legion 7 with Intel i7-10750H eight-CPU with a clock frequency of 2.6 GHz and 16 GB of DDR4 UDIMM memory.

d) Software Architecture

ROS Software Architecture

We used Robotic Operating System (ROS) (Wei et al., 2016) to have a distributed framework for the TADA software. This software using ROS (1) Noetic Ninjemys operated on the Raspberry Pi 4 and included the *Brain* and *Motor* nodes. The *Brain* node was the central program for user interaction, automated experimental protocols, and troubleshooting. It sent commands (published) of the final motor

position, max velocity, and max torque to the *Motor* node. The *Motor* node received (subscribed to) the motor commands and communicated with the motor controller using CANopen over EtherCAT for the position motor control to adjust ankle angles. A secondary computer receives ROS data over Wi-Fi to collect the experimental data. The code for the TADA software can be found in our GitHub repository (Nichols, 2022). The distribution of the ROS program on their specific hardware is described below:

- ***Raspberry Pi***

A precompiled image of the Debian Linux kernel was used based on LinuxCNC (Bu-Hai et al., 2017), which contains a PREEMPT real-time software patch. This software patch was necessary for real-time control as it allowed for deterministic systems with low latencies. Bash (Linux) terminal commands of "isolcpu" and "taskset" were used to ensure that each CPU was carefully used, to avoid thread racing issues and distribute the computational load. The Raspberry Pi has four CPUs; CPU0 was reserved for Linux kernel programs, CPU1 and 2 were reserved for general Linux programs, including TADA programs, and CPU3 was reserved for the clock synchronization process within the motor control component of the software. This clock synchronization process needed its own CPU to have uninterrupted execution for synchronizing the Linux clock with the motor driver clocks (*distributed clock synchronization*). The TADA programs were organized into several programs managed by Robot Operating System (ROS) software to ensure modularity and provide easy data transmission and logging.

1. Brain node

The *Brain* node functions as the central processing point for all nodes. It is a Python program with a multi-threaded structure. It receives and parses commands from the terminal, contains preset command instructions for specific experiments, and converts TADA control angle inputs to motor angle commands (position control). This node also monitors the CPU loads of the Raspberry Pi.

To initialize the homed position of the TADA, the peaks of both wedge cams were set to forward, corresponding to full Plantarflexion (toe-down 10 deg). Then, a user or program can issue control values to the *Brain* node, called theta, θ and alpha, α (Adamczyk, 2020). θ represents the foot's tilt angle (0 to 10 degrees) from the shank segment. α represents the "downward direction" – i.e., the projection direction in the transverse plane of the foot's tilt axis relative to the PF direction (ranging –180 to +180 deg) . Given the constraints of the U-joint and wedge cams, the ankle angle control was parameterized into θ and α to represent the 3D orientation of the foot. For example, (θ, α) of (10,0) represents the homed position where the toe is pointing downward, with (PF, IV) angles of (10,0).

PF	**IV**	**θ**	**α**
0	0	0	any
10	0	10	0
-10	0	10	180
0	10	10	-90
0	-10	10	90

Table 3: example angles of the TADA commands (θ, α) with their related PF, IV coordinates

The table to the left (Table 3) shows the notable positions of (PF, IV) and their corresponding (θ, α) combinations. The ankle angles were Plantarflexion PF (toe-down), Eversion EV (bottom of foot turning outward), Dorsiflexion DF (toe-up), and Inversion IV (bottom of foot turning inward). PF and DF are movements in the sagittal plane, and EV and IV are in the frontal plane.

Rotation matrices are applied to these values to determine the angles needed to move the foot correctly. The *Brain* node uses the previous motor angles and the new desired angles to calculate the motor rotation needed to arrive at the desired foot orientation. The motors can continuously rotate (above 180 deg and below -180), so conditional statements were added to ensure that the motor takes the shortest path and to avoid mathematical angle wrapping issues.

2. *Motor node*

The *Motor* node receives global motor commands from the *Brain* node and executes a position control of the two motors of the TADA. It is built with a mixture of C and C++ programming and has a multi-threaded structure, with a real-time thread for the clock synchronization and non-real-time threads for CANopen over EtherCAT (CoE) communication, error handling, and ROS data-processing. CPU3 is reserved for the clock synchronization thread and CPU2 is used for the CoE

communication thread. All motor threads were given higher thread priority to help the Linux task scheduler prioritize them in preference to other non-critical computer tasks.

The motor control is based on software from Single Open-source EtherCAT Master (SOEM) (Peekema et al., 2014). SOEM enables a control architecture for one manager (Raspberry Pi) with two clients (two motor controllers). This control progresses through a series of initialization and confirmation modes to set up the CoE connection.

Firstly, the ethernet connection and CoE manager on the Raspberry Pi is initialized. To begin the position controller, CoE Service Data Objects for motor driver configuration settings (slow updates) and CoE Process Data Objects for real-time data transfer (fast updates) are mapped to the clients using Cyclic Synchronous Position (CSP) Control (Hasan, 2021). CSP Control is useful because a desired end position is sent to motor drivers, but the motor drivers determine the appropriate trajectory, and there is a periodic, time-deterministic feedback loop to ensure that both motors achieve their trajectory. Next, the safety modes like safe stop and safe torque-off are turned off to allow for an operational motor. The operational mode is then started, and the controller waits for position commands from the *Brain* over ROS messages (it runs at 1000 Hz).

Three other threads are dedicated to ensuring that the motors stay in operational mode. The real-time clock synchronization thread syncs the Linux and Motor Driver clocks and ensures consistent movement data timing (250, 500, or 1000 microseconds for 4000, 2000, or 1000 Hz, respectively). The Error handling thread monitors for errors and corrects them if necessary (running roughly 1000 Hz). The slowest thread contains the data processing for ROS messages published to log the system's state, such as commands and feedback measurements (100 Hz).

To maintain a stable CoE connection, the clock synchronization thread sends and receives the CoE Process Data Objects (PDO) in a cyclic manner among the Raspberry Pi and motor drivers. Mutex locking is included to safeguard against thread racing (threads simultaneously trying to access the same resource). This thread initializes a timer and calculates the cycle time. Then, it waits until the next cycle starts based on the pre-selected thread sampling period and a wait time after the

previous cycle. This wait time is adjusted using pre-selected Proportional and Integral (PI) gains, with the proportional error defined as the difference between the time passed since the last cycle and the commanded sampling period. The integral error is based on an accumulation of the past proportional errors (if the recent past proportional errors are positive, then the integral error becomes more positive). This thread maintains the communication of PDOs among the Raspberry Pi and motor controller and maintains the sampling period of that communication.

- ***Windows laptop remote node***

3. Data collection

The experimental data were collected using the *rosbag* functionality of ROS. Using the Command terminal in a Microsoft Visual Studio instance of ROS, the *rosbag* command was entered to save data for each trial. The messages from all the nodes were streamed to a *rosbag* file. The Windows computer was connected to the Raspberry Pi's ROS manager (*rosmaster*) through a cellular device's hotspot using WIFI.

b) Experimental Methods

We designed experiments to test two aspects of the new TADA: (i) the function of the real-time operating system and CoE implementation and (ii) the TADA performance in achieving the target movements. Data collection involved moving the TADA through 33 pre-selected ankle configurations. Using the anatomical reference frame, the TADA control angles were combinations of Plantarflexion (PF) and inversion (IV). Starting at the neutral configuration (0 degrees PF and EV), the TADA was commanded to move to a new position and was given up to one second to complete the movement before moving again. Ankle configurations were chosen for eight directions combining PF and EV: combinations were specified in pure PF, DF, IV, and EV, and equal combinations of the two directions in all four quadrants (PF+IV (α = -45 deg), PF+EV (α = +45 deg), DF+IV (α = -135 deg), DF+EV (α = +135 deg)). Each direction contributed four settings, with total ankle angle magnitudes θ of 2.5, 5.0, 7.5, and

10.0 degrees for the pure directions and 1.25, 2.5, 3.75, and 5.0 for the combined directions. Each combination of direction and magnitude was converted into corresponding control angles for the wedge cams in the TADA and used to command the motors.

ROS data recording with the ROS tool, *rosbag*, was used to collect data at 100 Hz sampling frequency. The ROS system collected the TADA command angles, resulting motor commands, actual motor position, and current time. ROS also collected the actual sampling period (SP) of distributed clock synchronization thread and individual CPU load values. Two experiments were performed, to evaluate (i) the clock synchronization and CPU utilization and (ii) the kinematic motor response of the TADA system:

1) Clock Synchronization and CPU utilization

The TADA was moved through 33 ankle configurations with a total trial time of 33 seconds. There were seven trials for each set of PI gain and SP. This experiment focused on testing the reliability of the CANopen over EtherCAT communication, and the main results were the actual sampling period (mean value, mean error, and standard deviation) and CPU loads (mean and standard deviation).

2) Kinematic motor response

The TADA was randomly moved through 33 ankle configurations, each repeated nine times, for a total trial time of 297 seconds. The PI gain and SP of (0.1, 0.01, 500 μs) were used for this experiment. This experiment focused on testing the precision of motor control for ankle angles, and the main results were the final absolute PF error (absolute value of the difference between the command PF and actual PF angle when the motor first settles) and movement times (95% rise time and settling time). Statistics were calculated for the final absolute PF error and movement times for settling for absolute changes of the top and bottom motors in the form of regression slopes and intercepts, r^2 values (coefficient of determination), and p-values.

c) Results

1) Clock Synchronization and CPU utilization

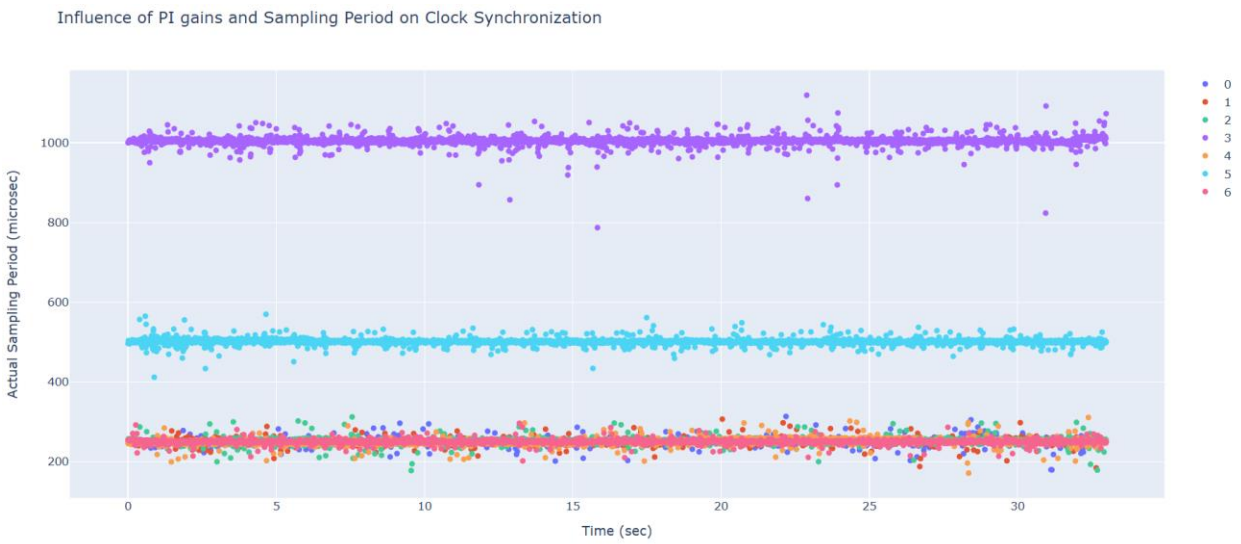

Figure 16: plot of the actual sampling period across the experiment time. Each color represents a different condition. These scatter plots show stable matching of the intended sampling period with some variability. There are three commanded sampling period of 250, 500, and 1000 µs.

Condition				Actual Sampling period (μs)			CPU load (%)	
#	P	I	SP (μs)	Mean	Mean Error	SD	Mean	SD
0	0.1	*0.002*	250	250.48	0.52	5.69	15.93	23.6
1	0.1	*0.05*	250	250.95	0.05	5.07	11.25	20.7
4	0.1	0.01	250	249.65	0.35	6.59	13.37	23.5
2	*0.02*	0.01	250	251.85	0.15	6.29	17.20	24.1
6	***0.5***	**0.01**	**250**	**249.98**	**0.02**	**4.51**	**12.48**	**21.3**
5	0.1	0.01	*500*	501.08	0.08	7.25	36.81	7.24
3	0.1	0.01	*1000*	1004.4	0.40	11.52	6.67	14.7

Table 4: various conditions with the resulting mean and standard deviation (SD) of Actual Sampling Period and CPU load. The bolded numbers for condition 6 represented the optimal condition with the lowest error and standard deviation in sampling period and modest CPU load. The condition are ordered in this table to group the changes in I first, then changes in P, and then changes in SP.

Condition 6, with the largest P value, presented the lowest mean error and standard deviation of the actual sampling period (Table 4 and Figure 16). Condition 0 with the lowest I value gave the higher mean error indicating some effect of reduced I value increasing the mean error. There is some effect of an increased sampling period on the reducing CPU load and increasing the variability of the sampling period, but not a consistent effect for CPU loads (500 μs does not have a lower CPU load). All conditions had mean errors less than 0.21% off the commanded sampling period. Condition 6, with the highest P and

moderate I gains, gave the lowest mean error and actual sampling period variability, and its command sampling period of 250 μs gave modest CPU loads. Overall, clock synchrony was maintained adequately across a wide range of settings, and CPU load was variable and not very sensitive to sampling period.

2) Kinematic motor response

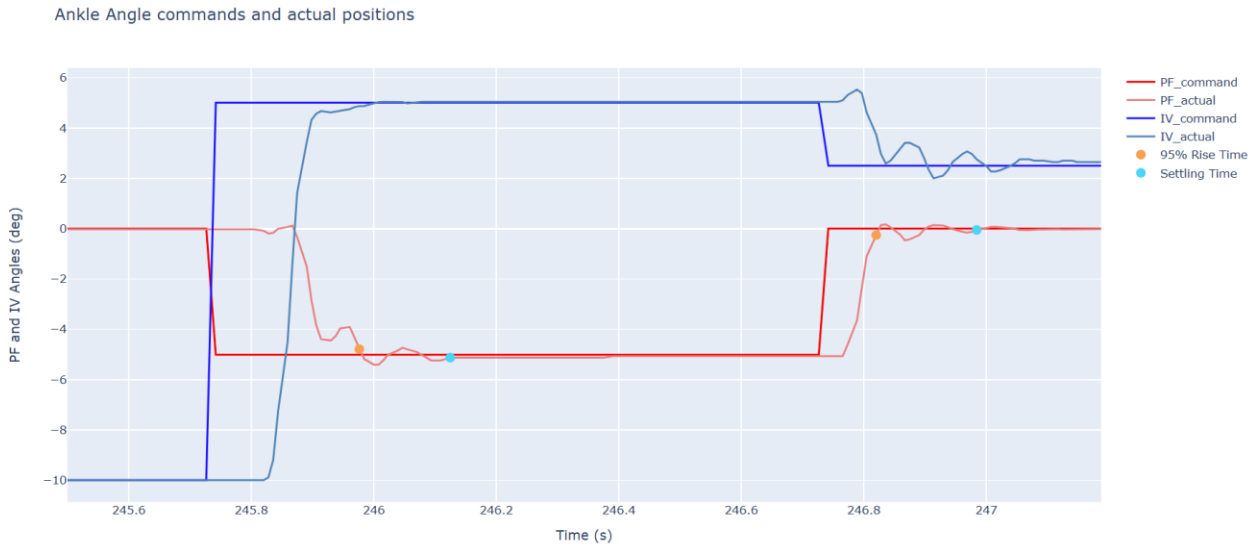

Figure 17: Example data from one movement, plotting ankle angle commands (intended angle) and actual ankle angle based on the motors' position sensors. The blue lines represent the IV angles and the red lines represent the PF angles. The orange dots are the 95% rise times and the light-blue dots are for the settling times.

The motors move the TADA to new ankle angles with small errors: 0.045 degrees for PF and 0.067 degrees for IV (Table 5). Figure 17 displays the trajectory of the ankle angle motions showing that when a command is sent, there is a slight delay (around 0.1 seconds). The motors move and then settle to the new commanded ankle angle (there is some oscillation with the settling). The 95% rise time is important to know the time taken to move most of the distance, and the settling time represents the time taken to arrive around 0.1 degrees of the final destination.

Metrics	Movement Time (seconds) based on PF error		Movement Error (degrees)	
	95% Rise Time	Settling Time	PF	IV
Mean	0.1278	0.1928	0.045	0.067
SD	0.037	0.076	0.01	0.04

Table 5: Mean and standard deviation (SD) of the movement times and errors of the ankle angle movements. 95% rise time is the movement time to achieve 95% of the intended change of PF angle. Settling time is the movement time to achieve an average error of less than 0.1 deg PF. The results excluded errors from 6 out of the 297 movements as the motors were briefly stuck.

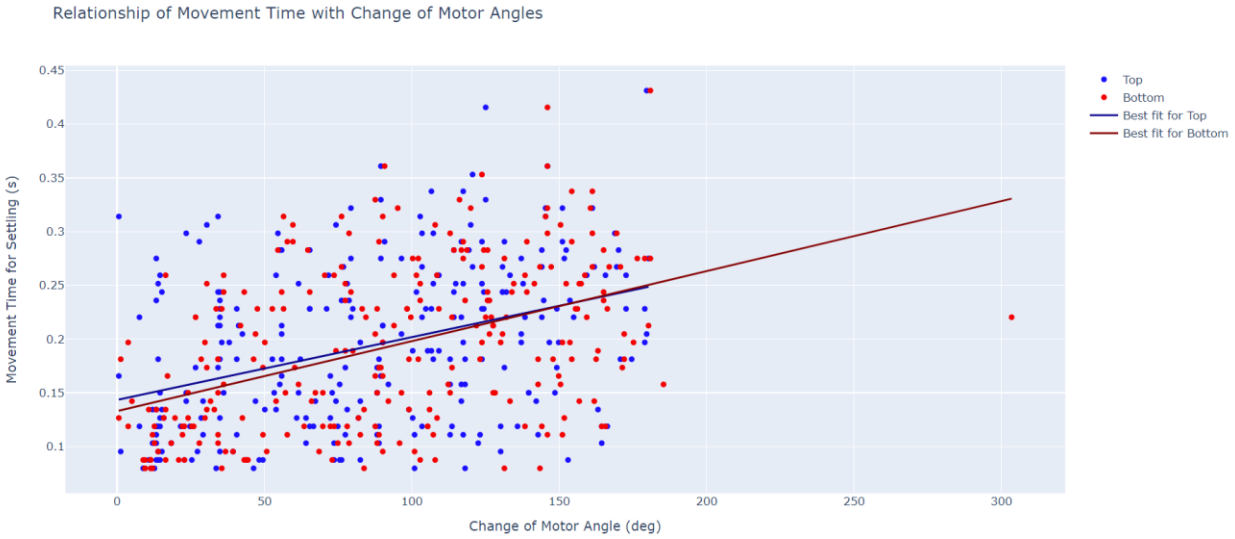

Figure 18: plot of movement times for settling with the motor angle changes for the top and bottom motors.

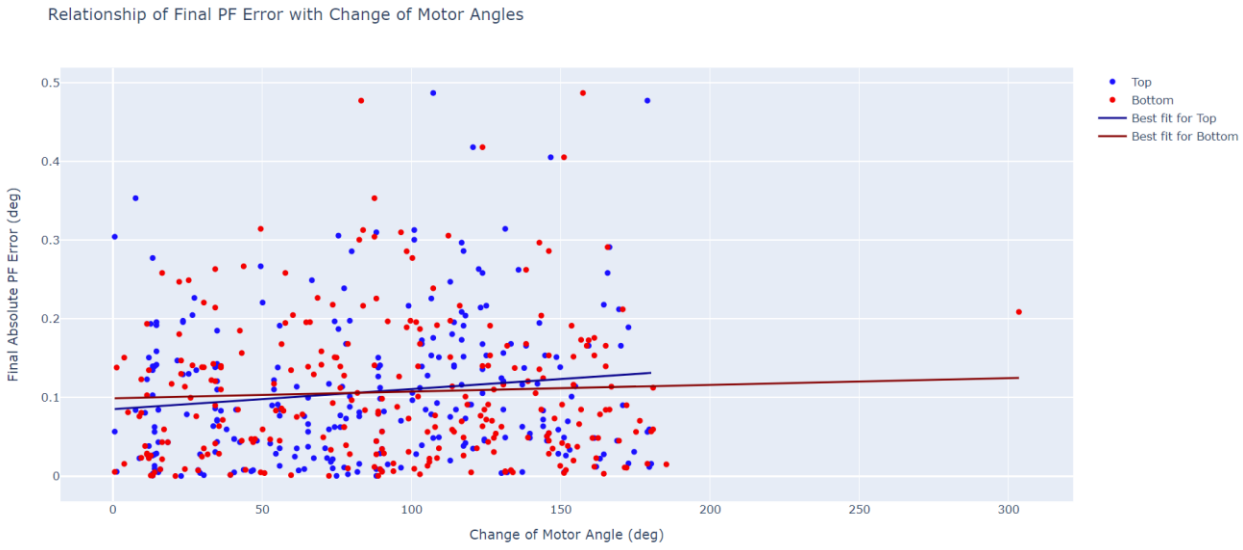

Figure 19: plot of Final Absolute PF error with the motor angle changes for the top and bottom motors.

Statistical analysis	Metric	Slope*10^{-4}	Intercept	r^2 value	P value
Settling Movement Time	Top	5.84 s/deg	0.121 s	0.145	<0.001
	Bottom	6.51 s/deg	0.111 s	0.202	<0.001
Final Absolute PF Error	Top	2.56 deg/deg	0.085 deg	0.139	0.024
	Bottom	0.858 deg/deg	0.099 deg	0.049	0.425

Table 6: statistical analysis for settling movement time and final absolute PF error for the top and bottom motors

Figures 18 and 19 show the variability of settling times and final PF error as a function of the change of top and bottom motor angles. In Figures 18 and 19, the bottom motor had one change of angle that was around 305 degrees, which warrants some investigation as motor angle changes should have been below 180 degrees. There was a weak trend (Table 6) that the larger the motor movement, the higher the movement time. There was a weak trend (Table 6) between PF error and change of motor angle for the top motors, but not the bottom motor. The important features of Figures 18 and 19 were that for most movements of the TADA, the movement times and final PF errors for settling had some variability that depended on how much the top and bottom motors moved, but the movements were small errors (less than 0.5 degrees with a mean of 0.045 degrees) and quick settling times (less 0.45 seconds with a mean of 0.19 seconds). Figure 20 displays the low variability of the PF and IV errors (0.01 and 0.04 degrees) by displaying the intended and actual positions.

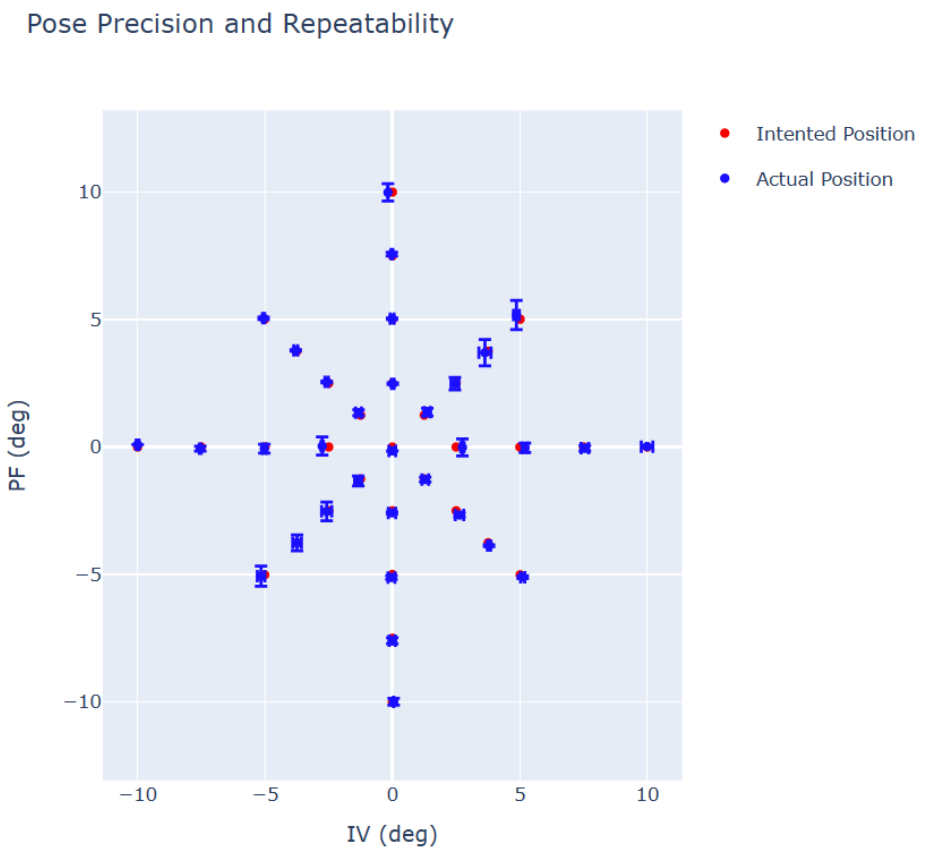

Figure 20: plot of PF and IV angles with the intended orientation (command with red marker) and actual position (based on the motors' position sensors). The actual orientation is represented by blue dots with error bars for PF and IV errors.

d) Discussion

This paper focused on the software and hardware improvements for the new version of the Two Axis aDaptable Ankle to use in prosthetic walking. The key method to the controller implementation is the software architecture using a real-time operating system and CANopen over EtherCAT to enable a reliable motor communication for continuous real-time control of two-directional ankle angle. For the condition with the optimal combination of sampling period error and computational load, a Proportional-Integral controller with gains of (P = 0.5, I = 0.01) and sampling period (SP) of 250 µs had averages of 249.98 µs for the actual sampling period (error offset of 0.023 µs) and 12.48% for CPU loads.

This paper serves as an example of how to set up a Raspberry Pi 4 as a real-time controller of brushless DC motors. The added real-time patch to the Linux kernel, overclocking of the CPUs, and

specific allocation of CPUs for the real-time synchronization thread all contributed to reliable motor communication. There are other recent examples of real-time motor prosthetic control (Hoover et al., 2013; Lenzi et al., 2019; Yuan et al., 2015). (Lenzi et al., 2019) presented a lightweight non-backdrivable robotic ankle prosthesis. Their motor control included a closed-loop velocity feedback computed on the main control computer, whose inputs were the motor's hall sensors and absolute encoder for the ankle angle position and whose output was a Pulse Width Modulation (PWM) voltage, to move the motor to a final range of positions within a deadband region. We considered Lenzi's method for controlling our prosthetic motors but ultimately settled on this current implementation due to its advantages of using the full capability of the motor controller to achieve high-bandwidth direct control of final motor position, trajectory control, error-correcting capabilities, and control of max motor speed and torque.

We could have used embedded hardware specifically designed for real-time systems like STM32 (Glanzer and Adamczyk, 2018) or ESP32 (Yuan et al., 2015), but settled on using a Raspberry Pi to use the Robotic Operating System (ROS), have capabilities of a graphical user interface, to be able to use a general-purpose Operating System, to be able to add other sensors and communication methods using GPIO, Bluetooth, or Wi-Fi. Instead of implementing a software controller to communicate with motor drivers through CoE, we could have used a separate CAN or EtherCAT hardware interface (e.g. PiCAT, CAN-Bus, or EPOS). These other communication interfaces have been used as a hardware bridge between the computer and a CANopen device (motor controller). At the time of the TADA development, the devices were difficult to access due to COVID restrictions, so we focused on developing our software by adapting the SOEM (Single Open EtherCAT Master) software to enable CANopen over EtherCAT communication. This reduced the hardware required for CoE implementation and provides a software controller platform that can be used beyond just prosthetic controllers. Anyone needing to communicate with motor drivers and brushless DC motors can use this software.

The TADA contains external U-joints angled wedge cams that allow the prosthetic ankle to plantarflex, dorsiflex, evert, and invert. The ankle angle movements had averages of 0.13 sec for 95%

Rise Time, 0.20 sec for Settling Time, and less than 0.1 degrees for Movement errors. These ankle angle movements had lower movement times and orientation errors than the previous version of the TADA (Adamczyk, 2020).

Given the low movement error, settling time, and rise time, the TADA can perform changes of ankle angles in one leg swing. Typical prosthetic-side leg swings are about 0.4 seconds in persons with transtibial amputations (Isakov et al., 1997). Since the movement time (~0.2 s) is much less than the average swing time, a toe-lift controller could be implemented for the TADA, so it goes from the original stance angle to 5 or 10 degrees dorsiflexed (toe-up), and then returns to the original stance angle or a new one. Toe-lift in prostheses has been broadly, though not universally, implemented (Johnson et al., 2014; Tran et al., 2022, p. 20); it would represent a valuable safety feature for this new, faster TADA. This toe-lift controller can help reduce toe-scuf (Wu and Kuo, 2016), a common issue in prosthetic walking. When the TADA is in contact with the floor, contact friction between the wedge cams makes the mechanism non-backdrivable and holds the ankle angle fixed. One future improvement is to send a torque command of 0 when the foot is on the floor, to ensure zero power consumption in the motors.

Some challenges remain in the implementation of the TADA. To have smooth and continuous ankle movements, it was important for the U-joint and wedge cams to have coincident centers. This TADA design included vertical and horizontal adjustability through shims added to the sides of the U-joint arms and below the plates that support the wedge cams. Practically, these features did reduce slop in the mechanism, though they were also challenging to use. The design also included brushless DC motors with higher speed and torque outputs. There were 2% of the movements where the motors were briefly stuck. This may have occurred due to brief off-centering of the U-joint and wedges, causing additional forces and high friction on the aluminum surfaces. The aluminum surfaces were lubricated, but over time there was some wear. Future design will use alternative materials such as steel or bronze to minimize material wear and will refine the centering mechanism.

Future work with the TADA prosthesis will center on its application as an adaptable prosthetic device to help persons with transtibial amputations adjust to various slopes, corners, and walking speeds. The first step of creating a reliable and precise control system was demonstrated in this paper. The next steps to integrate other kinematic and kinetic body-oriented sensors will be helpful in creating an adaptable system. The intention is for motion sensors (inertial measurement units, IMUs) to detect when the leg is swinging (i.e., when external load is low), to control when the mechanism changes the ankle angle. Kinetic sensors (pylon load cells and force sensing resistors) could also be useful for understanding the user's interaction with the prosthetic device and foot contact with the floor. We also plan to expand the software to include synchronous whole-body kinematic sensing using a whole-body IMU suit (Schepers et al., 2018). These sensors will enable additional control laws that aim to match the TADA's movements to the ground or provide benefits like controlling the moment at the prosthetic socket in different terrains or locomotion modes.

e) Conclusion

This paper presents a key method for motor controller implementation to control the ankle angle of the new Two Axis aDaptable Ankle (TADA), utilizing a ROS software architecture on a Raspberry Pi 4 with real-time capabilities. This approach enables continuous and reliable real-time motor communication using CANopen over EtherCAT (CoE), reducing the hardware needed for CoE implementation, and providing a versatile software controller platform applicable beyond prosthetic controllers. The software and hardware improvements to the TADA system allow quicker, more reliable, and more precise ankle angle changes compared to the original TADA. These improvements also led to higher data transmission rates, which offered modest CPU loads. These improvements aim to allow the TADA to efficiently adapt to various speeds and terrains, such as walking on slopes, stairs, or around corners.

f) References

Adamczyk, P.G., 2020. Chapter 9 - Semi-active prostheses for low-power gait adaptation, in: Dallali, H., Demircan, E., Rastgaar, M. (Eds.), Powered Prostheses. Academic Press, pp. 201–259. https://doi.org/10.1016/B978-0-12-817450-0.00009-2

Azocar, A.F., Mooney, L.M., Hargrove, L.J., Rouse, E.J., 2018. Design and Characterization of an Open-Source Robotic Leg Prosthesis, in: 2018 7th IEEE International Conference on Biomedical Robotics and Biomechatronics (Biorob). Presented at the 2018 7th IEEE International Conference on Biomedical Robotics and Biomechatronics (Biorob), pp. 111–118. https://doi.org/10.1109/BIOROB.2018.8488057

Bu-Hai, S., Yong-Zhi, W., Chuan, D., 2017. A design of real-time communication based on EtherCAT in industrial robot control system based on LinuxCNC, in: 2017 29th Chinese Control And Decision Conference (CCDC). Presented at the 2017 29th Chinese Control And Decision Conference (CCDC), pp. 5776–5780. https://doi.org/10.1109/CCDC.2017.7978198

Chen, Y., Chen, H., Zhang, M., Li, Y., 2010. The relevant research of CoE protocol in EtherCAT Industrial Ethernet, in: 2010 IEEE International Conference on Intelligent Computing and Intelligent Systems. Presented at the 2010 IEEE International Conference on Intelligent Computing and Intelligent Systems, pp. 67–70. https://doi.org/10.1109/ICICISYS.2010.5658844

Giridhar, A., Kumar, P.R., 2006. Distributed Clock Synchronization over Wireless Networks: Algorithms and Analysis, in: Proceedings of the 45th IEEE Conference on Decision and Control. Presented at the Proceedings of the 45th IEEE Conference on Decision and Control, pp. 4915–4920. https://doi.org/10.1109/CDC.2006.377325

Glanzer, E.M., Adamczyk, P.G., 2018. Design and Validation of a Semi-Active Variable Stiffness Foot Prosthesis. IEEE Transactions on Neural Systems and Rehabilitation Engineering 26, 2351–2359. https://doi.org/10.1109/TNSRE.2018.2877962

Hasan, M.K., 2021. P2P Motion: A Motion Planning Algorithm for Cyclic Synchronous Position Based Motion Control Systems, in: 2021 International Conference on Electronics, Communications and Information Technology (ICECIT). Presented at the 2021 International Conference on Electronics, Communications and Information Technology (ICECIT), pp. 1–4. https://doi.org/10.1109/ICECIT54077.2021.9641380

Hoover, C.D., Fulk, G.D., Fite, K.B., 2013. Stair Ascent With a Powered Transfemoral Prosthesis Under Direct Myoelectric Control. IEEE/ASME Transactions on Mechatronics 18, 1191–1200. https://doi.org/10.1109/TMECH.2012.2200498

Isakov, E., Burger, H., Krajnik, J., Gregoric, M., Marincek, C., 1997. Double-limb support and step-length asymmetry in below-knee amputees. Scand J Rehabil Med 29, 75–79.

Johnson, L., De Asha, A.R., Munjal, R., Kulkarni, J., Buckley, J.G., 2014. Toe clearance when walking in people with unilateral transtibial amputation: effects of passive hydraulic ankle. J Rehabil Res Dev 51, 429–437. https://doi.org/10.1682/JRRD.2013.05.0126

Lenzi, T., Cempini, M., Hargrove, L.J., Kuiken, T.A., 2019. Design, Development, and Validation of a Lightweight Nonbackdrivable Robotic Ankle Prosthesis. IEEE/ASME Transactions on Mechatronics 24, 471–482. https://doi.org/10.1109/TMECH.2019.2892609

Nichols, K.M., 2022. catkin_ws_tadaros [WWW Document]. URL https://github.com/kieran-nichols/catkin_ws_tadaros/tree/main (accessed 6.16.23).

Peekema, A., Renjewski, D., Hurst, J., 2014. Open-Source Real-Time Robot Operation and Control System for Highly Dynamic, Modular Machines. Presented at the ASME 2013 International Design Engineering Technical Conferences and Computers and Information in Engineering Conference, American Society of Mechanical Engineers Digital Collection. https://doi.org/10.1115/DETC2013-12493

Schepers, M., Giuberti, M., Bellusci, G., 2018. Xsens MVN: Consistent Tracking of Human Motion Using Inertial Sensing (No. MV0424P.A). XSens Technologies B.V. https://doi.org/10.13140/RG.2.2.22099.07205

Sung, M., Kim, K., Jin, H.-W., Kim, T., 2011. An EtherCAT-based motor drive for high precision motion systems, in: 2011 9th IEEE International Conference on Industrial Informatics. Presented at the 2011 9th IEEE

International Conference on Industrial Informatics, pp. 163–168. https://doi.org/10.1109/INDIN.2011.6034856

Tran, M., Gabert, L., Hood, S., Lenzi, T., 2022. A lightweight robotic leg prosthesis replicating the biomechanics of the knee, ankle, and toe joint. Science Robotics 7, eabo3996. https://doi.org/10.1126/scirobotics.abo3996

Voss, W., 2008. A Comprehensible Guide to Controller Area Network. Copperhill Media.

Wei, H., Shao, Zhenzhou, Huang, Z., Chen, R., Guan, Y., Tan, J., Shao, Zili, 2016. RT-ROS: A real-time ROS architecture on multi-core processors. Future Generation Computer Systems 56, 171–178. https://doi.org/10.1016/j.future.2015.05.008

Wu, A.R., Kuo, A.D., 2016. Determinants of preferred ground clearance during swing phase of human walking. Journal of Experimental Biology jeb.137356. https://doi.org/10.1242/jeb.137356

Yuan, K., Wang, Q., Wang, L., 2015. Fuzzy-Logic-Based Terrain Identification with Multisensor Fusion for Transtibial Amputees. IEEE/ASME Transactions on Mechatronics 20, 618–630. https://doi.org/10.1109/TMECH.2014.2309708

Chapter 4. Biomechanical Evaluation of the Two Axis aDaptable Ankle

Influence of Prosthetic ankle-angle and walking speed on pylon moments in the Two Axis aDaptable Ankle

Intended Journal: IEEE/ASME Journal of Mechatronics

a) Abstract

Persons with lower-limb amputations can replace their lost limbs using passive, active, or semi-active prostheses. Semi-active prostheses attempt to recover more of the biological ankle mechanics and can give functional benefits of adaptability compared to passive devices, and low cost and low weight compared to active devices. The Two Axis aDaptable Ankle (TADA) is a novel semi-active prosthetic ankle that allows for independent modulation of sagittal and frontal ankle angle (±10 degrees). This study investigates the influence of changes in frontal and sagittal TADA angles and walking speed on prosthetic pylon moments while users walk over flat ground. One unimpaired participant walked with the TADA on flat ground at three consistent self-selected speeds (slow, medium, or fast). The TADA was mounted lateral and distal to the participant's right foot using an ankle bypass orthosis. The TADA system involved dual motor control to set ankle angles, a load cell between the TADA and pylon, and a shank IMU for motion reconstruction. In addition, the participant wore an Xsens motion sensor suite for kinematic data of the lower-body movements. The control system was set up to synchronize all these systems for investigation of ankle angle and its effects on the user's biomechanics. Results showed that the peak sagittal (plantarflexor) moment and impulses increased with increased plantarflexion angles, frontal (evertor) impulses increased with increased Inversion angles, and peak frontal moments increased with increased plantarflexion angles. Also, the peak sagittal pylon moments increased with increased walking speed. The integrated system of the TADA can affect lower-body mechanical outcomes by controlling the 2D ankle angles.

b) Introduction

People with lower-limb amputations account for about one million people in the United States of America, with about 28% being individuals with transtibial amputation (TTA) (Ziegler-Graham et al., 2008). Besides the high average cost of about $81,000 for TTA amputation and associated rehabilitation services (Dillingham et al., 2005), prosthesis users spend about $1600 per year for a prosthetic device that lasts on average 1.3 years (Wanamaker et al., 2019). They have typical gait deviations and compensations of hip circumduction, toe scuffing, weak prosthetic side push-off, knee-hyperextension on the prosthetic side, higher intact side collision work, and knee osteoarthritis on the intact side. The problems of high cost and difficulty in recreating the human ankle-foot system instigate a need for improved mechanical adaptabilities and characteristics of the prostheses.

Prosthetic devices can be categorized in terms of adaptability into three main groups: passive, semi-active, and active (Adamczyk, 2020). Passive prostheses which have static mechanical properties are more widely accessible and affordable. On the other side of the adaptability spectrum, active (robotized) prostheses offer users an extensive range of biomimetic functions, including modulation of posture, impedance, and power. The disadvantages of active prostheses include their higher weight, increased size, expense, high-energy demand, and control complexity (Adamczyk, 2020). For lower-limb prostheses, semi-active devices attempt to optimize a combination of robotic and passive elements to recover some biological ankle-foot mechanics. Semi-active prostheses may not supply power to move the body when the prosthetic-side foot is on the ground like active prostheses, but it can supply minimal power to allow adaptable and adjustable walking (Glanzer and Adamczyk, 2018; Nichols and Adamczyk, 2023).

The Two Axis aDaptable Ankle (TADA) (Adamczyk, 2020) is a semi-active prosthetic ankle that allows for independent modulation of sagittal and frontal ankle angle (±10 in any combination of plantarflexion and eversion). The first design and the updated design and motor controller (Chapter 3) have been recently presented. This paper presents the instrumentation of TADA with additional kinematic

and kinetic sensors to detect lower-body mechanics and evaluate the sensitivity of the prosthetic system while the users walk over flat ground. We investigated flat-ground walking biomechanics with an unimpaired participant in preparation for use in persons with unilateral transtibial amputations. A future direction is to conduct a similar study with persons with amputations to help create a moment targeting controller to help the users adapt to various locomotion and terrain and improve socket comfort.

(Boone et al., 2013) investigated the perturbation effects of TTA prosthetic misalignment on the sagittal and frontal (coronal) socket reaction moments. These prostheses had misalignment perturbations of 3 and 6 deg rotation (adduction/abduction) and 5 and 10 mm translation (medial and lateral). Compared to normal alignment, frontal socket moments exhibited the most statistically significant differences at 30% and 75% of the stance phase for all angles and translation perturbations. Correct alignment is important for comfort and functionality of transtibial prostheses, and the results from the Boone et. al paper can be compared to how the various angles of the TADA affect the pylon moment. Also, (Molina-Rueda et al., 2014; Rueda et al., 2013) showed that participants with TTA walked with lower hip abductor and valgus (knee) moments on the prosthetic side compared to the intact side and unimpaired subjects. They also found that the thorax frontal range of motion increased, indicating mediolateral compensation to accommodate the prosthetic vs. intact frontal moments. A pylon load cell is important to help researchers understand the interaction of residual limb and the prosthetic device.

This paper aimed to create a lower-limb prosthesis that can record lower-body kinematics and kinetics and assess the sensitivity of those mechanics to different walking speeds and ankle angles using an unimpaired participant. The recording focused on the peaks and impulses of pylon moments. The sensitivity addressed the question: can we discern the relationship of the peaks and impulses pylon moment to different walking speeds and TADA angles. The main aim was to investigate the relationship of the average peaks and impulses of Plantaflexor (sagittal) and Evertor (frontal) pylon moments with changes in walking speed and TADA angles.

c) TADA Instrumentation for Control and Evaluation

The TADA's semi-active mechanism can only move during unloaded swing phases. Therefore, an integrated inertial measurement unit (IMU) was mounted to the TADA for swing-phase detection. (Formento et al., 2014) showed that gyroscopes in IMUs can be used to detect the leg swing initiation and termination in human walking; they showed that detection success for initial contact of the foot was over 93% and within 0.045 seconds of the reference comparison (in-shoe pressure measurements). We implemented a similar algorithm to detect swing phases and enable and disable the TADA's kinematic changes in real time. Typically, prosthetic-side leg swings are about 0.4 seconds (Isakov et al., 2000) and the TADA was designed to act within one swing-phase. Having a prosthetic device that can adjust to various walking speeds and locomotion mode (stairs, slopes, corners) can be advantageous for walking with lower-limb prostheses (Bartlett et al., 2019; Leestma et al., 2021).

Kinematic measurements of movement are made by two mechanisms: the internal sensing of the joint actuation motors, and an Xsens wearable inertial motion sensor lower-body suit. The motor angles are sensed by the hall effect sensors of the motor controllers and used with the known kinematics of the mechanism to compute ankle postures. The wearable Xsens system is used to estimate lower-body segment, joint, and center of mass movements. These measurements are streamed in real-time for concurrent logging in the TADA system (Schepers et al., 2018). Xsens is a suitable out-of-the-lab motion capture system to test the TADA through a variety of walking conditions like stairs, corners, and hills (Harper et al., 2020). Kinetic measurements are made by a load cell sensor (Europa+ Smart Pyramid), which attaches the prosthetic pylon to the TADA and measures axial pylon force and two-axis moments (sagittal and frontal) using Bluetooth streaming.

d) Software Architecture

The focus of building the TADA software system was to create an integrated control and data logging system that can enable a wide range of experiments with the TADA and can also readily be adapted to other prosthetic systems that have actuators and sensors. One main goal was to create an

adaptable controller that adjusts ankle angle depending on walking speed and pylon moments. We chose to use the distributed Robot Operation System (ROS) for the TADA modules (nodes) (see Fig. 21) to have a common messaging platform across multiple computer systems. The central controller of the TADA is located on a Raspberry Pi 4 computer embedded in a waist pack; it commands the motor controllers and receives signals from the kinetic sensors (Europa load cell) and kinematic sensors (IMU, Motors, and Xsens). There is also a secondary computer that receives the streamed data over a network and for data viewing and collection.

The TADA system consists of multiple ROS nodes and communication components, namely Brain, Europa, IMU, Motor and Xsens nodes, all running at 100 Hz. The Europa node serves as a multi-threaded node with custom Python software that transmits recorded values from Europa+; these signals include frontal and sagittal moments and axial force, along with the corresponding time data. It is connected to the Raspberry Pi via Bluetooth. The IMU node (Python) captures angular velocity, acceleration, detected swing/stance state, step, swing time and recorded time using the MPU6050 inertial sensor. The MPU6050 is connected to the Raspberry Pi through a wired I2C connection.

The Motor node (C/C++) receives motor commands from the Brain node and maintains communication with the two TADA motors using CANopen over EtherCAT (Chapter 3). This node is multi-threaded and has specific use of certain CPUs to maintain continuous real-time communication with the motors through the motor drivers.

The custom Xsens node (C++) operates on the secondary (remote) computer and is launched from a Windows laptop running Xsens MVN software. It is connected to the Xsens system using the Xsens Software Development Kit with custom adaptations to make it ROS-compatible. The Xsens node relays information back to the secondary computer using a multi-threaded approach, and reports various measurements, including angular and linear velocity and acceleration of each segment, joint angles, the position, velocity, and acceleration of the center of mass, and the recorded time.

The Brain node (Python) subscribes to the IMU, Europa, and Motor nodes, gathering data from these sources, and publishes motor commands to the motor node based on desired ankle angle. To capture

all the reported values from all nodes, we employ the use of *rosbag* software on the secondary computer (Windows laptop with ROS capabilities (Nichols, 2022)). The *rosbag* tool allows recording of messages across all topics and computer systems in one archive. We chose to use *rosbag* on the remote computer to reduce the embedded Raspberry Pi's processor load, to have a more capable GUI, and to quickly process and check the *rosbag* file contents for the collected nodes and topics.

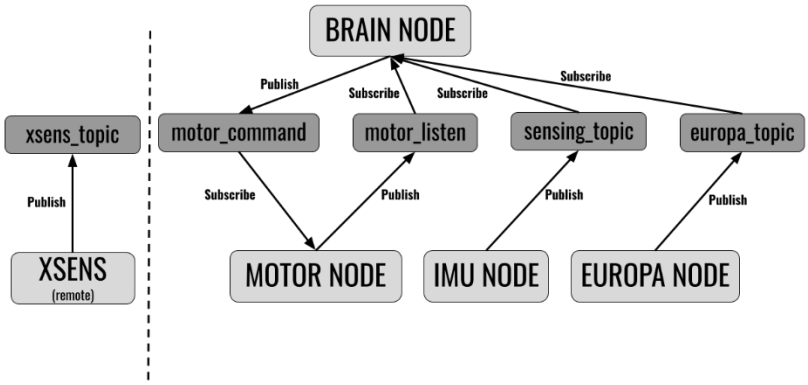

Figure 21: ROS subscribers and publishers for each message topic. The remote Xsens node runs on the secondary Windows computer. The Motor, IMU, Europa, and Brain nodes run on the Raspberry Pi.

e) Method

One unimpaired participant (female, body mass = 64.8 kg) was included in this study after giving written informed consent according to procedures approved by the University of Wisconsin-Madison Health Sciences Institutional Review Board (protocol #2020-0812). The participant was included under the criteria: comfortably walk a minimum of 30 minutes without aid and walk on level ground and ramps. Exclusion criteria included the presence of neuromuscular disorders, current injuries, or surgery within the past six months. The TADA was fitted onto the participant using a custom-made ankle bypass orthosis, where the TADA is mounted laterally and distally to the participant's right foot. The TADA was aligned in a neutral configuration (comfortable static sagittal angle of foot to lower leg and no inversion/eversion). The participant was then given a short (10 minute) acclimation period to walk freely through the hallway while the TADA was adjusted to its most extreme pure-axis angles (10 degrees in dorsiflexion (DF), plantarflexion (PF), eversion (EV), and inversion (IV)), to gain experience.

The participant then walked on flat ground at three consistent self-selected speeds (slow, medium, fast). The participant walked with 17 different TADA stance angles including neutral (0, 0 deg for PF, IV), purely sagittal angles (5 and 10 deg PF and DF), purely frontal angles (5 and 10 deg IV and EV), and combined angles with magnitudes of (2.5 and 5 deg, equal in PF/DF and IV/EV). The participant was instructed to walk continuously in a flat hallway. The TADA alternated between the neutral angle for 5 steps and a non-neutral angle for 6 – 10 steps. A random number between 0 and 4 was added to 6 steps in the non-neutral angle condition, to reduce the likelihood of the participant anticipating the TADA angle changes. The trial was paused after the participant walked for 4 conditions of the neutral angle and 3 conditions of the non-neutral angles, to allow the participant to turn around at the ends of the hallway. For the medium speed, there were 17 different TADA angles. For the slow and fast speeds, there were 5 different angles: neutral and the most extreme pure-axis angles (10 deg PF, IV, DF, and EV).

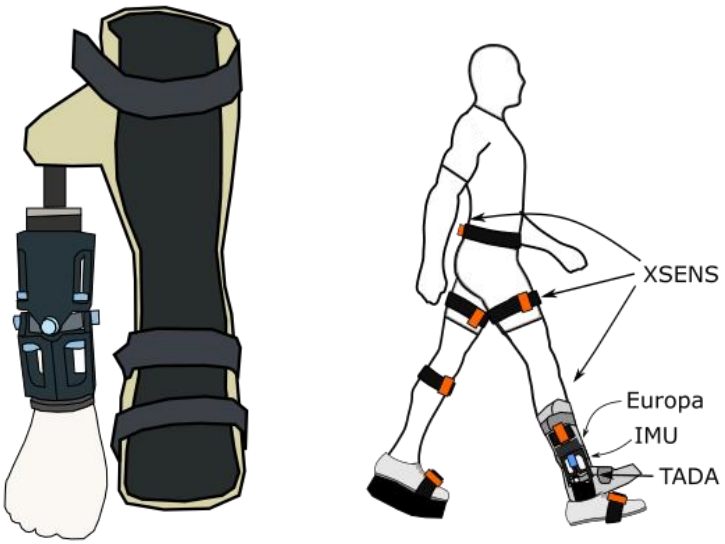

Figure 22: (Left) Front view of the custom-made ankle bypass orthosis connected to the TADA. (Right) Full experimental setup. The participant has the lower body Xsens suit, pylon load cell (Europa+), IMU, and TADA foot. A foam lift (5 cm) is added to the other shoe to match the height.

f) Data analysis

Walking speed from the Xsens node and TADA ankle angles from the Brain node were used as the independent variables of the main hypothesis. The peak pylon moments and moment impulses through the stance phase (sagittal and frontal) were used as the dependent variables. The Europa was

oriented such that plantarflexor and evertor moments when applied to the pyramid side of the Europa were positive when mounted on the right foot; values were calibrated by hanging static known weights at known distances from the load cell center in static trials. Secondary dependent variables of hip and knee angles from Xsens were also investigated.

For the kinetic data, the sagittal and frontal moments were low pass filtered (cutoff of 6 Hz) and the values were normalized by dividing by body mass. The units for peak moment and impulse were Nm/kg and Nm.s/kg, respectively. Then the sagittal and frontal averages for peak moment and impulses for each speed and TADA angle were found for the middle three strides of the 6 – 10 steps while the subject walked with the TADA. The Europa signal was found to have a time delay due to buffering; it was time-shifted backwards by roughly 2 seconds and verified that the kinetic and kinematic data were from matching strides. For the kinematic data, sagittal and frontal hip and knee angles from Xsens, and ankle angles were calculated in the Brain node.

For the medium speed, linear regressions were performed for the peaks and impulses of the sagittal and frontal moments for pure sagittal ankle angles (only plantarflexion) and pure frontal ankle angles (only IV). The slope, intercept, r^2 value, and p values are reported in Tables 8 and 9.

g) Results

The results consist of processed data from the IMU, Europa, and Xsens nodes. The participant walked at three self-selected speeds with neutral and various non-neutral TADA angles. At the medium walking speed, the TADA moved to purely PF, purely IV, and combinations of PF and IV ankle angles. At slow and fast, the TADA moved in purely PF and purely IV angles. The results start with Figure 23, showing time-based moment data for the 3 speeds while walking with the TADA angle of PF=10, IV=0, starting with one heel-strike and ending with the following heel-strike.

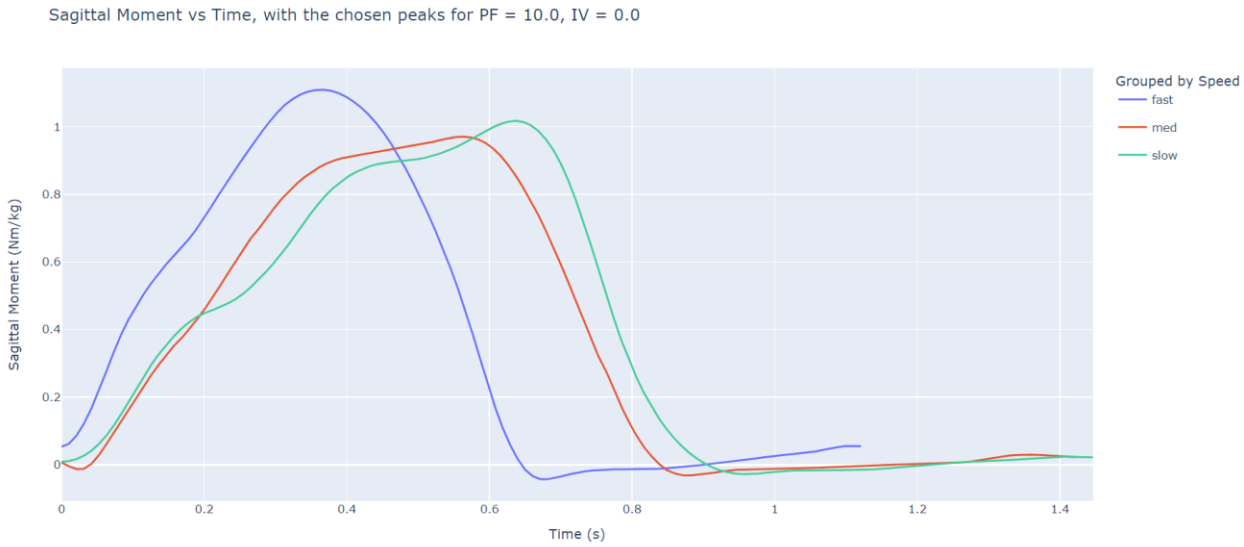

Figure 23: plot of sagittal moment vs time over one representative stride when the TADA was plantarflexed to 10 degrees. The fast moment profile had the largest peak Plantarflexor moment compared to other speeds, but the smallest stance time (when the moment is approximately larger than 0). The slow moment profile had a smaller peak than the fast profile and had the largest stance and stride times.

For this TADA angle (Figure 23), peak sagittal moments were lower and stride time were higher (time from one heel strike to another) for the slow and medium speeds compared to the fast speed. Stance time is a factor in impulse calculation, and impulse can give more information about the time and average moment characteristics than peak moment can. Figure 24 shows the frontal moment profiles for the TADA at 10 degrees PF for multiple walking speeds. The peak frontal moment (evertor) increases with increasing walking speed.

Figure 24: plot of frontal moment vs time over one representative stride when the TADA was plantarflexed to 10 degrees. It shows the frontal moment peaks and stances time increased with increasing speed for this TADA angle. The moment profiles are shown across time instead of as a percentage of stride (0 to 100% of heel-strike to heel-strike) to illustrate the effect of speed on stance and stride times.

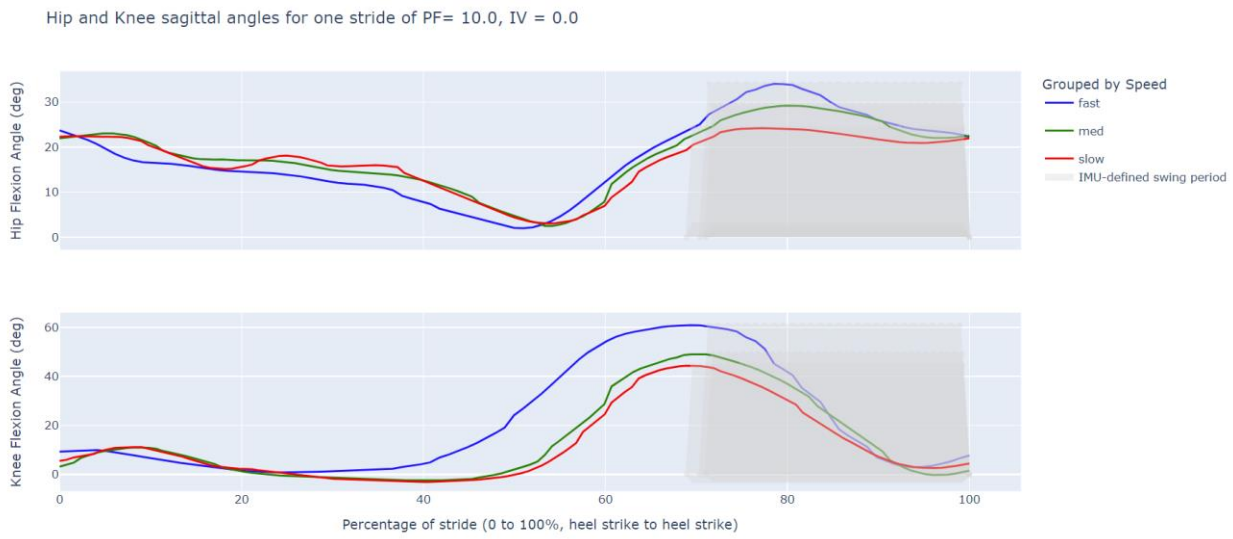

Figure 25: Plots of hip and knee sagittal angles for one representative stride when the TADA was plantarflexed to 10 degrees. These angles were from the Xsens node. The subplots also include grey regions which represent the swing period from the IMU swing detection.

In Figure 25, there were changes of hip and knee angles provided by Xsens for different speeds with the TADA angle of 10 degrees PF. The grey colored region represents conservative estimates of swing period based on the IMU signals. It is conservative to give the TADA motors sufficient time to move when the foot is not in contact with the floor. There is an upward vertical shift of the knee angles profiles for faster speeds from around mid-stance (40%) to mid-swing (85%), indicating a more flexed knee (less straight with faster speeds). Also, the peak knee and hip flexions increased with increases in walking speed.

Sagittal Moment	Metric	Slope ($*10^{-3}$) Peak units: Nm/kg/deg Impulse units: Nm/kg/deg*s	Intercept Peak units: Nm/kg Impulse units: Nm/kg*s	r^2 value	P-value
Purely changes in Inversion angles	Peak	4.14	0.917	0.400	0.253
	Impulse	2.28	0.360	0.478	0.195
Purely changes in Plantarflexion angles	**Peak**	**10.2**	**0.915**	**0.932**	**0.002**
	Impulse	**13.4**	**0.0381**	**0.897**	**0.004**

Frontal Moment	Metric	Slope ($*10^{-3}$) Peak units: Nm/kg/deg Impulse units: Nm/kg/deg*s	Intercept Peak units: Nm/kg Impulse units: Nm/kg*s	r^2 value	P-value
Purely changes in Inversion angles	**Peak**	**5.00**	**0.199**	**0.964**	**0.003**
	Impulse	**3.47**	**0.080**	**0.974**	**0.002**
Purely changes in Plantarflexion angles	**Peak**	**3.93**	**0.194**	**0.910**	**0.003**
	Impulse	1.05	0.081	0.174	0.410

Table 7 and 8: the slopes, intercepts, r^2 values, and p-values of the trends of the sagittal and frontal moments with changes in purely inversion and plantarflexion angles for the TADA angles for medium self-selected speed. The bolded text highlights the metrics that had high r^2 and low p values, above 0.85 and below 0.05, respectively.

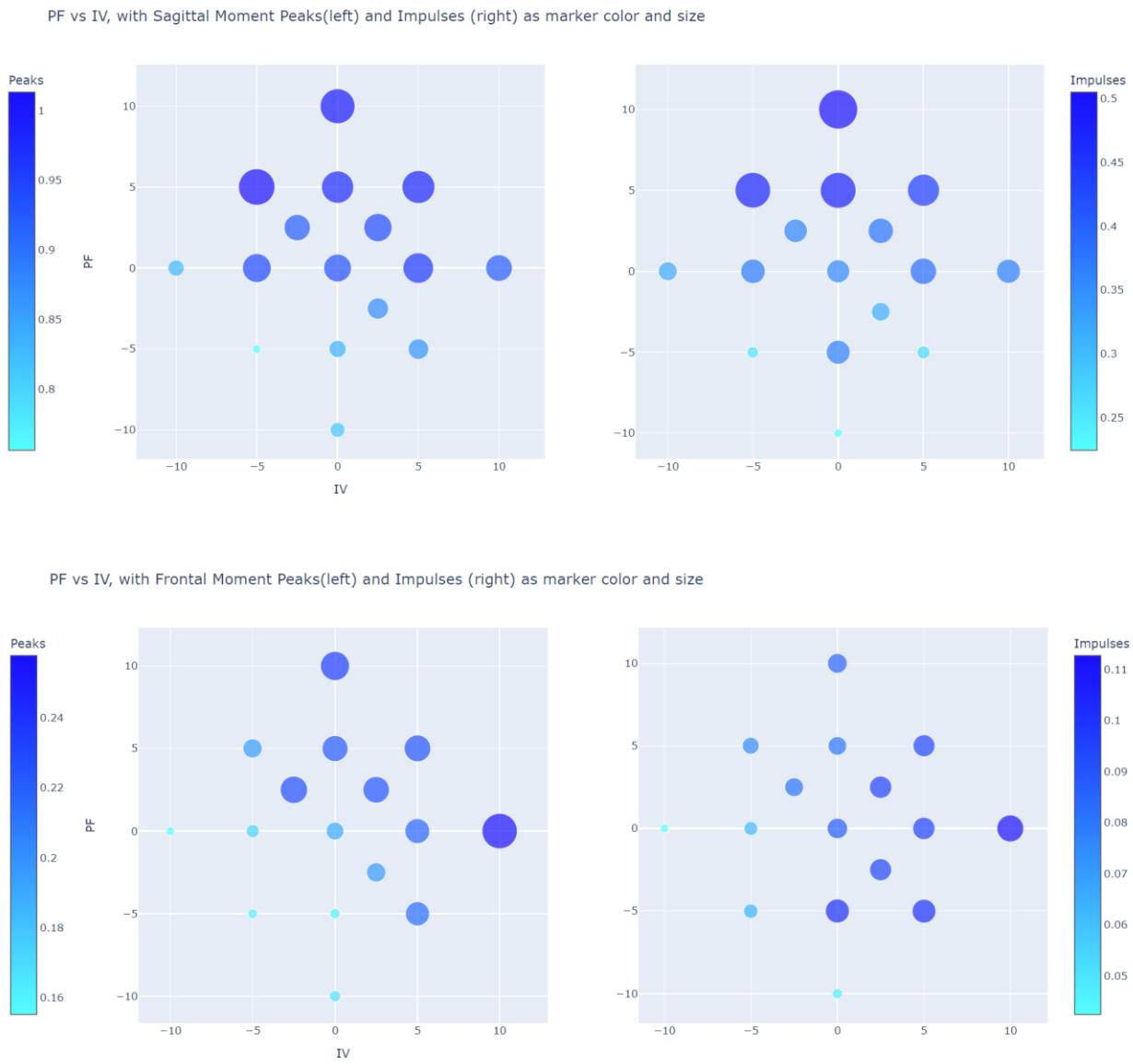

Figures 26 and 27: Plots of Sagittal (Top) and Frontal Moments (Bottom) for their respective PF and IV angles for the participant walking at medium speed. The left subplots are for peak pylon moments and the right subplots for pylon impulses. There is data missing for the PF, IV of -2.5,-2.5 due to a missed trial.

For medium walking speed, Table 7 and 8 and Figures 26 and 27 show strong trends of pure PF ankle angles leading to increased Plantarflexor (sagittal) pylon moment peaks ($r^2 = 0.932$) and impulses ($r^2 = 0.897$). There were also strong trends of pure IV ankle angles leading to increased pylon frontal moment peaks and impulses ($r^2 = 0.964$ and 0.974) and there were increased peaks for frontal pylon

moments with increased PF angles ($r^2 = 0.910$).

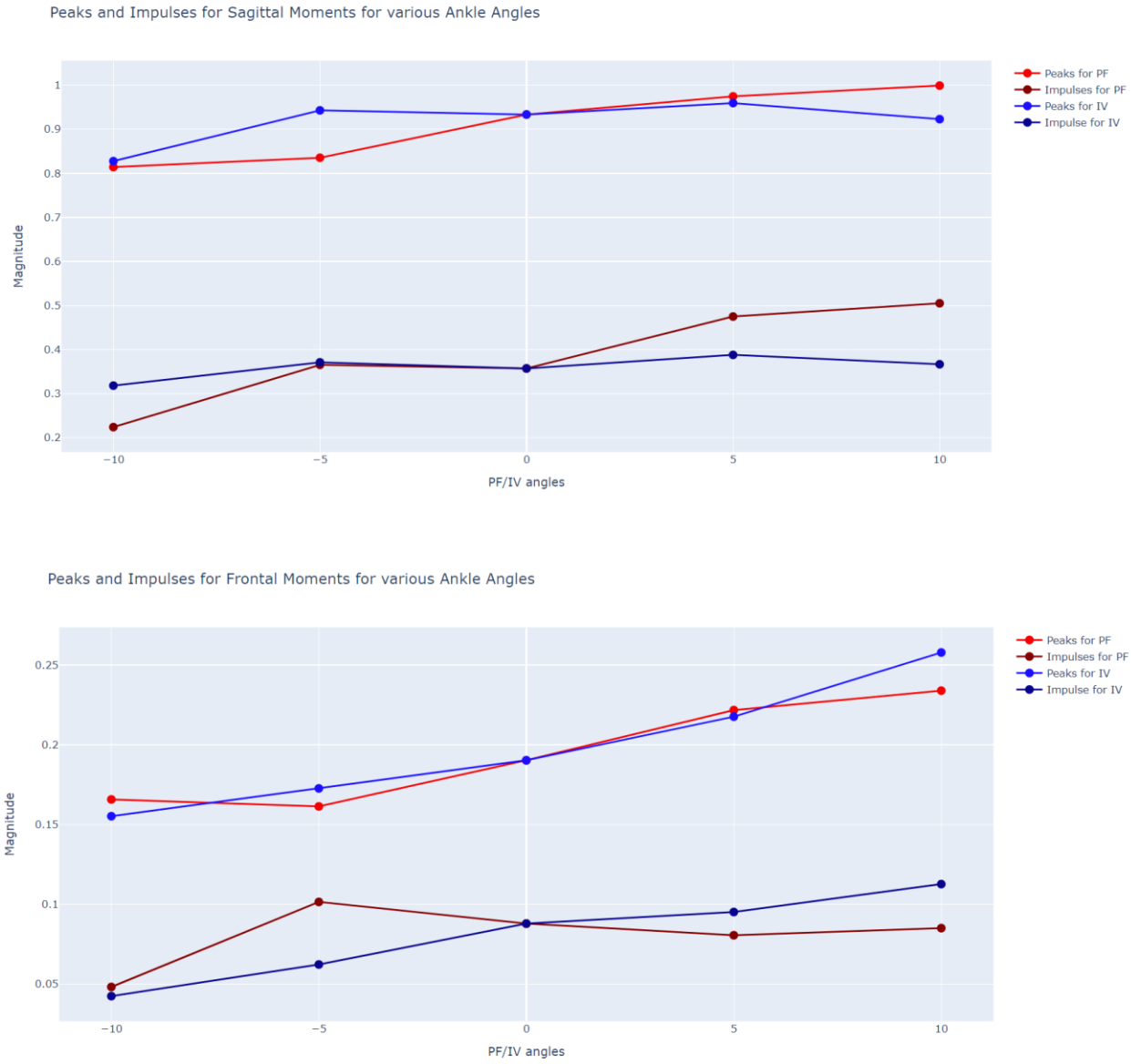

Figures 28 and 29: Regression plots of Sagittal (Top) and Frontal Moments (Bottom) for their respective PF and IV angles for the participant walking at medium speed. The lighter colored lines are for peak pylon moments and the darker colored lines for pylon impulses.

Figures 28 and 29 (above) show another graphical representation of the trends of the sagittal and frontal moments for purely changes in PF and IV of the TADA. There were generally positive trends of larger magnitudes for peaks and impulses for sagittal and frontal moments with increases in IV and PF ankle angles (more Inverted and more Plantarflexed ankle).

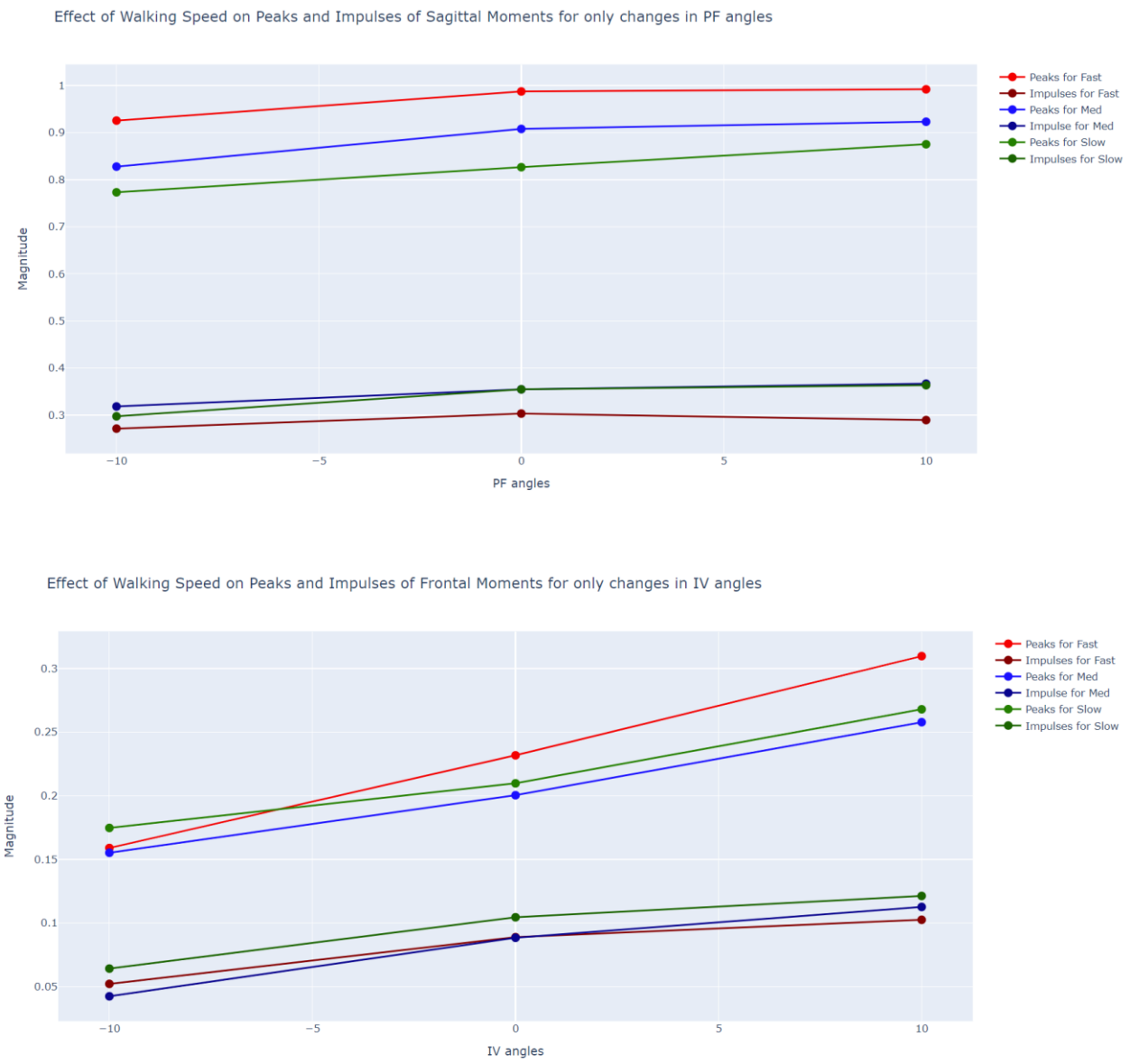

Figures 30 and 31: Regression plots of Sagittal (Top) and Frontal Moments (Bottom) for each speed. The lighter colored lines are for peak pylon moments and the darker colored lines for pylon impulses.

In Figures 30 and 31, there are general trends of sagittal moments with sagittal angles and frontal moments with frontal angles for the three walking speeds. There was some variety in differences of slope and vertical offsets of these trends across speeds, but a general summary is that peaks and impulses of sagittal and frontal moments increased with increased speed and increased PF. Additionally, increased peaks and impulses of Evertor moments increased with increased speed and increased IV. More trials and participants are needed to draw statistical conclusions about the differences of the various regression slopes and vertical offsets among the peaks and impulses of the moment data across walking speeds.

h) Discussion

a. Device Purpose:

The purpose of this paper is to present the kinematic and kinetic detection and sensitivity of Two Axis aDaptable Ankle (TADA) for various walking speeds and ankle angles. This study investigated the effect of walking speed and ankle angle on ankle pylon moments as a first step to building a controller that can adapt ankle angle to a variety of locomotive conditions like walking on slopes, stairs, around corners. The main advantages of the current implementation of the TADA system are the centralized software controller for the prosthetic ankle with independent power and functionality, an off-loaded computational processing for the Xsens motion capture system and data saving to a secondary computer, and the ability to view and save time-synchronized data into one file from the multiple devices connected to the TADA.

b. Device Evaluation:

Previous testing (Chapter 3) showed that the device is capable of successfully adjusting ankle orientation of subjects within one step while collecting data from various sensors, given that prosthetic-side leg swings are typically 0.4 seconds (Isakov et al., 2000). On average, the motors move the TADA within 0.1 degrees of the commanded angle and within 0.2 seconds. For this study, the signals from the Europa node were time-shifted by 2 seconds to synchronize the moment data to the other kinematic data post processing. This 2 second delay occurred due to the delay in the Bluetooth message in the raspberry pi receiving data from the Europa device and potentially with the nature of the software buffer. Future software development of the Europa node could reduce this delay to enable the use of the most recent step for a moment-based feedback controller for the TADA. The kinematic signals from the Xsens, IMU, and motors were synchronized, and preliminary results were shown in the results section.

The results showed that the average peaks and impulses of Plantarflexor (sagittal) and Evertor (frontal) pylon moments were higher at more plantarflexed and inverted ankle angles and higher for

higher walking speeds. Additionally, the peak frontal moments were shown to be higher for more plantarflexed angles.

c. Experimental pilot study:

The pylon moments of the pilot participant walking with the ankle bypass orthosis and TADA were evaluated through various speeds and ankle angles over level ground walking. A positive sagittal moment relates to the ground reaction force passing in front of the load cell, causing a Plantarflexor moment to be applied to the TADA (Boone et al., 2013). In other papers about prosthetic alignment (Hashimoto et al., 2021), the peak plantarflexor moment increased with more extension of the socket (which was related to more plantarflexion of their prosthesis). Our results (Table 6) presented the consistent effects to the Hashimoto study for the relationship of peak plantarflexor moment with plantarflexion.

In the frontal plane, a positive frontal moment indicates an Evertor moment is applied to the TADA (see Figure 24). Results (Table 8) showed that a *more inverted ankle led increased peak evertor moment (and impulses),* which was consistent with the trends seen in the other literature (Hashimoto et al., 2021), but the average value of their frontal pylon moment was invertor. They observed *increased invertor moments (also called varus moments) with more everted ankle angles*. The average value of evertor moment for this study (instead of invertor) is likely due to lateral placement of the TADA due to the ankle bypass orthosis (issue described in the Limitations).

Our participant showed that the sagittal pylon moment peaks were largest in Plantarflexed angles and smallest in Dorsiflexed and Everted angles. The peak values of the sagittal pylon moment of this paper (0.7 – 1.0 Nm/kg) were close to the peaks from other literature (0.62 – 0.81 Nm/kg) with ankle adaptors (Hashimoto et al., 2021; Kobayashi et al., 2013). In prosthetic walking, excessive peak plantarflexor moment at the socket can translate to high peak pressures on the patellar tendon and distal posterior regions of the residual limb when persons with amputations use conventional prostheses (LaPre et al., 2017). LaPre's objective was to reduce the high moment transfer through the socket by realigning

the socket center to be closer to the line of action of the ground reaction force during midstance. Reducing these peak moments on the socket can be beneficial to improving comfort (Boone et al., 2013), however, if we are aiming to reduce peak moments and maintain balanced walking, we need to consider an acceptable range of both peak pylon moments and pylon impulses. Pylon moment impulses are important to consider as they give information about the average moment for stance period. A moment target controller can be developed with the TADA to control ankle angles as a function of peak pylon moments, pylon moment impulse, and walking speed.

d. Future work:

In the future, a moment targeting control algorithm can attempt to alter the peaks and impulses of the pylon moments. One idea will be to first set a range of acceptable peaks and impulses based on walking with a neutral TADA angle at a self-selected walking speed. Then the TADA will adjust the ankle angle if the average values for the last three strides is outside of that range for both peak pylon moments and pylon impulses. Walking speed can be derived from the TADA's IMU using a motion reconstruction method for walking speed and foot movement previously published by our lab (Glanzer and Adamczyk, 2018). The Xsens also gives valuable insight into lower-body joint angles and a way to validate the motion reconstruction.

This moment targeting control could be useful for adjusting ankle angles while walking at different speeds, on slopes, stairs, and around corners. For a participant walking on level ground in the ankle bypass orthosis, if peak pylon moments and impulses for sagittal and frontal moments are too high, the TADA could move the ankle angle to be more dorsiflexed and/or everted. The purpose would be to reduce unnecessarily high peak pylon moments causing high pressure regions on the orthosis (which can be similar to socket pressures). If the peaks and impulse are too low, the TADA could become more plantarflexed and inverted. The controller can also be helpful for persons with amputations once we confirm the quantitative relationship of speed and TADA angle to frontal and sagittal peak pylon moment

on persons with transtibial amputations. The goal of moment targeting control would be to lower the socket moments by adjusting ankle angle without favoring the other leg.

Additionally, future directions of study could include investigations using whole-body angular momentum, balance augmentation, and transient and steady-state responses in the pylon moments/joint angles in steps immediately after foot angle changes. This research also feeds into research on neural interfaces for volitional control of prostheses. If integrated with such control, a user would be able to directly manipulate the ankle angle of the TADA using neural signal based off of obstacles in their vision and be able to sense the ankle angle.

e. Limitations:

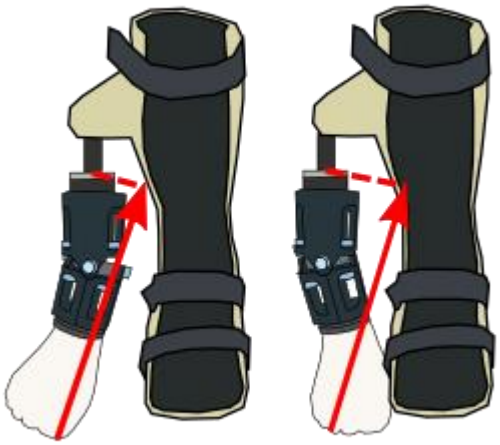

Figure 32: graphical representation of the moment arms of the ground reaction force and pylon-center for the ankle bypass orthosis for the everted TADA (left) and inverted TADA (right).

A current limitation of this study is our sample size of one participant; it would be beneficial to collect data on additional subjects to further evaluate our system. Another limitation is the ankle bypass orthosis significantly shifts the pylon laterally, which changes the frontal moment direction to be evertor. In persons with amputations, frontal moments were on average invertor moments (Hashimoto et al., 2021). The lateral placement of the TADA from to the anatomical knee joint contributed to the consistent evertor moment due to lateral location of the center of pressure of the foot from the knee. This effect causes a larger moment arm with similar GRF magnitude, and may also increase the medially-directed component of the GRF, increasing the evertor torque as seen in Figure 32. These issues would not be present in persons with transtibial amputations as the foot would be in the correct mediolateral location.

f. Conclusion

The integrated system of the Two Axis aDaptable Ankle (TADA) can detect lower-body mechanical outcomes using a combination of a shank inertial sensor, a pylon load cell, and a Xsens lower-body sensor suit, and can evaluate the effect of ankle angle and walking speed on sagittal and frontal pylon moments. For an unimpaired participant walking with the TADA using an ankle bypass orthosis, the peaks and impulses of sagittal and frontal pylon moment increased with increased plantarflexion and inversion, respectively. Automated, real-time moment-targeting control could allow users to adapt to terrain conditions, such as stairs and ramps, or to alter biomechanical loads like undesirable socket moments.

i) References

Adamczyk, P.G., 2020. Chapter 9 - Semi-active prostheses for low-power gait adaptation, in: Dallali, H., Demircan, E., Rastgaar, M. (Eds.), Powered Prostheses. Academic Press, pp. 201–259. https://doi.org/10.1016/B978-0-12-817450-0.00009-2

Bartlett, H.L., Lawson, B.E., Goldfarb, M., 2019. Design, Control, and Preliminary Assessment of a Multifunctional Semipowered Ankle Prosthesis. IEEE/ASME Transactions on Mechatronics 24, 1532–1540. https://doi.org/10.1109/TMECH.2019.2918685

Boone, D.A., Kobayashi, T., Chou, T.G., Arabian, A.K., Coleman, K.L., Orendurff, M.S., Zhang, M., 2013. Influence of malalignment on socket reaction moments during gait in amputees with transtibial prostheses. Gait & Posture 37, 620–626. https://doi.org/10.1016/j.gaitpost.2012.10.002

Dillingham, T.R., Pezzin, L.E., Shore, A.D., 2005. Reamputation, mortality, and health care costs among persons with dysvascular lower-limb amputations. Archives of Physical Medicine and Rehabilitation 86, 480–486. https://doi.org/10.1016/j.apmr.2004.06.072

Formento, P.C., Acevedo, R., Ghoussayni, S., Ewins, D., 2014. Gait Event Detection during Stair Walking Using a Rate Gyroscope. Sensors 14, 5470–5485. https://doi.org/10.3390/s140305470

Glanzer, E.M., Adamczyk, P.G., 2018. Design and Validation of a Semi-Active Variable Stiffness Foot Prosthesis. IEEE Transactions on Neural Systems and Rehabilitation Engineering 26, 2351–2359. https://doi.org/10.1109/TNSRE.2018.2877962

Harper, S.E., Roembke, R.A., Zunker, J.D., Thelen, D.G., Adamczyk, P.G., 2020. Wearable Tendon Kinetics. Sensors 20, 4805. https://doi.org/10.3390/s20174805

Hashimoto, H., Kobayashi, T., Kataoka, M., Okuda, K., 2021. Influence of coronal and sagittal prosthetic foot alignment on socket reaction moments in transtibial prostheses during walking. Gait & Posture 90, 252–260. https://doi.org/10.1016/j.gaitpost.2021.08.011

Isakov, E., Keren, O., Benjuya, N., 2000. Trans-tibial amputee gait: Time-distance parameters and EMG activity. Prosthetics and Orthotics International 24, 216–220. https://doi.org/10.1080/03093640008726550

Kobayashi, T., Orendurff, M.S., Zhang, M., Boone, D.A., 2013. Effect of alignment changes on sagittal and coronal socket reaction moment interactions in transtibial prostheses. Journal of Biomechanics 46, 1343–1350. https://doi.org/10.1016/j.jbiomech.2013.01.026

LaPre, A.K., Wedge, R.D., Umberger, B.R., Sup, F.C., 2017. Preliminary study of a robotic foot-ankle prosthesis with active alignment, in: 2017 International Conference on Rehabilitation Robotics

(ICORR). Presented at the 2017 International Conference on Rehabilitation Robotics (ICORR), pp. 1299–1304. https://doi.org/10.1109/ICORR.2017.8009428

Leestma, J.K., Fehr, K.H., Adamczyk, P.G., 2021. Adapting Semi-Active Prostheses to Real-World Movements: Sensing and Controlling the Dynamic Mean Ankle Moment Arm with a Variable-Stiffness Foot on Ramps and Stairs. Sensors 21, 6009. https://doi.org/10.3390/s21186009

Molina-Rueda, F., Alguacil-Diego, I.M., Cuesta-Gómez, A., Iglesias-Giménez, J., Martín-Vivaldi, A., Miangolarra-Page, J.C., 2014. Thorax, pelvis and hip pattern in the frontal plane during walking in unilateral transtibial amputees: biomechanical analysis. Braz. J. Phys. Ther. 18, 252–258. https://doi.org/10.1590/bjpt-rbf.2014.0032

Nichols, K.M., 2022. catkin_ws_remote [WWW Document]. URL https://github.com/kieran-nichols/catkin_ws_remote/tree/main (accessed 6.16.23).

Nichols, K.M., Adamczyk, P.G., 2023. Sensitivity of lower-limb joint mechanics to prosthetic forefoot stiffness with a variable stiffness foot in level-ground walking. Journal of Biomechanics 147, 111436. https://doi.org/10.1016/j.jbiomech.2023.111436

Rueda, F.M., Diego, I.M.A., Sánchez, A.M., Tejada, M.C., Montero, F.M.R., Page, J.C.M., 2013. Knee and hip internal moments and upper-body kinematics in the frontal plane in unilateral transtibial amputees. Gait & Posture 37, 436–439. https://doi.org/10.1016/j.gaitpost.2012.08.019

Schepers, M., Giuberti, M., Bellusci, G., 2018. Xsens MVN: Consistent Tracking of Human Motion Using Inertial Sensing (No. MV0424P.A). XSens Technologies B.V. https://doi.org/10.13140/RG.2.2.22099.07205

Wanamaker, A.B., Andridge, R.R., Chaudhari, A.M.W., 2019. Projected Health Care Associated Costs of Workplace-Related Traumatic Amputation After 10, 15, and 20 Years: Part I: Lower Limb. JPO: Journal of Prosthetics and Orthotics 31, 189–198. https://doi.org/10.1097/JPO.0000000000000260

Ziegler-Graham, K., MacKenzie, E.J., Ephraim, P.L., Travison, T.G., Brookmeyer, R., 2008. Estimating the Prevalence of Limb Loss in the United States: 2005 to 2050. Archives of Physical Medicine and Rehabilitation 89, 422–429. https://doi.org/10.1016/j.apmr.2007.11.005

Chapter 5. Discussion

(a) Introduction and Overview of Research Questions

My dissertation focused on the development and application of two Semi-Active Prosthetic Foot-Ankle Systems: Variable Stiffness Foot (VSF) and Two Axis aDaptable Ankle (TADA). This section focuses on a detailed summary of my work, helpful proposals for future directions for the TADA project, and an overview of my scientific and engineering contributions. The main research questions of my dissertation were as follows.

i) What are the biomechanical effects of modulating forefoot stiffness on knee and ankle mechanics on persons with transtibial amputations walking with the Variable Stiffness Foot?

ii) How to implement a real-time motor control for the new Two Axis aDaptable Ankle using a Raspberry Pi, ROS, and CANopen over EtherCAT?

iii) What is the Influence of Prosthetic ankle-angle and walking speed on Pylon moments of the Two Axis aDaptable Ankle?

(b) Summary of My Dissertation Work

(i) Biomechanical Analysis of the Variable Stiffness Foot

My dissertation work started with the VSF project (Chapter 2), where I completed the data collection for seven persons with transtibial amputations walking with the VSF in our motion capture lab. They walked with a self-selected speed for three different VSF stiffnesses (low, medium, and high). We investigated the knee and ankle angles and moments, prosthetic power flow and energy, and magnitude and offloading of the vertical ground reaction force under the prosthetic side. We published that a less stiff VSF led to higher ankle angle range of motion, lower peak moments for the ankle, knee, and hip, higher prosthetic energy storage and return and power, which may help reduce joint overuse in persons with transtibial amputations. This manuscript [70] addressed my first research question: "*What are the biomechanical effects of modulating forefoot stiffness on knee and ankle mechanics on persons with*

transtibial amputations walking with the Variable Stiffness Foot." This study included data collection using separate streams from reconstructed movement from motion capture cameras, two force plates, a pylon-mounted load cell, and an inertial measurement unit on the foot.

A time synchronization issue with the motion capture and force plate data required a post-processing correction based on the time point where the vertical force was close to 0 and the moment the toe left the floor. The load cell data were synchronized during post-processing to the other signals by aligning the force trace with the motion trace for the time periods when the subject tapped their foot a few times before each trial. Another difficulty was additional time spent synchronizing the multiple data files and accommodating issues of not consistently turning on and off the devices between trials. It was also difficult to share our motor control and lower-leg motion reconstruction software development as our software was compiled on an embedded system specifically catered to the VSF hardware.

(ii) Importance of an Integrated System for Prosthetic Devices

I then transitioned to work on the TADA. I entered the project to continue my work in prosthetic development, reduce the chances of synchronization issues, and have a centralized and generalizable controller to communicate with the motors and sensors usable by other collaborators or people curious about prosthetic or robotic systems.

(iii) Connection to my collaborative work in Biomechanical Simulations, the original Two Axis aDaptable Ankle, and the Wearables Review manuscripts

There was an original design paper (manuscript in progress) that I inherited from the previous TADA work. The previous generation of the TADA was built to control ankle angle using an inside U-joint and brushed DC motors which acted on the gears attached to the outside of the angled cams. It used a shifted bang-bang velocity-feedback controller. I am assisting with finishing the manuscript for resubmission and translating its software into the new TADA controller.

Also, I collaborated in the publications for the biomechanical simulations to replicate gait kinematics and the ground reaction force (resultant force and center of pressure) using the VSF [71,72] and

presentation [73] of a simulation-based analysis of the interface dynamics between the prosthetic socket and residual limb in walking with the VSF. The manuscript investigating the socket interface dynamics contributed a helpful foundation for simulation approaches to improving prosthetic socket issues for persons walking with transtibial prostheses. These simulation-based collaboration papers helped extend the application uses of the VSF and initialize the development of the TADA. The review manuscript (submitted) focused on presenting current literature on wearable sensing for understanding and influencing human movement in ecological (out-of-the-lab) contexts.

(iv) Design of the New Two Axis aDaptable Ankle Hardware and Software

The new TADA (Chapter 3) needed lighter, faster, and stronger motors to have a more precise and prosthetic responsive ankle. After exploring many computer boards, motor models, and motor controllers, we used the Robotic Operating System (ROS) on a Raspberry Pi 4 to control the ankle angle of the TADA using brushless Direct Current motors. To communicate with these motors, we used position motor control utilizing CANopen over EtherCAT communication between the Raspberry Pi and motor controllers. The Raspberry Pi was chosen as the central controller for the prosthetic system with independent functionality. Independence means that the TADA can function on its own, but external computers can be used to view the data and send commands to the Raspberry Pi but were not necessary for the TADA to operate. ROS was chosen as it allows for modular customization of its programs and has a built-in messaging system to communicate among multiple programs written in Python and C++ and among multiple computers over the same Wi-Fi connection.

Additionally, my lab mates and I updated the mechanical design of the TADA to have an outside U-joint, internal direct-drive motors, and angled cylindrical cams with a combination of machined aluminum and 3D printed material. We found (Chapter 3) that our software and hardware implementation to control the TADA's movement allowed quicker movement times, more reliable and precise ankle angle changes, and higher data transmission rates compared to the original TADA. These

results answered my second research question: "*How to implement a real-time motor control for the New Two Axis aDaptable Ankle using a Raspberry Pi, ROS, and CANopen over EtherCAT?"*

(v) Integrated system for the New Two Axis aDaptable Ankle

Building onto the ROS architecture (Chapter 4), custom programs for a shank-based inertial measurement unit (IMU) for prosthetic leg swing detection, load cell (Europa) for pylon moments, and Xsens lower-data motion capture suit for joint, segment, and center of mass data. The programs for the IMU, motors, and Europa were hosted on the Raspberry Pi and were controlled by a governing program called the "Brain." The Brain allowed the automated execution of experiments and terminal-based user interaction.

The Xsens program was executed using a secondary computer to offload the computation burden on Raspberry Pi. This secondary computer was also used to view the Raspberry Pi's GUI and send commands to the TADA to start and end experiments and troubleshoot the TADA system. The data collection used a ROS tool, "*rosbag*" to save data for all the devices into one file, with timestamps dedicated to when each program received data from their devices. This data collection method allowed the data to be easily synchronized in post-processing and allowed for real-time feedback.

(vi) Creation of an Evaluation Prosthetic Tool for out-of-the-lab experiments

Using the integrated TADA system, we performed a pilot study (Chapter 4) of an unimpaired person walking at three self-selected speeds (slow, medium, and fast) with the TADA attached to an ankle bypass orthosis. Results showed that peak sagittal moment (plantarflexor) and impulses increased with increased plantarflexion angles, frontal peaks and impulses (evertor) increased with increased inversion angles, and peak evertor moments increased with increased plantarflexion angles. Also, the peak sagittal pylon moments generally increased with increased walking speed. This pilot study showed that pylon moments can be influenced by changes in walking speed and TADA angles and addressed my third and last research question, *"What is the Influence of Prosthetic ankle-angle and walking speed on Pylon moments of the Two Axis aDaptable Ankle?"*

In the future, the TADA can be tested with persons with transtibial amputations to investigate the inter-subject sensitivity parameters of the influence of walking speed and TADA angles on pylon moment. These sensitivity parameters can be important for building an adaptable prosthetic ankle that controls ankle angle as a function of walking speed or pylon moments.

The TADA can be used for data collection both in the lab and for out-of-the-lab experiments. It has an integrated system with motors and multiple sensors that can first be used as an evaluative tool for prosthetic walking, and then be developed into an adaptable prosthetic ankle.

(c) Proposals for Future Work with the TADA

(i) Toe-lift Control

This controller will aim to lift the toe by dorsiflexing the TADA during every swing period of the prosthetic side and returning it to the previous stance ankle angle before the leg contacts the ground. The main metrics to consider are minimum toe clearance and stance knee angles. The results of Chapter 3 support that the TADA is fast enough to dorsiflex and return to the original stance angle during swing. The commanded movement time and range of dorsiflexion of the toe lift could depend on ground slope or stairs conditions. An experiment can be designed with unimpaired participants walking on flat, sloped, and stairs with the ankle bypass orthosis and TADA. The toe-lift controller will use the IMU swing detection software and could be designed to move from neutral (0 degrees dorsiflexion) to various angles of dorsiflexion, and back to neutral. Walking with various ground slopes and mid-swing dorsiflexion angles may affect prosthetic-side swing time and the minimum toe clearance.

To motivate the evaluative metrics to assess toe-lift, previous experiments on other semi-active prostheses with a toe-lift controller showed increased the minimum foot clearance on flat ground[74,75], increased early stance prosthetic-side knee flexion angles for ramp ascent (closer to unimpaired walking)[76], and increased median of the toe clearance with a lower coefficient of variability for descending and ascending ramps, compared to passive prostheses[73]. Also, Asha and Buckley[77] showed that minimum toe clearance on the prosthetic side does not increase with walking speed. The main

variables of interest are minimum toe clearance and knee flexion angle. The goal of the toe-lift controller is to reduce toe scuf and the risk of tripping.

(ii) Slope Adapting Control

This controller will aim to adjust the stance angle of the TADA to adjust the ankle angle based off of the detected ground slope. The results of Chapter 4 support that the TADA can detect changes in pylon moment and moment impulses for different speeds and TADA angles. A similar experimental protocol and data analyses from that study will be adapted to investigate sloped walking. One aim will be to characterize the peak pylon moments and moment impulses as the foot angle of the TADA matches the ground slope for uphill, downhill, and crosshill walking. A slope detecting algorithm will be developed similar to the approach shown by Chang et al (2019)[78]. They presented a smart prosthetic ankle device that controls ankle angle based on detected terrain. It used the shank ankle as input to a fuzzy-logic based terrain identification method where fuzzy logic refers to the statistical approach that uses degrees of truth rather than a binary (true/false) approach. Using one IMU and load cell, the system detected slopes between 5-8 degrees.

To motivate the evaluative metrics to assess the slope adaptation, other literature using semi-active prostheses showed that the Propio-Foot[79], which can sagittally change ankle angle for uphill and downhill walking, presented socket pressure data similar to level ground walking[80]. Also, Fardet et al (2010)[76] showed that the Propio-Foot kinematics and kinetics similar to unimpaired persons for uphill walking but not downhill. Also, Nickel et al (2014)[81] presented a prosthetic ankle-foot that can adapt to up and downhill walking (up to 10 deg) with the device shifting to plantarflexion for downhill walking and dorsiflexion for uphill walking, reporting increased scores for socket comfort and decreased rate of perceived exertion. The main variables of interest are peak pylon moment and moment impulse for slope-matched TADA angles and user-defined socket comfort. The goal of the slope adapting control is to evaluate if slope-matched angles of the TADA have lower peak pylon moments and impulses

compared to the moments of the neutral TADA and to seek out the ankle angle the user find the most comfort.

(iii) Moment Targeting Control

This controller will aim to adjust the stance angle of the TADA as a function of the lowering peak pylon moments and impulse. The results of Chapter 4 support that when an unimpaired person wearing the TADA using an ankle bypass orthosis, peak sagittal and frontal pylon moments and moment impulses were lowest for dorsiflexed ankle angles. At the time of writing this dissertation, not enough is known about the minimum necessary magnitude of peak pylon moments and moment impulses to maintain functional walking on flat and sloped walking.

Lapre et. al (2016)[82] presented that one objective to minimize high moment transfer through the socket would be to realign the socket center closer to the ground reaction force's line of action during mid-stance. Moment targeting control cannot just aim for peak moments and impulses to be as low as possible. One un-ideal solution to minimize lower peak moments and impulses is to limp more on the intact side and minimize time spent on the prosthetic side. Consequently, we need to also consider the effect of the ground reaction force about the center of mass to maintain walking balance. We can use the results from the slope adapting experiments to design a suitable range of the peak pylon moments and impulses.

"How specifically should a moment targeting controller be designed?" is a necessary scientific question. We do not have a specific algorithm yet for the moment targeting control. The biomechanical outcomes can be evaluated with the TADA for participants walking on flat and sloped ground, on stairs, and around corners. In future studies, the following questions need to be asked:

- Can the moment targeting control of the TADA in steady-state sloped walking achieve consistently lower peak moment and impulse?
- Does a moment targeting control give kinematics and kinetics closer to the intact side or unimpaired walking?

- Can it improve the prosthetic user's comfort or lower rates of exertion?
- Can a moment targeting controller be a more generalizable controller for different types of walking and standing? Instead of having multiple different types of controllers for specific use cases like slope, corner, or stairs adaptation.
- Can a moment target controller adapt to multiple conditions like up/down/cross-hill and up/down stair walking, different walking speeds, standing on level, sloped, or stairs?

(d) Scientific and Engineering Contributions

(i) Motor control and Sensors

To control the TADA angle, I developed an open-source motor controller on the Raspberry Pi that interacts with brushless DC motors using CANopen over EtherCAT. I also wrote programs to receive sensor signals from a load cell (Europa+), inertial measurement unit (MPU6050), and Xsens lower-body inertial sensor suit. These sensors were used to detect the kinematics and kinetics of the lower body in prosthetic walking.

(ii) Integrated System for Biomechanical Evaluation

To integrate the hardware and software for full system functionality, I developed and tested the waist pack to include the raspberry pi, motor drivers, batteries, voltage regulators, circuit board, and cable connectors. The TADA with the motors and IMU were powered, and signals were sent through a few cables strapped to the person’s leg. The software architecture was built with Python, C, and C++ programs using the Robotic Operating System to interact with the motors and multiple sensors. These programs are freely available online (open source) and can be applied for other use cases.

(iii) Biomechanical Analyses

Through my work on the VSF and TADA data analyses, I’ve developed various biomechanical software to evaluate kinematic and kinetic data. For the VSF, I developed a mixed linear effect regression to evaluate the sensitivity of the lower body joint angles and moments, prosthetic power flow,

energy storage and return, and vertical ground reaction force magnitude and off-loading rate with changes of forefoot stiffness. This data set was created using motion capture and force plate data using Motive, synchronized using MATLAB, solved inverse dynamics using Visual3D, and completed final post-processing and graphics with MATLAB. For the TADA, I developed data analyses to calculate peak sagittal and frontal moments and moment impulses for various walking speed and TADA angles. This data set was created from the ROS file with streamed data from the TADA devices and post-processing and graphics with Python.

(iv) Summary of Manuscripts and Patent

On the next page is a summary of my journal articles in progress, in review, and published, and the patent I helped create.

Journal Articles

In Progress

1. **Kieran M. Nichols**, Rebecca Roembke, Sofya Akhetova, Peter G. Adamczyk. “Influence of Prosthetic Ankle Angle and Walking Speed on Pylon Moments in the Two Axis aDaptable Ankle.” *IEEE/AMSE Transactions on Mechatronics*
2. **Kieran M. Nichols,** Rebecca Roembke, Peter G. Adamczyk. “Real-time control of the New Two Axis aDaptable Ankle using a Raspberry Pi and CANopen motor communication.” *MDPI Actuators*.
3. Michael J. Greene, Ivan F.E. Simones, Preston R. Lewis, **Kieran M. Nichols,** and Peter G. Adamczyk. “Non-backdrivable Wedge-Cam Mechanism for a Semi-Active Two-Axis Prosthetic Ankle.” *Elsevier Mechatronics*.

Submitted

4. Bartloff, Jenny, Boehm, Wendy L., **Kieran M. Nichols**, and Kreg G. Gruben. " Frequency-dependent behavior of paretic and non-paretic leg force during standing post stroke.” *Journal of Biomechanics*.

Published

5. Peter G. Adamczyk, Sara Harper, Rebecca Roembke, Alex Reiter, Yisen Wang, **Kieran M. Nichols,** Darryl Thelen. “Wearable sensing for understanding and influencing human movement in ecological contexts.” *Current Opinion in Biomedical Engineering*.
6. **Kieran M. Nichols** and Peter G. Adamczyk. "Sensitivity of Lower-Limb Joint Mechanics to Prosthetic Forefoot Stiffness with a Variable Stiffness Foot in Level-Ground Walking." *Journal of Biomechanics* (2023): 111436.
7. McGeehan, Michael A., Peter G. Adamczyk, **Kieran M. Nichols**, and Michael E. Hahn. A simulation-based analysis of the effects of variable prosthesis stiffness on interface dynamics between the prosthetic socket and residual limb. *Journal of Rehabilitation and Assistive Technologies Engineering*. no. 9 (2022).
8. McGeehan, Michael A., Peter G. Adamczyk, **Kieran M. Nichols**, and Michael E. Hahn. "A computational gait model with a below-knee amputation and a semi-active variable-stiffness foot prosthesis." *Journal of Biomechanical Engineering* 143, no. 12 (2021).
9. McGeehan, Michael A., Peter G. Adamczyk, **Kieran M. Nichols**, and Michael E. Hahn. "A Reduced-Order Computational Model of a Semi-Active Variable-Stiffness Foot Prosthesis." *Journal of Biomechanical Engineering* 143, no. 7 (2021).
10. Boehm, Wendy L., **Kieran M. Nichols**, and Kreg G. Gruben. "Frequency-dependent contributions of sagittal-plane foot force to upright human standing." *Journal of Biomechanics* 83 (2019): 305-309.
11. **Kieran M. Nichols**. “The Characterization of Foot Force Vector Control in Human Standing.” Master’s Thesis. University of Wisconsin-Madison (2016).

Patent

Kreg G. Gruben, Wendy L. Boehm, and **Kieran M. Nichols**. "Apparatus for Assessing Human Balance Capability." U.S. Patent, No. 15/354,254.

Chapter 6. NOMENCLATURE

Abbreviations	Definition
AOPA	American Orthotic and Prosthetic Association
BOS	Base of Support
BW	Body Weight
CANopen	Controller Area Network (Open-source)
CAREN	Computer Assisted Rehabilitation ENvironment
CESR	Controlled Energy Storage and Return
COM	Center of Mass
COP	Center of Pressure
DMAMA	Dynamic Mean Ankle Moment Arm
DOD	Department of Defense
EFLR	Effective Foot Length Ratio
ESR	Energy Storage and Release
EtherCAT	Ethernet for Control Automation Technology
GRF	Ground Reaction Force
GRFR	Ground Reaction Force Resultant
IMU	Inertial Measurement Unit
KEAM	Knee External Adductor Moment
LE	Low Energy
LME	Linear Mixed Effects
MATLAB	MATrix LABoratory
MOS	Margin of Stability
MTC	Minimum Toe Clearance
PWA	Person with Amputation
RMSE	Root Mean Squared Error
ROS	Robotic Operating System
STADA	Sheep Two Axis aDaptable Ankle
TADA	Two Axis aDaptable Ankle
TTA	Transtibial Amputation (unilateral)
UD	Unified Deformable
vGRF	vertical Ground Reaction Force
VSF	Variable Stiffness Foot
VSPA	Variable Stiffness Prosthetic Ankle
xCOM	extrapolated Center of Mass

Units	
Angle	Degrees (deg)
Moment	Newton-meter (Nm); Nm/kg if normalized to body mass
Impulse	Newton-meter (Nm*s); Nm/kg*s if normalized to body mass
Power	Watts (W)
Energy/Work	Joules (J)
Vertical GRF	Newtons (N)
Vertical off-loading rate	Newton/second(N/s)

Chapter 7. LISTS OF FIGURES AND TABLES

(a) List of Figures

(b) List of Tables

Chapter 8. REFERENCES

1. Lower limb amputations – Epidemiology and assessment – PM&R KnowledgeNow. https://now.aapmr.org/lower-limb-amputations-epidemiology-and-assessment/.
2. Ziegler-Graham, K., MacKenzie, E. J., Ephraim, P. L., Travison, T. G. & Brookmeyer, R. Estimating the Prevalence of Limb Loss in the United States: 2005 to 2050. *Arch. Phys. Med. Rehabil.* **89**, 422–429 (2008).
3. Dillingham, T. R., Pezzin, L. E. & Shore, A. D. Reamputation, mortality, and health care costs among persons with dysvascular lower-limb amputations. *Arch. Phys. Med. Rehabil.* **86**, 480–486 (2005).
4. Wanamaker, A. B., Andridge, R. R. & Chaudhari, A. M. W. Projected Health Care Associated Costs of Workplace-Related Traumatic Amputation After 10, 15, and 20 Years: Part I: Lower Limb. *JPO J. Prosthet. Orthot.* **31**, 189–198 (2019).
5. Vu, H. T. T. *et al.* A Review of Gait Phase Detection Algorithms for Lower Limb Prostheses. *Sensors* **20**, 3972 (2020).
6. Safaeepour, Z., Esteki, A., Ghomshe, F. & Abu Osman, N. Quantitative analysis of human ankle characteristics at different gait phases and speeds for utilizing in ankle-foot prosthetic design. *Biomed. Eng. OnLine* **13**, 19 (2014).
7. Rajťúková, V., Michalíková, M., Bednarčíková, L., Balogová, A. & Živčák, J. Biomechanics of Lower Limb Prostheses. *Procedia Eng.* **96**, 382–391 (2014).
8. Adamczyk, P. G. Chapter 9 - Semi-active prostheses for low-power gait adaptation. in *Powered Prostheses* (eds. Dallali, H., Demircan, E. & Rastgaar, M.) 201–259 (Academic Press, 2020). doi:10.1016/B978-0-12-817450-0.00009-2.
9. Adamczyk, P. G., Roland, M. & Hahn, M. E. Sensitivity of biomechanical outcomes to independent variations of hindfoot and forefoot stiffness in foot prostheses. *Hum. Mov. Sci.* **54**, 154–171 (2017).
10. Klodd, E., Hansen, A. H., Fatone, S. & Edwards, M. Effects of prosthetic foot forefoot flexibility on gait of unilateral transtibial prosthesis users. *J. Rehabil. Res. Dev.* **47**, 899–910 (2010).
11. Lehmann, J. F., Price, R., Boswell-Bessette, S., Dralle, A. & Questad, K. Comprehensive analysis of dynamic elastic response feet: Seattle ankle/lite foot versus SACH foot. *Arch. Phys. Med. Rehabil.* **74**, 853–861 (1993).
12. AOPA. *Prosthetic Foot Project Report*. https://www.aopanet.org/wp-content/uploads/2013/12/Prosthetic_Foot_Project.pdf (2010).
13. Major, M. J., Twiste, M., Kenney, L. P. J. & Howard, D. Amputee Independent Prosthesis Properties—A new model for description and measurement. *J. Biomech.* **44**, 2572–2575 (2011).
14. Foort, J. Alignment of the above-knee prosthesis. *Prosthet. Orthot. Int.* **3**, 137–139 (1979).
15. Endolite Elan. *Endolite Elan* http://www.endolite.com/products/elan.
16. Kinnex. *Freedom Innovations* http://www.freedom-innovations.com/kinnex/.
17. Meridium. https://www.ottobockus.com/prosthetics/lower-limb-prosthetics/solution-overview/meridium/.
18. Ossur Products: Feet. *Össur* https://www.ossur.com/prosthetic-solutions/products/all-products/feet (2019).
19. Raschke, S. U. *et al.* Biomechanical characteristics, patient preference and activity level with different prosthetic feet: A randomized double blind trial with laboratory and community testing. *J. Biomech.* **48**, 146–152 (2015).
20. Fey, N. P. The influence of prosthetic foot design and walking speed on below-knee amputee gait mechanics. (2011).
21. Glanzer, E. M. & Adamczyk, P. G. Design and Validation of a Semi-Active Variable Stiffness Foot Prosthesis. *IEEE Trans. Neural Syst. Rehabil. Eng.* **26**, 2351–2359 (2018).

22. Shepherd, M. K. & Rouse, E. J. The VSPA Foot: A Quasi-Passive Ankle-Foot Prosthesis With Continuously Variable Stiffness. *IEEE Trans. Neural Syst. Rehabil. Eng.* **25**, 2375–2386 (2017).
23. Quraishi, H. A. *et al.* A passive mechanism for decoupling energy storage and return in ankle–foot prostheses: A case study in recycling collision energy. *Wearable Technol.* **2**, (2021).
24. Adamczyk, P. G. Ankle Control in Walking and Running: Speed- and Gait-Related Changes in Dynamic Mean Ankle Moment Arm. *J. Biomech. Eng.* **142**, 071007 (2020).
25. Leestma, J. K., Fehr, K. H. & Adamczyk, P. G. Adapting Semi-Active Prostheses to Real-World Movements: Sensing and Controlling the Dynamic Mean Ankle Moment Arm with a Variable-Stiffness Foot on Ramps and Stairs. *Sensors* **21**, 6009 (2021).
26. Shepherd, M. K., Azocar, A. F., Major, M. J. & Rouse, E. J. Amputee perception of prosthetic ankle stiffness during locomotion. *J. NeuroEngineering Rehabil.* **15**, 99 (2018).
27. Azocar, A. F., Shorter, A. L. & Rouse, E. J. Damping Perception During Active Ankle and Knee Movement. *IEEE Trans. Neural Syst. Rehabil. Eng.* **27**, 198–206 (2019).
28. Ingraham, K. A., Choi, H., Gardinier, E. S., Remy, C. D. & Gates, D. H. Choosing appropriate prosthetic ankle work to reduce the metabolic cost of individuals with transtibial amputation. *Sci. Rep.* **8**, 15303 (2018).
29. Rose, J. & Gamble, J. G. *Human walking*. vol. 3 (Williams & Wilkins Baltimore, 1994).
30. Wu, A. R. & Kuo, A. D. Determinants of preferred ground clearance during swing phase of human walking. *J. Exp. Biol.* jeb.137356 (2016) doi:10.1242/jeb.137356.
31. Adamczyk, P. G. & Kuo, A. D. Mechanisms of Gait Asymmetry Due to Push-Off Deficiency in Unilateral Amputees. *IEEE Trans. Neural Syst. Rehabil. Eng.* **23**, 776–785 (2015).
32. Collins, S. H. & Kuo, A. D. Recycling Energy to Restore Impaired Ankle Function during Human Walking. *PloS One* **5**, e9307 (2010).
33. Segal, A. D., Orendurff, M. S., Czerniecki, J. M., Schoen, J. & Klute, G. K. Comparison of transtibial amputee and non-amputee biomechanics during a common turning task. *Gait Posture* **33**, 41–47 (2011).
34. Zelik, K. E. & Adamczyk, P. G. A unified perspective on ankle push-off in human walking. *J. Exp. Biol.* **219**, 3676–3683 (2016).
35. Zelik, K. E. *et al.* Systematic Variation of Prosthetic Foot Spring Affects Center-of-Mass Mechanics and Metabolic Cost During Walking. *IEEE Trans. Neural Syst. Rehabil. Eng.* **19**, 411–419 (2011).
36. Clites, T. R., Shepherd, M. K., Ingraham, K. A. & Rouse, E. J. Patient Preference in the Selection of Prosthetic Joint Stiffness. in *2020 8th IEEE RAS/EMBS International Conference for Biomedical Robotics and Biomechatronics (BioRob)* 1073–1079 (2020). doi:10.1109/BioRob49111.2020.9224405.
37. Kim, M., Lyness, H., Chen, T. & Collins, S. H. The Effects of Prosthesis Inversion/Eversion Stiffness on Balance-Related Variability During Level Walking: A Pilot Study. *J. Biomech. Eng.* **142**, (2020).
38. Reimann, H., Fettrow, T., Thompson, E. D. & Jeka, J. J. Neural Control of Balance During Walking. *Front. Physiol.* **9**, 1271 (2018).
39. Gates, D. H., Scott, S. J., Wilken, J. M. & Dingwell, J. B. Frontal plane dynamic margins of stability in individuals with and without transtibial amputation walking on a loose rock surface. *Gait Posture* **38**, 570–575 (2013).
40. Reimann, H. *et al.* Complementary mechanisms for upright balance during walking. *PLOS ONE* **12**, e0172215 (2017).
41. Velzen, J. M. van, Houdijk, H., Polomski, W. & Bennekom, C. A. M. van. Usability of gait analysis in the alignment of trans-tibial prostheses: A clinical study. *Prosthet. Orthot. Int.* **29**, 255–267 (2005).
42. van Hal, E. S., Curtze, C., Postema, K., Hijmans, J. M. & Otten, E. Frontal plane roll-over analysis of prosthetic feet. *J. Biomech.* **125**, 110610 (2021).

43. Segal, A. D. & Klute, G. K. Lower-limb amputee recovery response to an imposed error in mediolateral foot placement. *J. Biomech.* **47**, 2911–2918 (2014).
44. Segal, A. D., Shofer, J. B. & Klute, G. K. Lower-limb amputee ankle and hip kinetic response to an imposed error in mediolateral foot placement. *J. Biomech.* **48**, 3982–3988 (2015).
45. Ramstrand, N. & Nilsson, K.-Å. A Comparison of Foot Placement Strategies of Transtibial Amputees and Able-Bodied Subjects During Stair Ambulation. *Prosthet. Orthot. Int.* **33**, 348–355 (2009).
46. Boone, D. A. *et al.* Influence of malalignment on socket reaction moments during gait in amputees with transtibial prostheses. *Gait Posture* **37**, 620–626 (2013).
47. Royer, T. D. & Wasilewski, C. A. Hip and knee frontal plane moments in persons with unilateral, trans-tibial amputation. *Gait Posture* **23**, 303–306 (2006).
48. Morgenroth, D. C. *et al.* The effect of prosthetic foot push-off on mechanical loading associated with knee osteoarthritis in lower extremity amputees. *Gait Posture* **34**, 502–507 (2011).
49. Jin, L., Adamczyk, P. G., Roland, M. & Hahn, M. E. The Effect of High- and Low-Damping Prosthetic Foot Structures on Knee Loading in the Uninvolved Limb Across Different Walking Speeds. *J. Appl. Biomech.* **32**, 233–240 (2016).
50. Doyle, S. S., Lemaire, E. D., Nantel, J. & Sinitski, E. H. The effect of surface inclination and limb on knee loading measures in transtibial prosthesis users. *J. NeuroEngineering Rehabil.* **16**, 37 (2019).
51. Rueda, F. M. *et al.* Knee and hip internal moments and upper-body kinematics in the frontal plane in unilateral transtibial amputees. *Gait Posture* **37**, 436–439 (2013).
52. Molina-Rueda, F. *et al.* Thorax, pelvis and hip pattern in the frontal plane during walking in unilateral transtibial amputees: biomechanical analysis. *Braz. J. Phys. Ther.* **18**, 252–258 (2014).
53. Molina-Rueda1, F. *et al.* Joint internal moments in subjects with unilateral transtibial amputation during walking. *J. Orthop. Orthop. Surg.* **2**, (2021).
54. Ventura, J. D., Klute, G. K. & Neptune, R. R. The effects of prosthetic ankle dorsiflexion and energy return on below-knee amputee leg loading. *Clin. Biomech.* **26**, 298–303 (2011).
55. McAndrew Young, P. M., Wilken, J. M. & Dingwell, J. B. Dynamic Margins of Stability During Human Walking in Destabilizing Environments. *J. Biomech.* **45**, 1053–1059 (2012).
56. Beltran, E. J., Dingwell, J. B. & Wilken, J. M. Margins of stability in young adults with traumatic transtibial amputation walking in destabilizing environments. *J. Biomech.* **47**, 1138–1143 (2014).
57. Sheehan, R. C., Beltran, E. J., Dingwell, J. B. & Wilken, J. M. Mediolateral angular momentum changes in persons with amputation during perturbed walking. *Gait Posture* **41**, 795–800 (2015).
58. Miller, S. E. Balance recovery mechanisms used by below-knee amputees following mediolateral perturbations. (2017). doi:10.15781/T20V89V4K.
59. Shell, C. E., Segal, A. D., Klute, G. K. & Neptune, R. R. The effects of prosthetic foot stiffness on transtibial amputee walking mechanics and balance control during turning. *Clin. Biomech.* **49**, 56–63 (2017).
60. Vitali, R. V., McGinnis, R. S. & Perkins, N. C. Robust Error-State Kalman Filter for Estimating IMU Orientation. *IEEE Sens. J.* **21**, 3561–3569 (2021).
61. Washabaugh, E. P., Kalyanaraman, T., Adamczyk, P. G., Claflin, E. S. & Krishnan, C. Validity and repeatability of inertial measurement units for measuring gait parameters. *Gait Posture* **55**, 87–93 (2017).
62. Li, Q., Young, M., Naing, V. & Donelan, J. M. Walking speed and slope estimation using shank-mounted inertial measurement units. in *2009 IEEE International Conference on Rehabilitation Robotics* 839–844 (2009). doi:10.1109/ICORR.2009.5209598.
63. Rebula, J. R., Ojeda, L. V., Adamczyk, P. G. & Kuo, A. D. Measurement of foot placement and its variability with inertial sensors. *Gait Posture* **38**, 974–980 (2013).

64. Kitagawa, N. & Ogihara, N. Estimation of foot trajectory during human walking by a wearable inertial measurement unit mounted to the foot. *Gait Posture* **45**, 110–114 (2016).
65. Ojeda, L. V., Rebula, J. R., Kuo, A. D. & Adamczyk, P. G. Influence of contextual task constraints on preferred stride parameters and their variabilities during human walking. *Med. Eng. Phys.* **37**, 929–936 (2015).
66. Gao, F., Liu, G., Liang, F. & Liao, W.-H. IMU-Based Locomotion Mode Identification for Transtibial Prostheses, Orthoses, and Exoskeletons. *IEEE Trans. Neural Syst. Rehabil. Eng.* **28**, 1334–1343 (2020).
67. Sup, F., Varol, H. A. & Goldfarb, M. Upslope Walking With a Powered Knee and Ankle Prosthesis: Initial Results With an Amputee Subject. *IEEE Trans. Neural Syst. Rehabil. Eng.* **19**, 71–78 (2011).
68. Best, T. K., Embry, K. R., Rouse, E. J. & Gregg, R. D. Phase-Variable Control of a Powered Knee-Ankle Prosthesis over Continuously Varying Speeds and Inclines. 8.
69. Takahashi, K. Z., Kepple, T. M. & Stanhope, S. J. A unified deformable (UD) segment model for quantifying total power of anatomical and prosthetic below-knee structures during stance in gait. *J. Biomech.* **45**, 2662–2667 (2012).
70. Nichols, K. M. & Adamczyk, P. G. Sensitivity of lower-limb joint mechanics to prosthetic forefoot stiffness with a variable stiffness foot in level-ground walking. *J. Biomech.* **147**, 111436 (2023).
71. McGeehan, M. A., Adamczyk, P. G., Nichols, K. M. & Hahn, M. E. A Reduced-Order Computational Model of a Semi-Active Variable-Stiffness Foot Prosthesis. *J. Biomech. Eng.* **143**, (2021).
72. McGeehan, M. A., Adamczyk, P. G., Nichols, K. M. & Hahn, M. E. A Computational Gait Model With a Below-Knee Amputation and a Semi-Active Variable-Stiffness Foot Prosthesis. *J. Biomech. Eng.* **143**, (2021).
73. McGeehan, M. A., Adamczyk, P. G., Nichols, K. M. & Hahn, M. E. A simulation-based analysis of the effects of variable prosthesis stiffness on interface dynamics between the prosthetic socket and residual limb. *J. Rehabil. Assist. Technol. Eng.* **9**, 20556683221111984 (2022).
74. Johnson, L., De Asha, A. R., Munjal, R., Kulkarni, J. & Buckley, J. G. Toe clearance when walking in people with unilateral transtibial amputation: effects of passive hydraulic ankle. *J. Rehabil. Res. Dev.* **51**, 429–437 (2014).
75. Lenzi, T., Cempini, M., Hargrove, L. J. & Kuiken, T. A. Design, Development, and Validation of a Lightweight Nonbackdrivable Robotic Ankle Prosthesis. *IEEEASME Trans. Mechatron.* **24**, 471–482 (2019).
76. Fradet, L., Alimusaj, M., Braatz, F. & Wolf, S. I. Biomechanical analysis of ramp ambulation of transtibial amputees with an adaptive ankle foot system. *Gait Posture* **32**, 191–198 (2010).
77. De Asha, A. R. & Buckley, J. G. The effects of walking speed on minimum toe clearance and on the temporal relationship between minimum clearance and peak swing-foot velocity in unilateral trans-tibial amputees. *Prosthet. Orthot. Int.* **39**, 120–125 (2015).
78. Chang, M., Kim, K. & Jeon, D. Research on Terrain Identification of the Smart Prosthetic Ankle by Fuzzy Logic. *IEEE Trans. Neural Syst. Rehabil. Eng.* **27**, 1801–1809 (2019).
79. Össur Proprio Foot. *Össur Proprio Foot* http://www.ossur.com/prosthetic-solutions/bionic-technology/proprio-foot.
80. Alimusaj, M., Fradet, L., Braatz, F., Gerner, H. J. & Wolf, S. I. Kinematics and kinetics with an adaptive ankle foot system during stair ambulation of transtibial amputees. *Gait Posture* **30**, 356–363 (2009).
81. Nickel, E., Sensinger, J. & Hansen, A. Passive prosthetic ankle-foot mechanism for automatic adaptation to sloped surfaces. *J. Rehabil. Res. Dev.* **51**, 803–14 (2014).
82. Kennedy LaPrè, A., Umberger, B. R. & Sup, F. C. A Robotic Ankle–Foot Prosthesis With Active Alignment. *J. Med. Devices* **10**, 025001 (2016).